Theory and Application of Induced Higher Order Color Aberrations

Dissertation
zur Erlangung des akademischen Grades

Doktor-Ingenieur (Dr.-Ing.)

vorgelegt dem Rat der Physikalisch-Astronomischen Fakultät
der Friedrich-Schiller-Universität Jena

von M.Eng. Andrea Berner
geboren am 10.09.1986 in Nordhausen

Gutachter

1. Prof. Dr. Herbert Gross, Friedrich-Schiller-Universität Jena

2. Prof. Dr. Alois Herkommer, Universität Stuttgart

3. Prof. Dr. Burkhard Fleck, Ernst-Abbe-Hochschule Jena

Tag der Disputation: 09.06.2020

Contents

1 Motivation and Introduction **5**

2 Theory and State of the Art **8**

2.1 Paraxial Image Formation 8

2.1.1 Paraxial Region 8

2.1.2 Paraxial Properties of an Optical Surface 9

2.1.3 Paraxial Raytrace and Lagrange Invariant 11

2.1.4 Refractive Power of a Thick and a Thin Lens 13

2.2 Aberration Theory 15

2.2.1 Wavefront Aberration Function 15

2.2.2 Transverse Ray Aberration Function 20

2.2.3 Seidel Surface Coefficients 21

2.3 Chromatic Aberrations 23

2.3.1 Axial Color Aberration 26

2.3.2 Lateral Color Aberration 28

2.4 Design Process 30

2.5 State of the Induced Aberration Problem 32

2.5.1 Induced Monochromatic Aberration 33

2.5.2 Induced Axial and Lateral Color 34

2.5.3 Induced Chromatic Variation of 3rd-order Aberrations 35

3 Extended Induced Color Aberration Theory **36**

3.1 The Concept of Induced Color Aberrations 36

3.1.1 Characteristics 36

3.1.2 Aberration Classification 37

3.1.3 Overview of new Results in this Chapter 38

3.2 Induced Axial Color 39

3.2.1 Surface Contribution of Intrinsic and Induced Axial Color . . . 39

3.2.2 Lens Contribution of Intrinsic and Induced Axial Color 43

3.2.3 Discussion 45

3.3 Induced Lateral Color 47

3.3.1 Surface Contribution of Intrinsic and Induced Lateral Color . . 47
3.3.2 Lens Contribution of Intrinsic and Induced Lateral Color 53
3.3.3 Discussion 55
3.4 Induced Spherochromatism 58
3.4.1 Definition of Spherochromatism 58
3.4.2 Surface Contribution of Intrinsic and Induced Spherochromatism 60
3.4.3 Thin Lens Contribution of Intrinsic and Induced Spherochromatism 65
3.4.4 Discussion 67
3.5 Induced Chromatic Variation of 3rd-order Seidel Aberrations 70

4 Application of the New Theory 73
4.1 Classical Design Examples 73
4.1.1 8f-imaging System 73
4.1.2 Thick Meniscus 77
4.1.3 Schupmann Achromat 78
4.1.4 Catadioptric System 81
4.1.5 Split Achromat 84
4.2 Complex Design Example - A Microscope Objective Lens 89
4.2.1 Design Specifications 89
4.2.2 Design Analysis 92
4.2.3 Improved Analysis by the New Theory 94

5 Summary 102

A Appendix i

Bibliography vii

List of Figures xii

List of Tables xiv

Zusammenfassung

Ehrenwörtliche Erklärung

Danksagung

1 Motivation and Introduction

Optical design describes an optimization process for lens systems combining applied aberration theory, system engineering and the experience of the designer. Meeting a set of optical performance specifications as well as manufacturing and costs constraints, very often complex lens systems with a multi-dimensional solution space are required. Prior to the development of digital computers, lens optimization was a hand-calculation task using trigonometric and logarithmic tables to calculate selected single rays trough a lens system up to the image. Nowadays, for this purpose, the main tool of an optical designer is the computer. Since computational power became available, the emphasis quickly shifted to powerful optimization techniques. They can navigate the design through the multi-dimensional solution space and push it to different local minima. To evaluate the several found solutions, a merit function is set up by the optical designer. Ensuring the final performance at the end of the optical system, typically this merit function is based on ray intersection operands at the final image plane and on some 1st-order parameters, e.g. focal length, magnification or intersection length. An explicit control of certain 3rd-order or even higher-order aberrations is unusual to give meaningful measures of the final image quality. Hence, because of the ability to do many computations simultaneously and due to the associated tendency to treat lens systems as black boxes, a deeper understanding about how and why a lens design works can only be achieved by a systematic and constant analysis of the different optimized design states.

The best way to find out the inner workings of an optical systems is to understand why aberrations arise and how they sum up surface by surface to their final amount at the image plane. Such a surface or lens resolved analysis describes the key method for achieving a deeper understanding and better optimizations of the designs. Its main advantage is the identification of performance dominating surfaces or lenses, referring to the five primary, 3rd-order aberrations, which are spherical aberration, coma, astigmatism, field curvature and distortion as well as to the chromatic aberrations. Furthermore, well balanced aberration contributions additionally indicate the system insensitivity to large tolerances, which always is an intended characteristic of a good lens design. Ludwig Seidel [Sei56] derived these well-known coefficients in 1856 and established the basic principles of aberration correction. Knowing the single contribu-

tions of every lens within the optical system enables the designer to work with determined steps like decreasing ray angles at dominating surfaces, add lenses at stressed positions or changing glasses of lenses with less or inverted chromatic contributions. Re-optimization after such determined system changes can push the design quickly to better or simpler states.
As today a multitude of the lens designs are specified to work in broad wavelength ranges, providing large field of views and apertures within very compact lens dimensions, higher-order aberrations are often the factor that at the end limits the resolution a lens can give [KT02]. Hence, although the correction of the five 3rd-order aberrations and the 1st-order chromatic aberration is a necessary condition to guarantee a good overall aberration correction, the influence of higher-order aberrations can not be neglected in all cases. Assuming the same ray-based approach like Seidel, Buchdahl and Rimmer[Buc54], [Rim63] derived the 5th- and 7th-order surface contributions of the monochromatic aberrations in 1963. Hoffman [Hof93] and Sasian [Sas10] completed 5th-order surface contribution theory in terms of wavefront aberration in 1993 and 2010. Clearly, those coefficients are not that reasonably simple anymore, but they are well described and discussed today.
In contrast to the 3rd-order aberrations, which are completely independent of each other, 5th-order aberrations are characterized by additional aberration parts that are induced by prior generated aberrations of lower-order. This special differentiation between induced and intrinsic contributions allows the lens designer not only to analyze, if there are dominating 5th-order aberrations, but it also tells how well the intrinsic and induced parts are balanced. Thereby, large induced aberrations parts refer to either unbalanced great 3rd-order aberrations somewhere inside the system or in some special cases large induced contributions even helps to correct the remaining intrinsic parts.

The present investigation now applies to the induced surface contributions of color aberrations. Especially for today's advanced applications, different challenges regarding the chromatic correction of optical systems have to be managed. For instance, in case of consumer optics, where mostly only plastic lenses can be applied because of weight and cost specifications, or in case of freeform optics, where the overall number of optical elements is often limited by compactness requirements, the options for color correction regarding glass choice and an appropriate refractive power distribution are highly restricted. Other applications, like hyper spectral imaging systems, IR- and Raman microscopy, again have to cover and correct an extreme broad wavelength band by the optical elements of the systems. Hence, for these cases the lens designer has to go further than the classical 1st-order color correction of axial and lateral color by considering also higher-order color aberrations and by taking advantage of induced aberration effects. To enable the designer to understand and to push its optical system

concerning these aberrations, the new expressions for induced surface contributions of color aberrations were derived in this investigation.

In contrast to the monochromatic aberrations, here, induced influences are already observable in the paraxial regime, since even paraxial rays are affected by dispersion. In analogous manner, lower-order aberrations picked up surface by surface in the preceding optical system, generates induced aberrations of higher order. In case of axial color and lateral color, different orders refer to the dependency of paraxial rays on dispersion. Concerning the chromatic variation of 3rd-order aberrations, different orders refer to the dependency of monochromatic 3rd-order aberrations on 1st-order color aberrations. In overcoming the analytical gap discussed in Section 2.5 for induced surface contributions of color aberrations in literature, the derivations for both cases will be given in this investigation. Spherochromatism as the most significant and most discussed chromatic variation of 3rd-order aberration is particularly emphasized. Finally, five classical and academic examples for induced color aberrations as well as one complex microscope lens design will be analyzed extensively. Here, the new theory is applied, in order to understand how the higher-order color aberrations behave in real optical systems and to demonstrate how their induced and intrinsic aberration parts can influence the overall performance of the optical system.

2 Theory and State of the Art

2.1 Paraxial Image Formation

The paraxial approximation of imaging considers the properties of light only in the region infinitesimally close to the optical axis. This area is usually known as the paraxial region or the Gaussian region. Inside this, all paraxial rays starting at one point $O(x, y)$ of the object plane OP will perfectly meet at an image point $O'(x', y')$ at the conjugated paraxial image plane IP. Figure 2-1 shows this main concept of paraxial imaging.

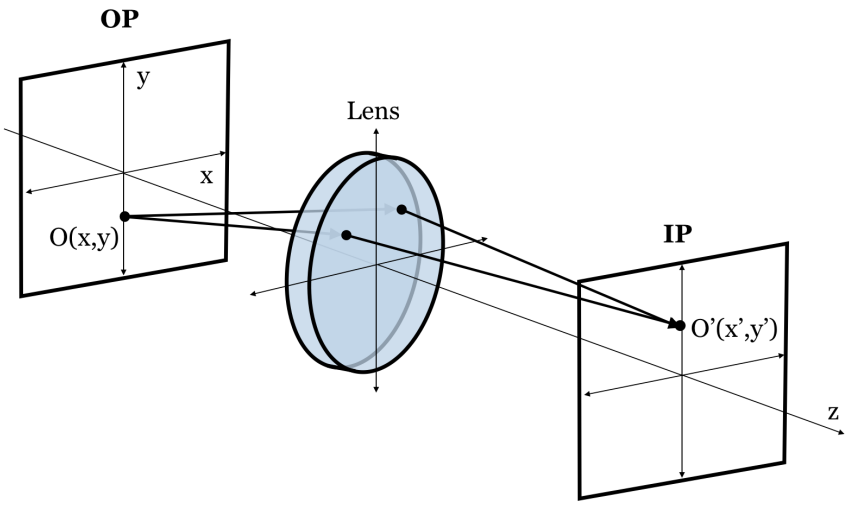

Figure 2-1: Paraxial approximation of imaging, assuming all rays starting at one point of the object plane OP perfectly meeting at an image point of the conjugated image plane IP.

2.1.1 Paraxial Region

The domain of paraxial rays is valid, if they are close enough to the optical axis to ensure that all terms of higher order of magnitude than quadratic in heights and in angles are to be neglected. Hence, to define the paraxial region, three assumptions have to be taken into account. Initially, any refracting or reflecting surface with an

curvature of c can be described by the first term in power series of a spherical surface sag z:

$$z \approx \frac{1}{2} c y^2 \tag{2.1}$$

Furthermore, the extension of the object and the image surfaces in x- and y-coordinates are limited to terms proportional to the square of the real object and image size. Finally, any ray angle is assumed to be sufficiently small so that its sine and the tangent function can also be linear approximated by[KT02]:

$$\sin i \approx \tan \approx i \tag{2.2}$$

The cosine function is set equal to 1 in this approximation.
Although these assumptions limit the validity of the paraxial approach to a very small area enclosing the optical axis, the paraxial approximation enables the calculation of the basic properties of an optical system like working distance, total track length, the Lagrange Invariant as well as the entrance and exit pupil positions. Even the estimation of the system performance based on paraxial relationships are of tremendous utility. Their simplicity makes calculation and manipulation quick and easy. Optical systems of practical value forming good images, apparently show that most of the light rays originating at an object point must pass at least reasonably close to the paraxial image point. Hence, the image point locations given by the paraxial relationships serve as an excellent approximation for the imaging of a well-corrected optical system [Smi66]. For this reason, paraxial imaging represent the point of reference for the definition of all aberrations.

2.1.2 Paraxial Properties of an Optical Surface

For the present investigation in this work, especially the surface related paraxial relations will be of greater interest. Figure 2-2 shows the imaging of an optical surface by refraction, assuming rotational symmetry along the z-axis. Please note, the marginal ray is defined as the paraxial ray starting at the optical axis passing through the edge of the aperture stop. The chief ray is defined as the ray starting at the maximum object height, passing through the center of the aperture stop.
The refractive spherical surface has a radius R with a center of curvature at c and separates two media of refractive index n and n' in front and behind, respectively. The marginal ray intersects the surface at a ray height y. Its incident ray encloses the angle u with the axis before refraction and u' after refraction. The angle i describes the angle between the incident marginal ray and the normal to the surface and the angle i' is the angle between the refracted ray and the normal. Please note, all of the above described ray parameters similarly apply for the chief ray. Those quantities are labeled

with bars. The distance of the object is denoted by the intersection length s and its height by y_O. After imaging through the surface, the image arises at an intersection length of s' and its height is y_I.

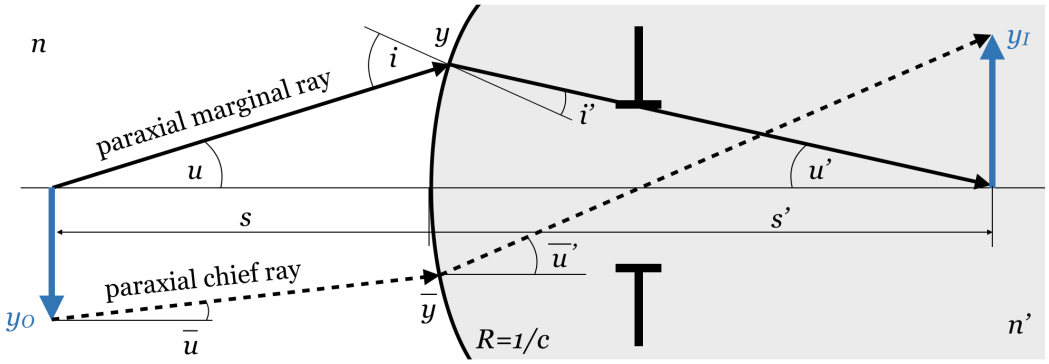

Figure 2-2: Refraction at an optical surface, assuming rotational symmetry along z-axis.

Generally, the normal Cartesian sign convention is applied, including these extensions:

- Light travels from left to right in z-direction.
- Ray heights above the optical axis are positive and under the optical axis are negative.
- Distances to the right of the surface are positive and to the left are negative.
- A radius is positive if the center of curvature lies to the right of the surface.
- Ray angles are positive if the slopes of the rays are positive.
- The angles of incidence and refraction are positive if the ray is rotated clockwise to reach the normal.

Determining the ray path from surface to surface through the optical system, Snell's law of refraction at dielectric interfaces or mirrors, $n \sin i = n' \sin i'$, has to be applied [Gro+07]. Following Equation 2.2, in paraxial approximation this is written as

$$ni = n'i' \tag{2.3}$$

Furthermore, simple trigonometric considerations reviewing Figure 2-2 concerning the ray angles u and u' as well as the marginal incident angle i and the emergent angle i' lead to (2.4).

$$u' = u - i + i' \tag{2.4}$$

$$i = u + yc \tag{2.5}$$

$$i' = u' + yc = \frac{ni}{n'} \tag{2.6}$$

By equivalent trigonometric treatment of the ray height y and the intersection lengths s as well as s', Equations (2.7) and (2.8) are obtained.

$$u = -\frac{y}{s} \tag{2.7}$$

$$u' = -\frac{y}{s'} \tag{2.8}$$

Now, if the two relations (2.3) and (2.4) as well as the paraxial approximation of (2.1) is assumed, the imaging equation of 2.9 for a refracting spherical surface can be deduced [Smi66].

$$\frac{n'}{s'} - \frac{n}{s} = (n' - n)c = F \tag{2.9}$$

Here, F is the refractive power of the surface. A surface with positive power will bend a ray toward the axis and a negative-powered surface will bend a ray away from the axis.

2.1.3 Paraxial Raytrace and Lagrange Invariant

Paraxial Raytrace If now calculations are to be continued through more than one surface, paraxial ray tracing is required. Reviewing the imaging equation of (2.9) and rearranging it by separating quantities before refraction and quantities after refraction, the following relation is obtained:

$$\frac{n'}{s'} = \frac{n}{s} + (n' - n)c \tag{2.10}$$

Multiplying both sides of the equation by y leads to

$$\frac{n'y}{s'} = \frac{ny}{s} + (n' - n)yc \tag{2.11}$$

and by substituting y/s and y/s' according to Equation (2.7) and (2.8), the relation describing the ray angle u' after refraction at a single spherical surface yields:

$$n'u' = nu - yc(n' - n) = nu - yF \tag{2.12}$$

To continue the calculation to the next surface of the system, a set of transfer equations are required. Figure 2-3 shows two spherical surfaces, j and $j+1$, of an arbitrary optical system separated by an axial distance d. The ray is shown after refraction by surface j; its slope is the angle u'_j. The intersection heights of the ray at the surfaces are y_j

and y_{j+1}, respectively.

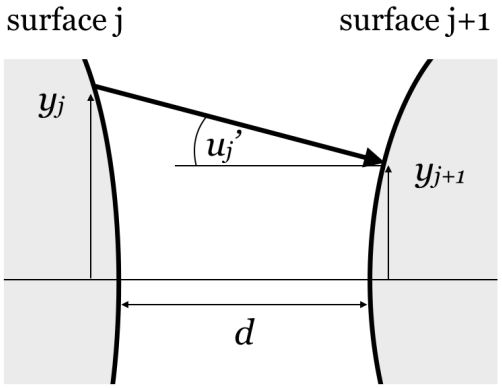

Figure 2-3: Paraxial ray transfer at an arbitrary surface j of an optical system to surface $j+1$.

The triangle formed by the distance d and both ray intersection points results in the trigonometric relation:

$$\tan u'_j = \frac{y_j - y_{j+1}}{d} \tag{2.13}$$

Within the paraxial approximation and by rearranging to obtain the ray height at the second surface $j+1$, this relation simplifies to:

$$y_{j+1} = y_j + du'_j \tag{2.14}$$

Since the slope of the ray incident on surface $j+1$ is the same as the slope after refraction by surface j, a second transfer equation is achieved:

$$n'_j u'_j = n_{j+1} u_{j+1} \tag{2.15}$$

Therefore, only the two Equations (2.12) and (2.14) are necessary to calculate a raytrace of any paraxial ray through an arbitrary optical system up to the image plane [Smi66]. Please note, if the marginal ray is chosen, like exemplary did in the equations above, the position of the image formed by the complete optical system can be determined and if the chief ray is chosen, the image size is obtained.

Lagrange Invariant A second important concept in paraxial optics, should also be emphasized here, since it is fundamental in calculating the 3rd-order aberrations, the Lagrange Invariant H. Reviewing the raytrace Equation (2.12) for the marginal ray, the same can be applied for the chief ray:

$$n'\bar{u}' = n\bar{u} + \bar{y}c(n' - n) = n\bar{u} + \bar{y}F \tag{2.16}$$

Here, the barred ray parameters refer to the chief ray. By eliminating $c(n'-n)$ in both equations, the following relation, known as the Lagrange Invariant or optical invariant at spherical surfaces is obtained:

$$n(u\bar{y} - \bar{u}y) = n'(u'\bar{y} - \bar{u}'y) = H \tag{2.17}$$

Since it is also invariant after transfer from one surface to another, the relation is identical at all surfaces in a lens system. It can be shown that the square of the Lagrange Invariant is proportional to the energy transmitted by the lens, assuming that the object radiates uniformity [KT02]. Hence, the Lagrange Invariant can be understood as a consequence of the law of conversation of energy in refracting optical systems [Wel86].

2.1.4 Refractive Power of a Thick and a Thin Lens

The refractive power F of an optical element is defined as the reciprocal of its effective focal length *f*. In general, the focal length of an optical system can simply be calculated by tracing a ray through the optical system, coming from infinity, with an initial ray angle u equal to zero. The effective focal length then is defined as the relation of the ray height at the first surface and the ray angle after emerging from the last surface. Similarly, for the back focal length the ray height at the last surface is taken into account. In a system with k surfaces, Equation (2.18) and (2.19) show the definitions of the effective focal length *f* and the back focal length *f'*, respectively[Smi66].

$$f = -\frac{y_1}{u'_k} \tag{2.18}$$

$$f' = -\frac{y_k}{u'_k} \tag{2.19}$$

Assuming now a thick lens in air, having a refractive index of n, the effective focal length can easily be calculated by tracing a parallel ray through the two surfaces of the thick lens. The surface radii are R_1 and R_2 and the surface curvatures are c_1 and c_2. The lens' thickness is t. Figure 2-4 illustrates these relevant quantities for the thick lens approach. If the lens is surrounded by air, the indices of refraction can be assumed to be $n_0 = n_2 = 1$.

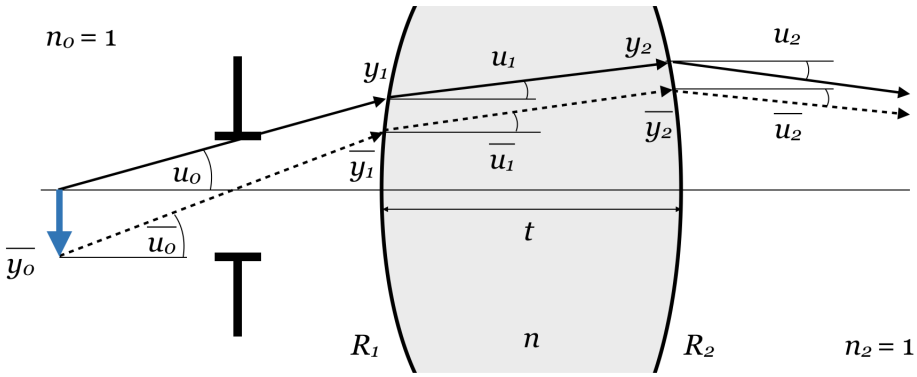

Figure 2-4: Refraction of the marginal ray (solid line) and the chief ray (dashed line) at a thick lens.

Applying the raytrace equations of Subsection 2.1.3, the refractive power F^{tL} of a thick lens, or the reciprocal of its effective focal length, can now be expressed by [Smi66]:

$$\begin{aligned} F^{tL} &= \frac{1}{f} = -\frac{u_2}{y_1} \\ &= (n-1)\left(c_1 - c_2 + t c_1 c_2 \frac{n-1}{n}\right) \\ &= (n-1)\left(\frac{1}{R_1} - \frac{1}{R_2} + \frac{t(n-1)}{n R_1 R_2}\right) \end{aligned} \tag{2.20}$$

Referring to the definition of the refractive power of a single surface, as shown in (2.9), the refractive power of a thick lens can also be calculated by considering the single surface powers F_1 and F_2 and the thickness t:

$$F^{tL} = F_1 + F_2 - \frac{t F_1 F_2}{n} \tag{2.21}$$

Reviewing this relation, also an equivalent expression for thin lenses can be found. By considering the limiting behavior of Equation (2.20) for t converging to zero, the refractive power F^L of a thin lens is described by:

$$\begin{aligned} F^L &= (n-1)(c_1 - c_2) \\ &= (n-1)\left(\frac{1}{R_1} - \frac{1}{R_2}\right) \\ &= F_1 + F_2 \end{aligned} \tag{2.22}$$

2.2 Aberration Theory

In Section 2.1 the perfect imaging characteristics of optical systems, limited to an infinitesimal close region to the optical axis, were discussed. Here, a lens forms an image without any aberrations. The image size as well as the location are given by the equations for the paraxial region. Leaving this paraxial region of an imaging system, in general, real optics with finite ray heights and ray angles do not perform ideal imaging. Hence, rays emerging from one object point *O(x,y)* will not all perfectly meet at a single image point *O'(x',y')*. Figure 2-5 shows an example with three random rays of the y-z-plane.

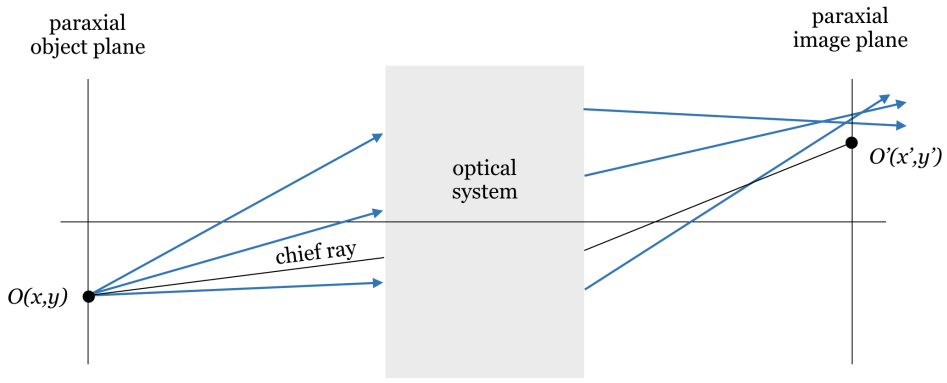

Figure 2-5: Real imaging of an optical system, considering real optics with finite ray heights and ray angles.

To determine the aberrations by the amount by which the real rays miss the paraxial image point, several methods are used for description. Deviations from perfect imaging can either be described in terms of wavefront aberrations, measured in optical path length differences, or in terms of the geometrical ray interception errors, measured in transverse or longitudinal aberrations at the image plane.

2.2.1 Wavefront Aberration Function

Wavefront Definition The fundamental law for defining wavefront aberrations is the theorem of Malus and Dupin. It states the definition of a wavefront by a surface of constant optical path length measured from a point at the object plane. Figure 2-6 illustrates this principle. Here, several rays are traced from a source point O at the object plane. The points P_1, P_2 and P_3 all represent points, having the same optical path length $|OP_1| = |OP_2| = |OP_3|$ starting at O. This is also true for any other ray outside the y-z-plane starting at O. In case of an isotropic material having a refractive index of n, the wavefront is the locus of the points P_1, P_2, P_3 etc., since it represents the surface of constant optical path length. Please note, the wavefront containing the

points P_1 up to P_n is a sphere centered on O. However, if the points Q_1 up to Q_n of the image space are taken, the wavefront is not in general a sphere anymore, since it was aberrated by the preceding optical system [KT02]. Here, it is easy to see, that the theorem of Malu and Dupin can also be interpreted in such a way that geometrical wavefronts always are perpendicular to the rays starting at the same object point [Wel86].

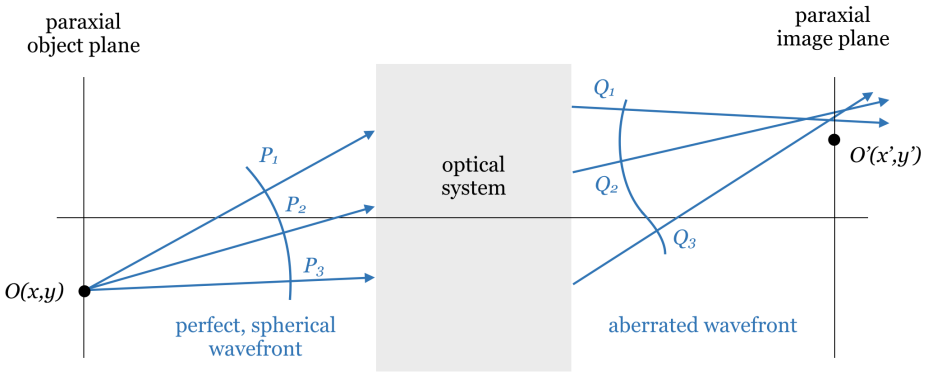

Figure 2-6: Definition of wavefronts as a surface of constant optical path length measured from a point at the object plane.

Wavefront Aberration After describing the wavefront itself, a definition for the wavefront errors is introduced. Spherical wavefronts in image space converge to a single, unblurred image point. However, aberrated wavefronts deviate from a perfect sphere. Therefore, it is suitable to express the wavefront aberration W with respect ot a reference sphere. It is measured in terms of optical path length difference along the ray. In general, the reference sphere is determined by its center O', which is the assumed paraxial image point, and by its radius R. Usually, R is defined by the location of the exit pupil, so that the reference sphere contains the intersection point of the chief ray with the optical axis. Figure 2-7 illustrates these conditions.

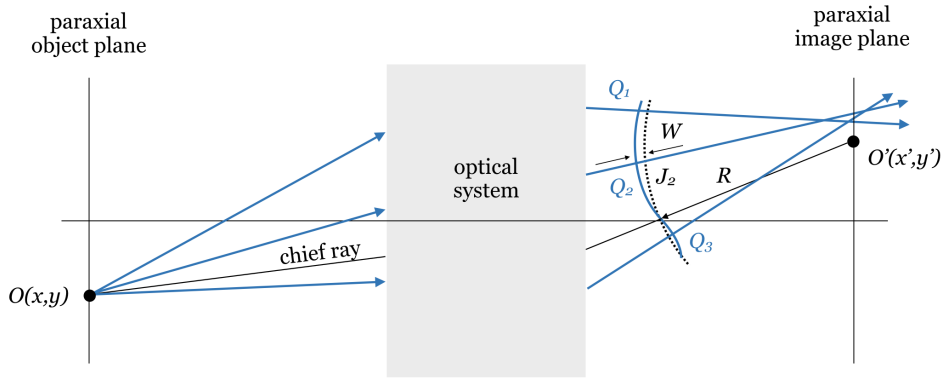

Figure 2-7: Wavefront aberration defined as the deviation of the wavefront to a reference sphere (dotted line). This is determined by the paraxial image point O' as center and the intersection point of the chief ray with the optical axis.

By considering the definition of the wavefront aberration W, the optical path measured along the ray from the reference sphere to the wavefront is obtained by [Gro+07]:

$$W = [OQ_2] - [OJ_2] \tag{2.23}$$

In this case, the wavefront aberration is negative, $W < 0$.

Power Series Expansion The example above shows, that the wavefront aberration clearly depends on the chosen ray. If the wave aberration is to be described for all rays emerging from the object point O and passing through the exit pupil, all concerned rays can be identified by their pupil coordinates x_p and y_p. Hence, the wave aberration $W(x_p, y_p)$ then becomes a function of two variables. However, this function only describes the aberrations for the chosen object point O. A complete information about the total system aberrations is only obtained by considering the whole object field. Therefore, if an object point is characterized by its object plane coordinates x and y, then the wavefront aberration becomes a function of four variables $W(x, y, x_p, y_p)$. This function of four variables is essential, if optical systems without rotational symmetry are investigated [Gro+07]. For reasons of simplification, Figure 2-8 only shows the object plane and the exit pupil plane of an optical system.
Here, a single ray is regarded, starting at the object coordinates x and y and passing through the pupil coordinates x_p and y_p. For this ray the wavefront aberration is defined by $W(x, y, x_p, y_p)$. In the more common case of a rotational symmetric system, this ray can be rotated about the optical axis by an arbitrary amount, but the wavefront aberration will still be the same.

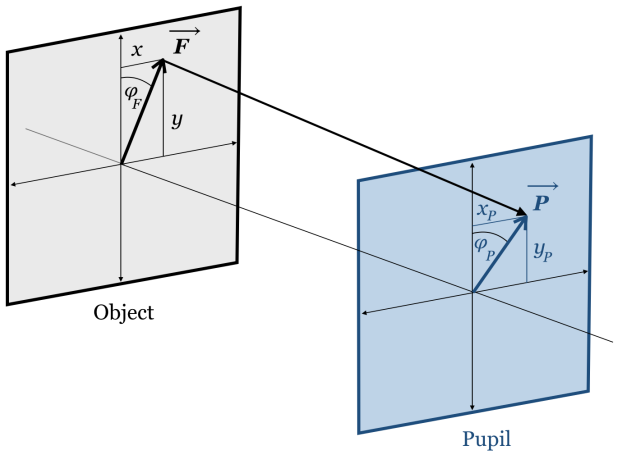

Figure 2-8: Definition of field vector $\vec{F}$ at the object plane and pupil vector $\vec{P}$ at the pupil plane of an optical system.

Hence, instead of describing the ray by the above mentioned four variables of the Cartesian object and pupil coordinates, adapted variables which are invariant with respect to rotation about the optical axis, can be found. Consequently, if $\vec{F}$ indicates the field vector within the object plane origin to the object point $(x,\ y)$ and if $\vec{P}$ is the pupil vector from the pupil plane origin to the pupil point (x_p, y_p), the rotational invariant variables are:

$\lvert\vec{F}\rvert^2 = x^2 + y^2$	the square of the field vector length
$\lvert\vec{P}\rvert^2 = x_p^2 + y_p^2$	the square of the pupile vector length
$\vec{P} \cdot \vec{F} = \lvert P\rvert\lvert F\rvert \cos(\varphi) = x_p x + y_p y$	the scalar product of $\vec{P}$ and $\vec{F}$

In addition to the lengths of both vectors, the last quantity also contains the information about the angle $\varphi = \varphi_F - \varphi_P$ between the two vectors. With these new rotational invariant variables the wavefront aberration for an arbitrary ray can be stated as $W(x^2 + y^2\,,\ x_p^2 + y_p^2\,,\ x_p x + y_p y)$, depending only on the length of the object vector, the length of the pupil vector and on the angle between the object and pupil vector. Now, without loss of generality, one more simplification can be assumed as the object point can be chosen to lay on the y-axis. Therefore, by setting $x = 0$ the wave aberration then is defined by [Gro+07]:

$$W(y^2, x_p^2 + y_p^2, y_p y) \tag{2.24}$$

An equivalent and also often used expression for W is found by changing from Cartesian coordinates to a polar coordinate description. In this case, the field coordinate y stays

the same, as it was chosen to lay on the y-axis . For the pupil parameters, the radial coordinate r is assumed to be $r^2 = x_p^2 + y_p^2$ and the angular coordinate is defined by $\cos\varphi = y_p/r$. Hence, in polar coordinates the wavefront aberration function reads:

$$W(y^2, r^2, y\, r \cos\varphi) \tag{2.25}$$

To classify now the different types of image errors comprised by the wavefront aberration function and to understand the behavior of each type, W can be written in the most general power series of its three variables. The result is shown in Equation (2.26). Here, again polar coordinates were assumed.

$$\begin{aligned}
W &= W(y, r, \varphi) \\
&= + w_{020}r^2 + w_{111}yr\cos\varphi && \text{Defocus and scale error} \\
&\quad + w_{040}r^4 + w_{131}yr^3\cos\varphi + w_{222}y^2r^2\cos^2\varphi && \text{Primary aberrations} \\
&\quad + w_{220}y^2r^2 + w_{311}y^3r\cos\varphi \\
&\quad + w_{060}y^6 + w_{151}yr^5\cos\varphi + w_{242}y^2r^4\cos^2\varphi && \text{Higher-order aberrations} \\
&\quad + w_{240}y^2r^4 + w_{331}y^3r^3\cos\varphi + w_{333}y^3r^3\cos^3\varphi \\
&\quad + w_{422}y^4r^2\cos^2\varphi + w_{420}y^4r^2 + w_{511}y^5r\cos\varphi
\end{aligned} \tag{2.26}$$

Please note, since a power expansion is strictly mathematical, but the wavefront aberration is not an arbitrary function to be expanded, a constant term and all coefficients with no dependence on pupil parameters were set to zero within this mathematical expression [Gro+07]. The latter is due to the fact that those wavefront parts are associated to the chief ray and therefore would cause $W(y, r, \varphi)$ to be zero for this point [Hop50].

Equation (2.26) now shows the classification of the different aberrations types. The coefficient's notation by $w_{i,j,k}$, which is due to Hopkins [Hop50], indicate the nature of the different aberrations by their suffixes, concerning on how they depend on the field, which is the first suffix, on the pupil, which is the second suffix, as well as in which power they depend on the azimuth angle φ, described by the third suffix. However, the classification to primary and higher-order aberrations is only based on their dependence on the field coordinate y and the aperture coordinate r. Considering this, in axially symmetrical systems, the sum of field and pupil powers only gives even-order terms. Odd-order terms may not exist. Therefore, primary aberrations include all terms that are dependent on the fourth power in field and aperture and higher-order aberrations show a total power sum of sixth-, eighth- and tenth-order etc. The defocus and the scale error, are usually not considered as aberrations at all, since those terms do not prohibit perfect imaging. Defocus only shifts the perfect image to another image plane

in z-direction and the magnification error generates a perfect image but of different size.

To specify the primary aberration more detailed, the five terms shown in Equation (2.26) are spherical aberration, coma, astigmatism, field curvature and distortion, respectively. The spherical aberration term $w_{040}r^4$ is the only one, which is independent of the object size y and the azimuth angle φ, so it is constant over field and azimuth angle. Expressed as a wavefront aberration, it is proportional to r^4 and therefore the only monochromatic aberration that can occur on-axis. However, coma, $w_{131}yr^3\cos\varphi$, is proportional to r^3 in the y-z section, but within the x-z-section, when $y_p = 0$ and $\cos\varphi = 0$, this wavefront aberration is zero. Since coma is linearly proportional to y, at small field angles coma is the most important off-axis aberration. In contrast, the wavefront aberrations associated with astigmatism and field curvature, $w_{222}y^2r^2\cos^2\varphi$ and $w_{220}y^2r^2$ respectively, are both proportional to r^2. Hence, these aberrations generate a defocus effect of some extent. Specifically, the field curvature term represents a defocus that is proportional to y^2 and therefore causes a curved image plane and corresponding to this, astigmatism is a similar aberration, but it is purely cylindrical. Therefore, astigmatism gives only a defocus for the tangential section. The fifth primary aberration is distortion,$w_{311}y^3$. Comparable to the scale error, distortion also produces a lateral displacement of the image, but in this primary aberration case it additionally varies with field y and is proportional to the third power of it [KT02].

2.2.2 Transverse Ray Aberration Function

The transverse ray aberration $\Delta x'$ and $\Delta y'$ give the lateral displacement components in x- and y-direction of the ray intersection point with a reference plane measured from a reference point. Usually, the paraxial image plane and the intersection point of chief ray are used for these references. Figure 2-9 illustrates the transverse ray aberration in the y-z-plane of an optical system.

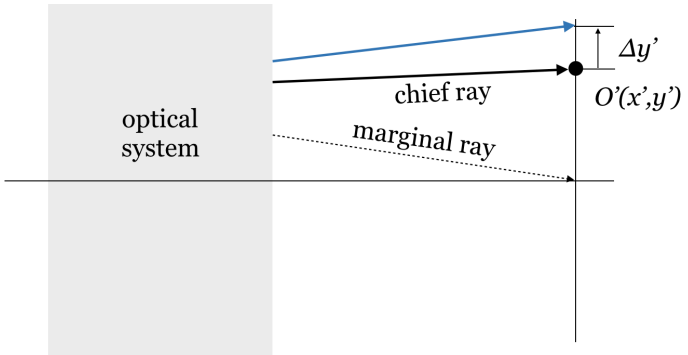

Figure 2-9: Transverse ray aberration $\Delta y'$ in the y-z-plane of an optical system.

According to Equations (2.27) and (2.28) the transverse ray aberrations can be calculated by differentiating with respect to x_p and y_p, respectively [Gro05].

$$\Delta x' = -\frac{R}{n'} \cdot \frac{\partial W}{\partial x_p} \tag{2.27}$$

$$\Delta y' = -\frac{R}{n'} \cdot \frac{\partial W}{\partial y_p} \tag{2.28}$$

Here, R is again the radius of reference sphere, n' is the index of refraction at image space and x_p and y_p are the ray exit pupil coordinates. By applying these equations to the primary aberrations of the power series expansion of Equation (2.26), the aberration polynomial for the primary transverse ray aberrations is obtained and shown in Equation (2.30).

$$\Delta x' = -\frac{R}{n'} \left[2b_1 x_p + 4c_1 r^3 \sin\varphi + c_2 y r^2 \sin 2\varphi + 2c_4 y^2 r \sin\varphi\right] \tag{2.29}$$

$$\Delta y' = -\frac{R}{n'} \left[2b_1 y_p + b_2 y + 4c_1 r^3 \cos\varphi + c_2 y r^2 (2 + \cos 2\varphi) + 2(c_3 + c_4) y^2 r \cos\varphi + c_5 y^3\right] \tag{2.30}$$

Here, the coefficients were renamed to b_1, b_2 and c_1 up to c_5, but the arrangement of the terms is still in the same proper order from defocus and scale error to spherical aberration, coma, astigmatism, field curvature and distortion. As the transverse aberrations are derived from the wavefront aberrations by differentiation with respect to the pupil coordinate, the power sum of a transverse aberration term is always one less than the power sum in the corresponding wavefront aberration term. Therefore, these aberrations, consisting of terms with the lowest powers, which are regarded as primary aberrations, are also called 3rd-order aberrations or Seidel aberrations. Please note, the naming "third-order" refers to the above shown power series for the transverse aberrations, although considered as wave aberrations the order for the primary aberrations is four [Gro+07].

2.2.3 Seidel Surface Coefficients

The last section showed that the wavefront aberration can be written as the difference between the optical path lengths along a system's chief ray and any other ray, starting from the same object point. This can be calculated as a part of ray tracing and it is used to analyze the optical performance of a system, concerning the different types of aberrations. However, the wavefront analysis only gives information about the aberrations at the image plane of a lens. Characteristic data helping to understand why

a lens shows its aberrations or what parameters should be changed, in order to reduce them, is missing. For this purpose, aberration coefficients, describing the contributions of the individual surfaces in a lens, are needed.
Figure 2-10 illustrates a lens with three surfaces, an object at O and an image at O'.

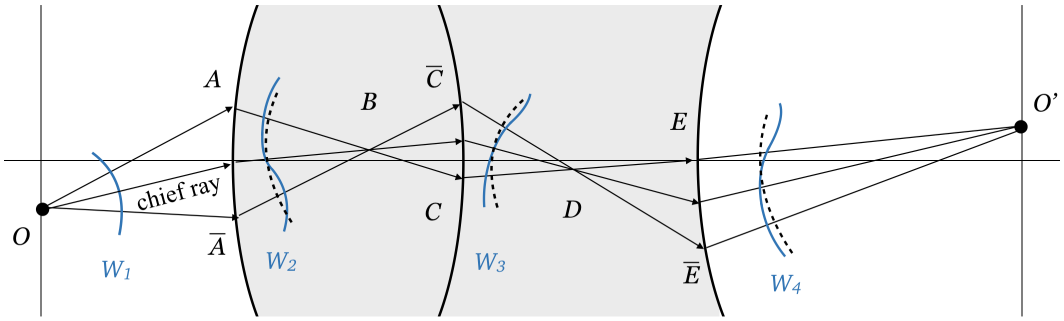

Figure 2-10: Lens example with three surfaces, forming a real intermediate image in each space in between the surfaces.

Here, a real intermediate image in each space between the surfaces is formed. Referring to the wavefront definition in 2.2.1, the wavefront aberration at the image point O' can be expressed by:

$$W = [O\bar{A}B\bar{C}D\bar{E}O'] - [OABCDEO'] \tag{2.31}$$

Because of the intermediate images, which each become the object of the following surface, this relation can also be rewritten by summing up the three optical path lengths from one intermediate image to the next:

$$W = [O\bar{A}B] - [OAB] + [B\bar{C}D] - [BCD] + [D\bar{E}O'] - [DEO'] \tag{2.32}$$

Hence, it can be seen from Equation (2.32) that the wavefront aberration of an optical system can also be expressed as the sum of the wavefront aberration contributions of the individual surfaces in the lens. In case of the five primary aberrations, these contributions can be evaluated independently, since they do not affect each other from surface to surface and furthermore only paraxial ray data, like ray heights and angles of the marginal and the chief ray, can be applied. This described approach represents the basis of Seidel's aberration analysis [KT02]. Please note, although it can not be identified directly as an intermediate image in between two surfaces like in the shown example, every optical surface either generates a real or a virtual intermediate image, which then becomes the object of the following surface.
Based on the paraxial quantities introduced in Section 2.1.2 and 2.1.3, the following expressions for the so-called Seidel sums $S_I, S_{II}, S_{III}, S_{IV}$ and S_V can be derived [Wel86]. These sums represent the summation of the single surface contributions in an optical system according to the five primary aberrations. They can be understood as a new

set of coefficients instead of the five coefficients w_{040} to w_{311} used in the mathematical derivation of the power series in Section 2.2.1 [Gro+07].

$$S_I = -\sum A^2 y\,\Delta\left(\frac{u}{n}\right) \qquad \text{Spherical aberration} \tag{2.33}$$

$$S_{II} = -\sum \bar{A} A y\,\Delta\left(\frac{u}{n}\right) \qquad \text{Coma} \tag{2.34}$$

$$S_{III} = -\sum \bar{A}^2 y\,\Delta\left(\frac{u}{n}\right) \qquad \text{Astigmatism} \tag{2.35}$$

$$S_{IV} = -\sum H^2 c\,\Delta\left(\frac{1}{n}\right) \qquad \text{Field curvature} \tag{2.36}$$

$$S_V = -\sum \frac{\bar{A}}{A}(S_{III} + S_{IV}) \qquad \text{Distortion} \tag{2.37}$$

In this equations, $A = ni$ and $\bar{A} = n\bar{i}$ are the refraction invariants at the chosen surface for the marginal ray and the chief ray, respectively. The Δ stands for the difference of the particular quantities after and in front of the surface. Hence, $\Delta\,(u/n) = u'/n' - u/n$. It should be emphasized, how reasonable simple these Seidel surface contributions are and that they enable the lens designer to distinguish between the influence of every single surface to a particular aberration. Listing the Seidel contributions of an optical system allows to find performance dominating surfaces and also shows, what parameters should be changed in order to reduce their contribution.
In general, the Seidel sums are calculated with maximum aperture and maximum field. So, to find an equivalent expression for the wave aberration function in terms of the Seidel sums, the pupil coordinate r and the field coordinate y have to be redefined as relative coordinates $\rho = r/r_{max}$ and $\eta = y/y_{max}$, respectively. With these, the total primary monochromatic wave aberration reads [Gro+07]:

$$\begin{aligned} W &= W(\eta, \rho, \varphi) \\ &= \frac{1}{8}S_I\rho^4 + \frac{1}{2}S_{II}\eta\rho^3\cos\varphi + \frac{1}{2}S_{III}\eta^2\rho^2\cos^2\varphi + \frac{1}{4}(S_{III} + S_{IV})\eta^2\rho^2 + \frac{1}{2}S_V\eta^3\rho\cos\varphi \end{aligned} \tag{2.38}$$

2.3 Chromatic Aberrations

Generally, optical systems have to be corrected within a certain wavelength range. The optical properties as well as the aberration of an optical system depend on the refractive index n characterizing the required glasses. Since the refractive index of any medium other than vacuum varies as a function of the light's wavelength, also

the optical properties of a lens inherently depend on the wavelength. This variation of n is known as the dispersion and it is exemplary shown in Figure 2-11. Here, the dependence of the refractive index of the optical glass BK7 over the visual wavelength range is plotted [Nak15].

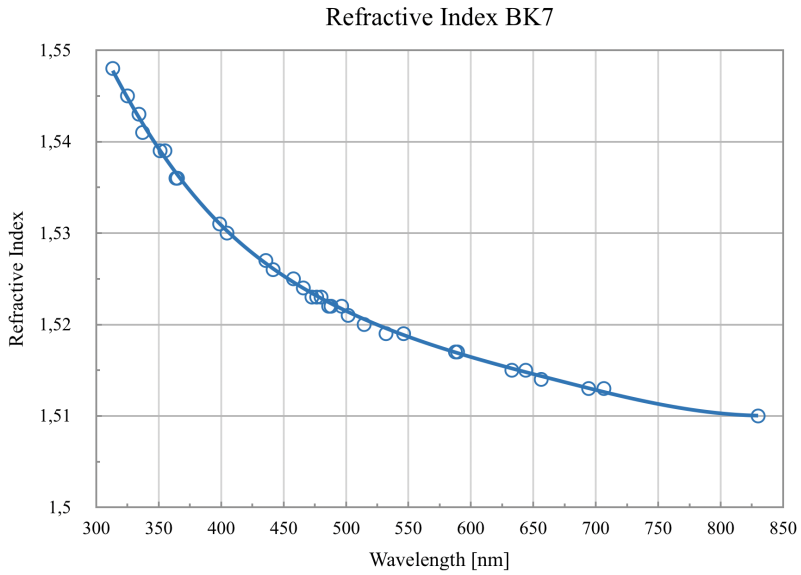

Figure 2-11: Variation of the refractive index n with wavelength for BK7

In general, the index of refraction of optical materials is higher for short wavelengths than for long wavelengths. Therefore, the short wavelengths are refracted more strongly at each surface of a lens than the longer wavelengths. Reviewing the wave aberration function of Section 2.2.1, based on the optical path length concept, as well as the Seidel coefficients in Section 2.2.3, clearly, all of the monochromatic aberrations will show their chromatic variation effects caused by dispersion. Usually, this is called colored coma, colored astigmatism, etc. For the chromatic variation of spherical aberration, there is a separate denotation, known as spherochromatism. But by varying the refractive indices, not only the aberration, even the paraxial quantities, such as the image position and the image size, will show chromatic variations. These change in focus and image size represent the primary chromatic aberrations known as axial color aberration and lateral color aberration, respectively.

The parameters, which determine those variations, are well-known as the Abbe number ν and the partial dispersion P. The Abbe number describes the dispersive character of an optical glass by the relation of its refractive indices at three characteristic wavelengths. Within the visible spectrum, it is common to measure the value of refractive index at 587.6 nm, which represents the yellow helium Fraunhofer d-line. The dispersion is conventionally taken to be the difference between the refractive indices at the hydrogen blue F- and red C-line wavelengths. These are traditionally Fraunhofer line values at 486.13 nm and 656.27 nm, respectively. Some design software and glass man-

ufacturer also prefer to use the mercury green line at 546.1 nm instead of the helium yellow line, since it is closer to the peak of the visual response of the human eye. In this case, the dispersion is measured between the F'-line at 479.99 nm and C'-line at 643.85 nm. Equation (2.39) and (2.40) shows those two definitions for the Abbe number ν_d and ν_e.

$$\nu_d = \frac{n_d - 1}{n_F - n_C} \tag{2.39}$$

$$\nu_e = \frac{n_e - 1}{n'_F - n'_C} \tag{2.40}$$

To categorize different types of optical glasses, the Abbe diagram, also called 'the glass map', plots the Abbe number ν_d of an optical material versus its refractive index n_d. Therefore, glasses can then be selected according to their positions on the diagram, describing their optical properties. An example Abbe diagram of the manufacturer Schott is shown in Figure 2-12.

However, some optical systems are required to operate at other wavelength bands, different from the visual spectrum, determined e.g. by the spectral emission of the source or by the spectral sensitivity of the detector. In this case, a glass map for an appropriate set of wavelengths should be generated and be used [KT02].

Consequently, since the curve of refractive index versus wavelength shown in Figure 2-11 follows a nonlinear behavior, also its gradient varies with wavelength. Therefore, a second relation for optical glasses characterizing the waveband starting at the d-line up to the F-line, was introduced by the well-known partial dispersion P:

$$P = \frac{n_F - n_d}{n_F - n_C} \tag{2.41}$$

Plotting this value versus the Abbe number ν_d leads to a second classical glass diagram type. Here, the majority of the glasses lay on the so-called normal glass line drawn through the glasses K7 and F2. The slope of this line is constant at $\Delta P/\Delta\nu_d = -0.0005$. Glasses distant from the line are called anomalous glasses. Because of their special properties, they are in most of the cases expensive materials. But they are necessary to reduce the secondary spectrum, when primary color aberrations are corrected.

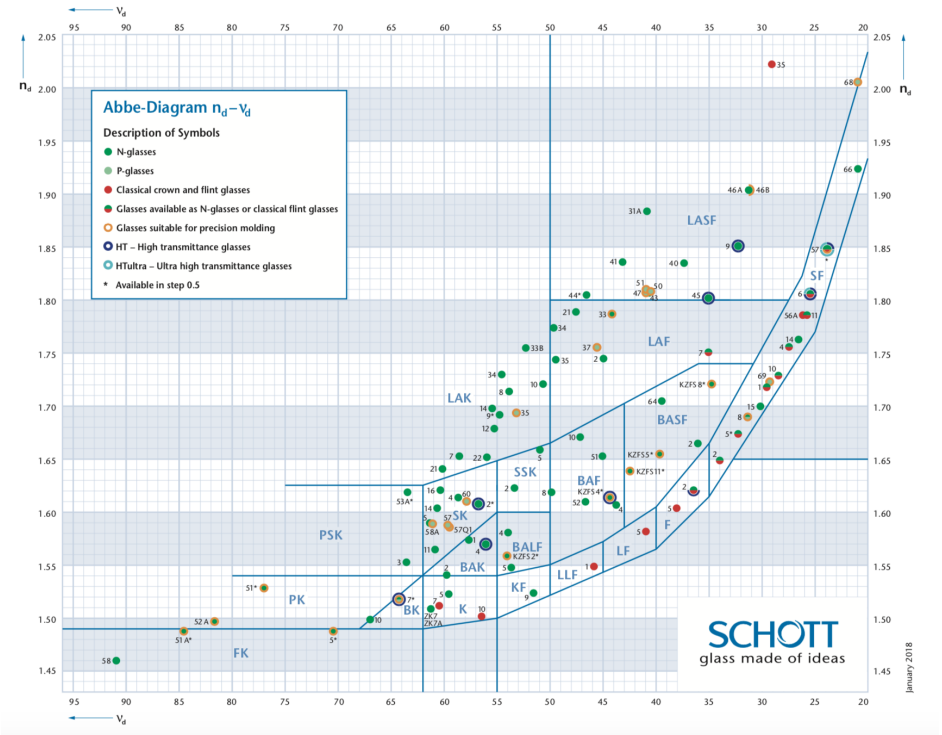

Figure 2-12: Abbe diagram of the manufacturer Schott

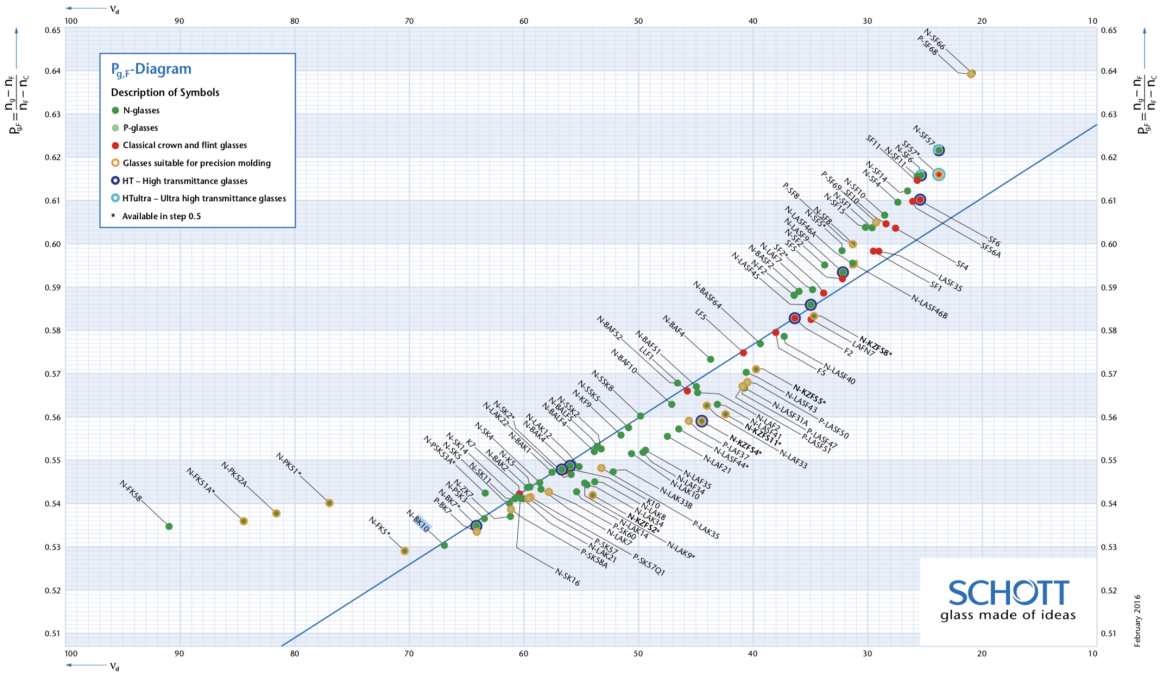

Figure 2-13: Partial Dispersion of the manufacturer Schott

2.3.1 Axial Color Aberration

The chromatic variation of the paraxial focus position is called axial color aberration. Therefore, it is a 1st-order chromatic aberration and can be described as the change of

intersection length $\Delta s'$ of an optical system with wavelength:

$$\Delta s' = s'_{blue} - s'_{red} \tag{2.42}$$

Here s'_{blue} and s'_{red} are the intersection lengths for the blue and the red wavelength. Assuming a single positive thin lens, focusing light coming from infinity, the intersection length s' equals to the focal length $f = 1/F$. Equation (2.22) in Section 2.1.4 gives its refractive power $F = (n_{green} - 1)(c_1 - c_2)$ with an refractive index of n_{green} for a central green wavelength. The power will be larger at short wavelengths and its focal point for red light will be farther from the lens than for the blue light. This is shown in 2-14.

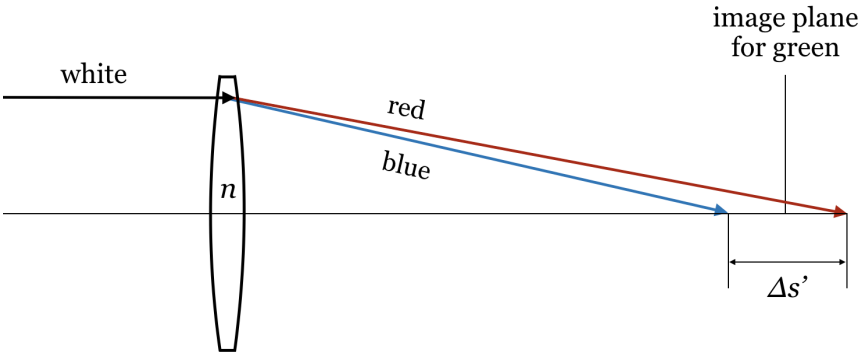

Figure 2-14: Axial color aberration $\Delta s'$ of a single positive thin lens

If the dispersion of its glass between the blue and the red wavelength is $\Delta n = n_{blue} - n_{red}$, the change in focal power $\Delta F = F_{blue} - F_{red}$ will be [KT02]:

$$\Delta F = \Delta n(c_1 - c_2) \tag{2.43}$$

$$= \frac{\Delta n}{n_{green} - 1} F$$

$$= \frac{F}{\nu} \tag{2.44}$$

This result emphasizes the definition of axial color and simultaneously shows how it can be corrected. If the same refractive power F is provided by two cemented lenses, axial color aberration between the blue and the red wavelength will vanish by combining a positive and negative lens in a way that both ΔF contributions will cancel out each other. The refractive power values of those both lenses, F_1 and F_2, that satisfy these two conditions for an achromatic doublet are presented in (2.45).

$$F_1 = \frac{F\nu_1}{\nu_1 - \nu_2} \qquad \text{and} \qquad F_2 = \frac{-F\nu_2}{\nu_1 - \nu_2} \tag{2.45}$$

This relation is called the achromatism condition. Figure 2-15 illustrates a typical achromatic case, plotting the intersection length over wavelength. If the blue and red foci coincide, then the focal length for the green wavelength will be shorter. This remaining effect is known as secondary spectrum and is commonly corrected by using anomalous glasses.

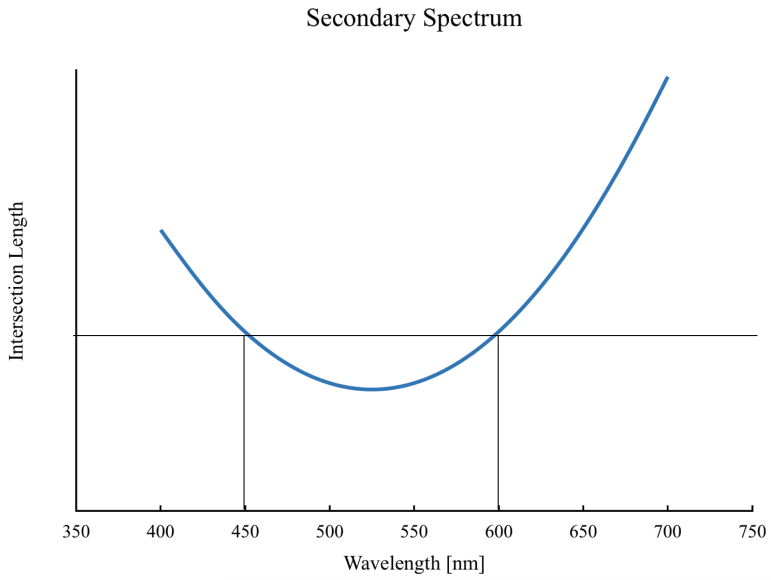

Figure 2-15: Achromatic case, where the blue and red foci show the same intersection length. The green focal length is shorter.

Furthermore, Welford [Wel86] showed how the Seidel approach, considering Conrady's so-called D-minus-d expression, can be applied to derive a surface contribution for axial color aberration. Following this, the sum over the system's surface coefficients for axial color can be written as:

$$C_1 = \sum niy\left(\frac{\Delta n'}{n'} - \frac{\Delta n}{n}\right) \tag{2.46}$$

Here, Δn and $\Delta n'$ describe the dispersion of the optical materials in front of the surface and behind the surface, respectively.
An equivalent thin lens contribution was obtained by:

$$C_1^L = \sum y^2 \Delta n_L (c_1 - c_2) \tag{2.47}$$

Here, the dispersion of the lens is Δn_L.

2.3.2 Lateral Color Aberration

The chromatic variation of the paraxial image size is called lateral color aberration. Hence, it is also a 1st-order chromatic aberration and can be described as the change

of the paraxial chief ray height $\Delta\bar{y}'$ at the image of an optical system with wavelength:

$$\Delta\bar{y}' = \bar{y}'_{blue} - \bar{y}'_{red} \tag{2.48}$$

Here, $\bar{y}'_{blue}$ and $\bar{y}'_{red}$ are the chief ray heights for the blue and the red wavelength at an image plane. Assuming again a single positive thin lens arranged in a front stop setup, the effect of the chromatic variation of refractive index causes a separation of the chief rays for the red and blue wavelength. Since the lens' power is larger at short wavelengths, the image size for the blue light is smaller than the red image size. Figure 2-16 illustrates this arrangement.

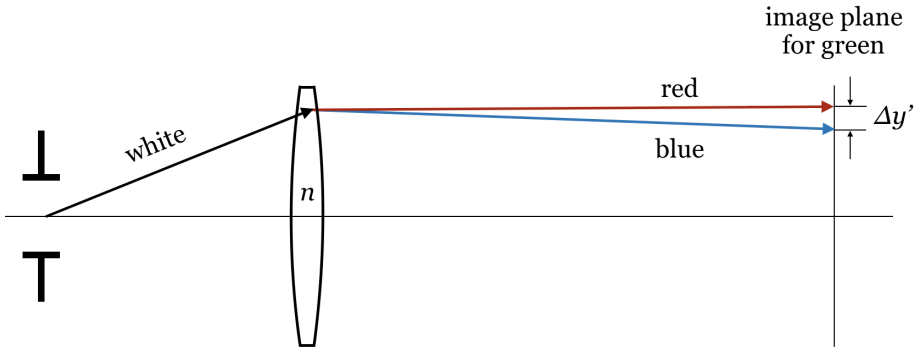

Figure 2-16: Lateral color $\Delta\bar{y}'$ of a single positive thin lens

If here the image plane is assumed to be at the focal plane for a central green wavelength, the image height of the red and blue chief ray can be calculated by the raytrace formula given in (2.14). Here, distance t has to be considered as $t = f = 1/F$. Therefore, the lateral color in this case reads:

$$\begin{aligned}
\Delta\bar{y}' &= \bar{y} + \frac{\bar{u}'_{blue}}{F} - \bar{y} - \frac{\bar{u}'_{red}}{F} \\
&= \frac{\bar{u} - \bar{y}F_{blue}}{F} - \frac{\bar{u} - \bar{y}F_{red}}{F} \\
&= -\frac{\bar{y}}{F}\Delta F \\
&= -\frac{\bar{y}}{\nu}
\end{aligned} \tag{2.49}$$

Again, the result of this simple example emphasizes the definition of lateral color. To correct this chromatic effect, Equation (2.49) tells that a second lens with an inverted chief ray height can correct the lateral color. Hence, since the way of light is invertible, a symmetrical setup of two identical lenses around the stop with the same object size as image size, will lead to an 1:1 imaging system with inverted chief ray heights and therefore with a completely corrected lateral color aberration.

A surface resolved contribution like the Seidel coefficients again was derived by Welford [Wel86], using a similar approach as for axial color. The result for the system's sum of lateral color surface contributions is given in Equation (2.50).

$$C_2 = \sum n\bar{i}y\left(\frac{\Delta n'}{n'} - \frac{\Delta n}{n}\right) \tag{2.50}$$

Here, again Δn and $\Delta n'$ describe the dispersion of the optical materials in front of the surface and behind the surface, respectively. An equivalent thin lens contribution was obtained by:

$$C_2^L = \sum y\bar{y}\Delta n_L(c_1 - c_2) \tag{2.51}$$

Here, the dispersion of the lens is Δn_L.

2.4 Design Process

During the lens design process, aberration theory and especially the concept of the Seidel coefficients are the main tools to control and to direct the optimization of an optical system. Considering the given degrees of freedom a lens design contains; like radii, air spaces, glass selection and stop position, the solution space becomes extremely wide and multi-dimensional [Smi04]. In most of the cases, there are different local minima, meeting a set of optical performance specifications as well as manufacturing and costs constraints. To find the several local solutions, a merit function is set up by the optical designer. Ensuring the final performance after passing the optical system, typically this merit function is based on ray intersection operands at the final image plane and on some 1st-order parameters, e.g. focal length, magnification or intersection length. An explicit control of certain 3rd-order or even higher-order aberrations is unusual to give meaningful measures of the final image quality. To evaluate the different solutions found by the optimizing algorithm, a deeper understanding about how and why the lens design works can be achieved by a systematic and continuous analysis of the different design states.

The best way to find out the inner workings of an optical systems is to understand why the present left aberrations arise and how they sum up surface by surface to its final amount at the image plane. This surface or lens resolved analysis is applied by the Seidel surface or lens contributions. Its main advantage is the identification of performance dominating surfaces or lenses referring to the five primary, 3rd-order aberrations, which are spherical aberration, coma, astigmatism, field curvature and distortion as well as to the chromatic aberrations. Knowing the single contributions of every lens within the optical system enables the designer to work with determined steps like decreasing

ray angles at dominating surfaces, split lenses at stressed positions or changing glasses of lenses with less or inverted chromatic contributions. Re-optimization after such determined system changes can push the design quickly to better or simpler states. Figure 2-17 shows an illustration of the seven Seidel contributions as bar plots. A photographic lens was chosen as an example lens design.

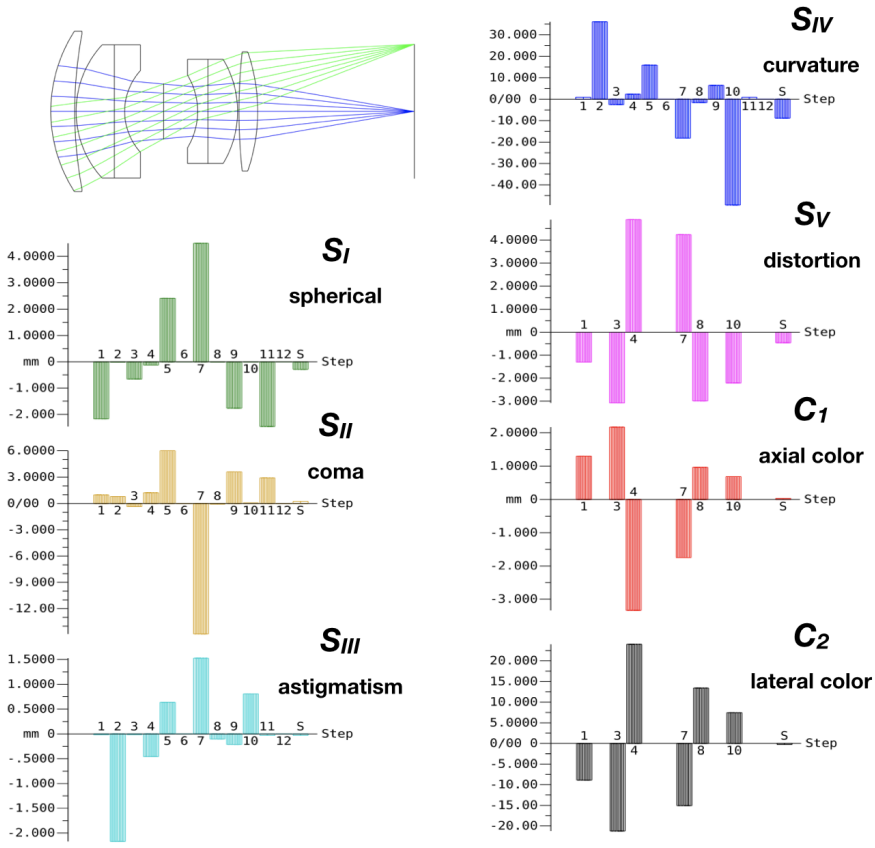

Figure 2-17: Bar plots of Seidel surface contribution for a given lens design.

The main goal for a good lens design is to find an correction state, where all of the seven Seidel contributions sum up to zero at the final image plane. If a lens design suffers from one dominant aberration, this kind of plot directly shows the designer, which kind of aberration has to be corrected and also where the greatest contributors can be found within the system. Additionally, the minimization of the absolute values of all single surface contributions for all aberrations is a second important property of a good lens design. Allowing large single contributions within the optical system would always lead to very sensitive and uncontrollable designs regarding tolerances and adjustment. Therefore, in questions of sensitivity a well-balanced optical system has to be found.

For color correction the discrete glass selection given by the available optical glasses, e.g. by Schott (2-12), plays a special role. Since therefore only discrete n, ν and P combinations can be chosen, the final glass selection still can not be solved by

a continuously working optimization algorithm, like a damped least squares (DLS) or orthogonal descent (OD) algorithm. Here, an experienced designer is supposed to find the best glass combination by carefully chosen incremental steps inside the Abbe diagram. The main contributors on color aberrations again can be found by the Seidel contributions. But in this case, not only the single surface but the whole lens contribution has to be considered, since a change of glass always influences the color effects of both surfaces of the lens.
Although the correction of the five 3rd-order aberrations and the two 1st-order chromatic aberration is a necessary condition to guarantee a good overall aberration correction, the influence of higher-order aberration can not be neglected in many cases. In contrast to the 3rd-order aberrations, which are completely independent of each other, 5th-order aberrations are characterized by additional aberration parts that are induced by prior generated aberrations of lower-order. This special differentiation between induced and intrinsic contributions allows the lens designer not only to analyze, if there are dominating 5th-order aberrations, but it also tells how well the intrinsic and induced parts are balanced. Thereby, large induced aberrations parts refer to either unbalanced large 3rd-order aberration somewhere inside the system or in some special cases large induced contributions even helps to correct the remaining intrinsic parts. This is often used for higher-order color aberrations without direct intention of the designer. An analytical tool like the Seidel contributions does not exist so far. For higher-order monochromatic aberrations some special design features like aspherical surfaces can help to correct them, without increasing the amount of elements and the total track length. A Seidel equivalent analysis tool for this was found by Buchdahl [Buc54] and Rimmer [Rim63]. 5th-order surface contributions theory in terms of wavefront aberrations was completed by Hoffman [Hof93] and Sasian [Sas10], which also can be found in some of today's lens design software.

2.5 State of the Induced Aberration Problem

The 1st-order theory of the color aberrations and the 3rd-order theory of the monochromatic aberrations are based on a linearized perturbation theory [Gro+07]. Therefore, a clear surface contribution formula can be derived for all of those aberrations and the total amount of the system aberrations can be expressed by the sum over all contributions. This was shown in Section 2.2.3 and 2.3. However, in realita, ray data deviates from the paraxial ones during its path in the optical system. The results are small, but present differences in ray heights (Δy) and ray angles (Δu) at the refractive surfaces compared to the paraxial ray data. Induced aberrations are caused by these differences. Therefore, they only occur at higher order aberrations [Ber+15].
As today, a multitude of the lens designs are specified to work in broad wavelength

ranges, providing large field of views and large apertures within very compact lens dimensions, higher-order aberrations are often the factor that at the end limits the resolution a lens can give [KT02]. Hence, although the correction of the five 3rd-order aberrations and the two 1st-order chromatic aberrations is a meaningful condition to guarantee a good overall aberration correction, the influence of higher-order aberrations and therefore also of induced aberrations can not be neglected in most cases.

2.5.1 Induced Monochromatic Aberration

When considering these higher orders of aberrations, the linearity of the 3rd-order monochromatic theory is no longer valid and mixing effects of higher perturbation terms occur. In consequence, at every optical surface, two types of aberration characteristics can be distinguished [Ber+15]:

1. Intrinsic aberration contributions, that are generated directly at the surface itself. Here it is assumed, that the incoming ray is a paraxial aberration free ray.

2. Induced aberration contributions, which occur, because of the prior summed up aberrations affecting the ray, hitting the surface.

This understanding of monochromatic intrinsic and induced aberration parts is shown in Figure 2-18 for the simple example of a single lens.

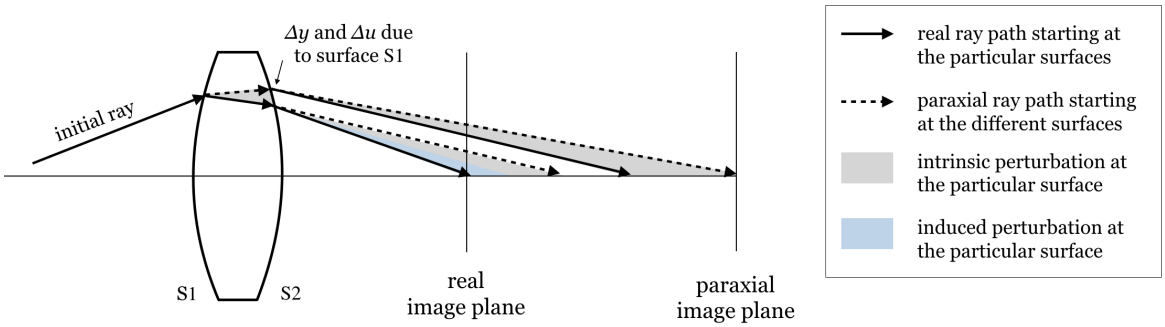

Figure 2-18: Monochromatic intrinsic and induced ray aberration parts

Assuming the same ray based approach like Seidel, Buchdahl [Buc54] and Rimmer [Rim63] derived the 5th- and 7th-order surface contributions of the monochromatic aberrations in 1963. Hoffman [Hof93] and Sasian [Sas10] completed 5th-order surface contributions theory in terms of wavefront aberration in 1993 and 2010. Clearly, the analytic expressions for these higher-order surface contributions are no longer as simple as the originally Seidel surface contributions. However, they are well described today, including the differentiation of intrinsic and induced aberration parts.

2.5.2 Induced Axial and Lateral Color

In case of color aberrations, different orders do not refer to their dependency on the ray field and pupil coordinates, only. They can also be considered with respect to their dependency of dispersion. Hence, this approach extends the paraxial theory to second and higher-order effects regarding the paraxial ray dependency on dispersion. Thus, the primary axial and lateral color aberration description, introduced in section 2.3, linearly depend on the dispersive behavior of the glasses. Nevertheless, in 1987 Wynne [Wyn77] [Wyn78] has already shown analytically that for every optical systems, axial color and lateral color are additionally influenced by non-linear contributions, in which induced aberrations are part of these nonlinear effects. He found that induced aberrations can have a significant impact on the correction of secondary axial color and he identified a way to determine the contribution of induced axial and lateral color by tracing two paraxial rays with different wavelengths. Also in present research today, for single selected design examples and certain special cases Roger[Rog13b] [Rog13a] and McCarthy [Mcc55] obtained analytical expressions for secondary axial color including induced aberration parts. Actually, they showed, that there are certain types of optical systems that exclusively take advantage of induced aberration effects to obtain a chromatically corrected image. In addition to those special cases, a more general description of the 2nd-order axial color distribution of thin lenses in air was under present investigation by Nobis [Nob14] [Nob15]. He derived an axial color contribution including higher orders by considering ray based parameters like ray angles, ray heights and the refractive power of the thin lens. Comparing these different approaches, there is one particular benefit of Nobis' descriptive, analytical formula for longitudinal lens contributions to axial color up to 2nd-order [Nob15]. In contrast to Wynne [Wyn78], his calculation requires ray data of the reference wavelength, only. Hence, a second ray of the other wavelength is not needed to be traced. This was similar to the Seidel surface contribution approach for primary color aberration and resulted in the following equation for the 2nd-order axial color contribution CHL_{2nd} of a thin lens in air:

$$CHL^{L}_{2nd} = \frac{F}{uu'} CHL^{2}_{1st} + \frac{2y\Delta F}{u'} CHL_{1st} + \frac{y^3 \Delta F^2}{u'} \tag{2.52}$$

Here, a prior 1st-order axial color aberration CHL_{1st}, summed up lens by lens in the previous optical system, was assumed. Reviewing the general definition and differentiation of intrinsic and induced aberration parts, described before for monochromatic aberrations, clearly, two terms of induced character are included here. These two terms are the first and second one, since they are depending on the prior summed up 1st-order axial color aberration. However, a comparable and equivalent expression for a surface contribution on axial and also on lateral color up to 2nd-order is missing literature.

2.5.3 Induced Chromatic Variation of 3rd-order Aberrations

Concerning the chromatic variation of 3rd-order aberrations, in particular e.g. for spherochromatism, different orders refer to the dependency of 3rd-order spherical aberration on 1st-order color aberrations. In this case, there were useful results due to Slyusarev [Sli84], Conrady [Con14] and Hopkins [Hop50]. However, Slyusarev [Sli84] considered only the special case of an object at infinity and also didn't include the 1st-order derivatives of the ray based parameters with respect to the refractive index to his approach. Hence, a general expression for spherochromatism was missing here. Furthermore, Conrady [Con14] permits the calculation of all chromatic aberrations, including spherochromatism, by tracing an exact ray at a single wavelength. But, the terms which were ignored during his derivation can become significantly high, in case that one part of a lens shows a large amount of color aberration, which is corrected in another widely separated part of the lens [KT02]. In other words, induced effects are not considered within Conrady's approach. Since Hopkin's solution in [Hop50] is also based on Conrady's idea, his results for spherochromatism suffer from the same disadvantages. To emphasize, in 1986 also Welford [Wel86] already mentioned the simple idea for specifying all of the chromatic variations of aberrations only by differentiating the Seidel contributions with respect to refractive index. But he also called the expected results to be cumbersome and too unwieldy for general use.
Hence, in case of the chromatic variation of 3rd-order aberrations, there is a great analytical gap concerning Seidel equivalent surface resolved expressions for spherochromatism, colored coma, colored astigmatism, colored field curvature and for colored distortion. Furthermore, following the basic idea of induced aberrations, these missing expressions are expected to also include induced aberration parts caused by 1st-order color aberrations.

3 Extended Induced Color Aberration Theory

3.1 The Concept of Induced Color Aberrations

In analogous manner to the monochromatic aberrations, in general induced aberrations are higher-order aberrations. They are caused by ray perturbations of lower order, picked up surface by surface in the preceding optical system. This monochromatic concept can be transferred to the color aberrations.
Please note, the following chapter includes a revised version of [BNG17] and [Ber+18], which have been published in advance in 2017 and 2018.

3.1.1 Characteristics

Following the monochromatic approach, induced color aberrations are higher-order aberrations, caused by small ray perturbations of lower-order color aberrations. These lower-order color aberrations sum up surface by surface on the light's way through the optical system. Therefore, a surface or lens resolved approach is the key method for characterizing and understanding them.
Regarding a single surface of an optical system, a polychromatic ray trace results in small ray deviations for the different wavelengths at the investigated surface. The reason for this is the wavelength depending law of refraction, $n \sin i = n' \sin i'$. Since the refractive index n varies with different wavelengths, every refractive surface in front of the investigated surface leads to small differences in ray angles Δu and therefore, after transferring to the next surface, also to small differences in ray heights Δy. The raytrace equations (2.12) and (2.14) of Section 2.1.3 illustrates these relations. To that effect, the prior summed up color aberrations, causing the induced aberration parts, appear as ray perturbations in ray angles and ray heights for the different wavelengths at the investigates surface of the optical system.
Following those considerations, the total amount of a surface contribution on color aberrations can always be divided into two parts:

1. the intrinsic aberration part, which is generated by the dispersion Δn of the surface itself, assuming a perfect, color aberration free incoming ray.

2. the induced aberration part, which is only generated, if a prior color aberrated ray hits the surface.

In other words, the intrinsic aberration part ignores all dispersive effects before and the induced aberration part is only present if a certain separation of the different wavelengths in ray angles and ray heights occurred before. Please note, all of these definitions are also true for a lens resolved analysis, assuming thin lenses. Hence, Figure 3-1 illustrates these considerations by a simple lens design and its differentiation of the total axial color aberration into the intrinsic and induced parts.

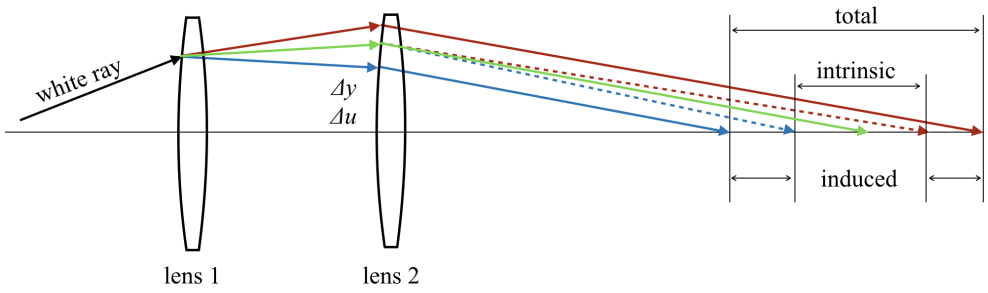

Figure 3-1: Intrinsic and induced color aberration parts

3.1.2 Aberration Classification

In case of induced color aberrations, the definition of different aberration orders do not refer to the ray dependency on field and pupil coordinates only, this approach extends the aberration theory to higher-order effects regarding the ray dependency on dispersion.

Following this, originating from the paraxial parameters of the intersection length s and the image height y, 1st-order terms result in the well-known Seidel contributions of axial color (2.50) and lateral color (2.46) shown in Section 2.3, since they are linearly depending on dispersion. Consequently, further differentiation with respect to dispersion then leads to 2nd- or higher-order terms, respectively. In contrast to the 1st-order, these terms also comprise the interaction of linear and higher-order terms. Therefore, dispersive effects between different elements of the optical system are considered. In consequence, they include induced color effects by definition, caused by lower 1st-order color aberrations, picked up in the preceding optical system.
Increasing as a next step the order of pupil and field dependency, the paraxial region is left and the primary monochromatic aberrations are obtained. Clearly, these primary

monochromatic aberrations as well as all higher-order monochromatic aberrations are of zero-order in color, since they do not depend on dispersive effects. However, by differentiation with respect to the wavelength, the chromatic variations of the monochromatic aberrations are found. They describe the interaction of monochromatic aberrations with dispersive effects of the optical systems. Therefore, in case of chromatic varying monochromatic aberrations, induced aberration terms already occur, if higher-order monochromatic aberrations depend on lower-order color aberrations, picked up in the preceding optical system.

(a)

Seidel
Buchdahl
induced

			Δn expansion ⟶			
			monochr.	1st order	2nd order	3rd order
			Δn^0	Δn^1	Δn^2	Δn^3
aperture ↓	paraxial	r^0	s	C_1	C_1^{2nd}	C_1^{3rd}
	primary	r^2	S_I	cS_I	cS_I^{2nd}	cS_I^{3rd}
	5th order	r^4	B5	cB5	$cB5^{2nd}$	$cB5^{3rd}$
	7th order	r^6	B7	cB7	$cB7^{2nd}$	$cB7^{3rd}$

(b)

Seidel
Buchdahl
induced

			Δn expansion ⟶			
			monochr.	1st order	2nd order	3rd order
			Δn^0	Δn^1	Δn^2	Δn^3
field ↓	paraxial	y	y	C_2	C_2^{2nd}	C_2^{3rd}
	primary	y^3	S_V	cS_V	cS_V^{2nd}	cS_V^{3rd}
	5th order	y^5	E5	cE5	$cE5^{2nd}$	$cE5^{3rd}$
	7th order	y^7	E7	cE7	$cE7^{2nd}$	$cE7^{3rd}$

Figure 3-2: Classification of different color aberration orders exemplary shown, starting at (a) paraxial intersection lengths s and (b) image height y. The green and yellow colored quantities mark the well-known Seidel and Buchdahl coefficients, respectively. The blue framed quantities include induced color aberrations.

Figure 3-2 (a) and (b) illustrate exemplary these classifications, starting at the paraxial parameters of the intersection lengths s and the image height y. The monochromatic aberration denotations are based on Seidel's [KT02] and Buchdahl's definitions [Buc54]. The prefix "c" indicates the chromatic variation of the individual quantity. Please note, all of the blue framed quantities consist of an intrinsic as well as an induced aberration part.

3.1.3 Overview of new Results in this Chapter

The Sections 2.5.2 and 2.5.3 already gave information about the current state of the induced color aberration problem. There were noteworthy contributions by Nobis

[Nob15], Wynne [Wyn78], Slyusarev [Sli84] and Conrady [Con14]. The overview presented in Figure 3-3 summarizes this state of the art (grey colored) regarding surface or lens contribution formulas, differentiating between two facts, firstly, if there are existing formulas describing the single quantity and secondly if those derivations completely include all induced terms. In comparison to the state of the art, additionally also the new derived quantities and their denotations of this Chapter (blue colored) are added to Figure 3-3. As can clearly be seen, the obvious analytical gaps as well as the missing derivations including a complete differentiation of intrinsic and induced color effects are filled. Please note, the thin lens formula for axial color by Nobis [Nob15] was derived, considering the same analytical approach as in this thesis. Hence, his thin lens contribution formula for 2nd-order axial color is kept within this overview and has not to be improved.

✓ *including all induced terms* x *without induced terms*	**State of the Art Coefficients**						**New Coefficients**					
	Surface		**Thin Lens**		**Thick Lens**		**Surface**		**Thin Lens**		**Thick Lens**	
2nd order axial color	Wynne	x	Nobis	✓			AXC_{2nd}^{S}	✓	Nobis	✓	AXC_{2nd}^{tL}	✓
2nd order lateral color	Wynne	x					LAC_{2nd}^{S}	✓	LAC_{2nd}^{L}	✓	LAC_{2nd}^{tL}	✓
Sphero-chromatism			Slyusarev	x			G^{S}	✓	G^{L}	✓		
chrom. var. Coma	Conrady	x					cS_{II}	✓				
chrom. var. Astigmatism	Conrady	x					cS_{III}	✓				
chrom. var. Field Curv.	Conrady	x					cS_{IV}	✓				
chrom. var. Distortion	Conrady	x					cS_{V}	✓				

Figure 3-3: Overview of the current state of the induced color aberration problem and the new derived quantities within this thesis. Please note, Since Wynne identified a way to determine the contribution of induced axial and lateral color by tracing two paraxial rays with different wavelengths, his induced terms are not wrong, but can be simplified within this new approach.

3.2 Induced Axial Color

3.2.1 Surface Contribution of Intrinsic and Induced Axial Color

Following the lens-resolved approach of [Nob15], general relations and parameters defining axial color conditions at an arbitrary surface S in an optical system are given in Figure 3-4. Considering a single refractive surface S with a curvature c hit by a paraxial marginal ray of the reference wavelength $\lambda = \lambda_1$, the ray height at the surface is

y, the ray angle before the surface is u, and the ray angle after the surface is u'. The materials before and after the surface are characterized by their individual refractive indices n and n' , respectively.

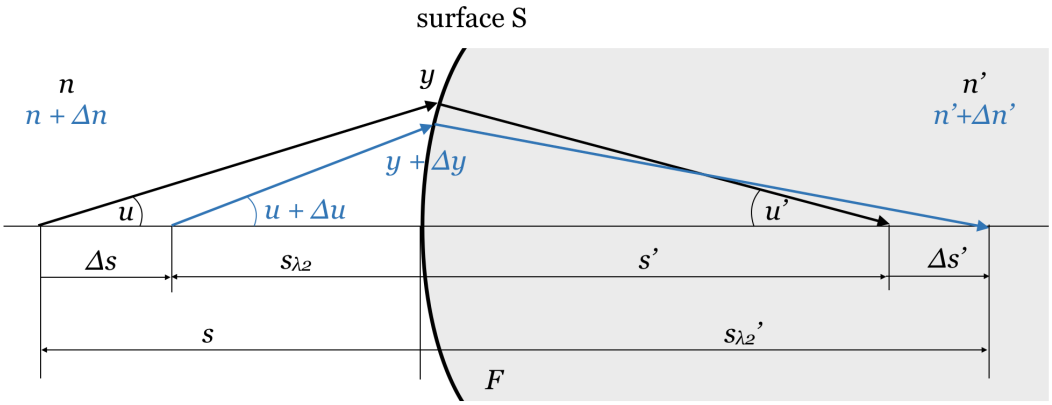

Figure 3-4: Refraction of two paraxial marginal rays with different wavelengths (black and blue line) at an arbitrary surface S

The intersection length s between the refractive surface and the intermediate image before, which is assumed to lie on a finite distance, is the result of

$$s(y,u) = -\frac{y}{u} \tag{3.1}$$

To define the intersection lengths s' after refraction, the definition for the refractive power F of a single surface (2.9) and the paraxial ray trace formula (2.12) have to be considered. Consequently, the intersection lengths s' after refraction results in:

$$\begin{aligned} s'(y,u,n,n') &= -\frac{y}{u'} \\ &= -\frac{yn'}{nu - y(n'-n)c} \end{aligned} \tag{3.2}$$

Considering a second wavelength $\lambda_2 = \lambda_1 + \Delta\lambda$, the corresponding ray height y_2 at the surface is $y_2 = y + \Delta y$ and the ray angles before and after the surface are $u_2 = u + \Delta u$ and $u'_2 = u' + \Delta u'$. Similarly, the refractive indices show a wavelength dependent, dispersive behavior with $n_2 = n + \Delta n$ and $n'_2 = n' + \Delta n'$. Reviewing now the definition in Section 2.3.1, axial color can be described as the change of intersection length of an optical system with wavelength. Hence, the axial color aberrations before and after

the surface, Δs and $\Delta s'$, within a wavelength range fromλ_1 to λ_2 are given by

$$\begin{aligned}\Delta s &= s_{\lambda 2} - s \\ &= s(y + \Delta y, u + \Delta u) - s(y, u)\end{aligned} \tag{3.3}$$

$$\begin{aligned}\Delta s' &= s'_{\lambda 2} - s' \\ &= s'(y + \Delta y, u + \Delta u, n + \Delta n, n' + \Delta n') - s'(y, u, n, n')\end{aligned} \tag{3.4}$$

If the differences $\Delta y, \Delta u, \Delta n$ and $\Delta n'$ are small, a Taylor series expansion can be applied. Since all of these differences occurred because of dispersion within the optical system, an expansion up to second order refer to the 2nd-order color aberration classification of Section 3.1.2. Hence, the following expressions for the intersection lengths $s_{\lambda 2}$ and $s'_{\lambda 2}$ are obtained:

$$s_{\lambda 2} = s(y, u) + \frac{\partial s}{\partial y}\Delta y + \frac{\partial s}{\partial u}\Delta u + \frac{1}{2}\frac{\partial^2 s}{\partial y^2}\Delta y^2 + \frac{\partial^2 s}{\partial y \partial u}\Delta y \Delta u + \frac{1}{2}\frac{\partial^2 s}{\partial u^2}\Delta u^2 \tag{3.5}$$

$$\begin{aligned}s'_{\lambda 2} = s'(y, u, n, n') &+ \frac{\partial s'}{\partial y}\Delta y + \frac{\partial s'}{\partial u}\Delta u + \frac{\partial s'}{\partial n}\Delta n + \frac{\partial s'}{\partial n'}\Delta n' \\ &+ \frac{1}{2}\frac{\partial^2 s'}{\partial y^2}\Delta y^2 + \frac{\partial^2 s'}{\partial y \partial u}\Delta y \Delta u + \frac{\partial^2 s'}{\partial y \partial n}\Delta y \Delta n + \frac{\partial^2 s'}{\partial y \partial n'}\Delta y \Delta n' \\ &+ \frac{1}{2}\frac{\partial^2 s'}{\partial u^2}\Delta u^2 + \frac{\partial^2 s'}{\partial u \partial n}\Delta u \Delta n + \frac{\partial^2 s'}{\partial u \partial n'}\Delta u \Delta n' + \frac{1}{2}\frac{\partial^2 s'}{\partial n^2}\Delta n^2 \\ &+ \frac{\partial^2 s'}{\partial n \partial n'}\Delta n \Delta n' + \frac{1}{2}\frac{\partial^2 s'}{\partial n'^2}\Delta n'^2\end{aligned} \tag{3.6}$$

Inserting this into Equation (3.3) and (3.4), the axial color before and after the refractive surface results in:

$$\Delta s = \frac{\partial s}{\partial y}\Delta y + \frac{\partial s}{\partial u}\Delta u + \frac{1}{2}\frac{\partial^2 s}{\partial y^2}\Delta y^2 + \frac{\partial^2 s}{\partial y \partial u}\Delta y \Delta u + \frac{1}{2}\frac{\partial^2 s}{\partial u^2}\Delta u^2 \tag{3.7}$$

$$\begin{aligned}\Delta s' = &\frac{\partial s'}{\partial y}\Delta y + \frac{\partial s'}{\partial u}\Delta u + \frac{\partial s'}{\partial n}\Delta n + \frac{\partial s'}{\partial n'}\Delta n' \\ &+ \frac{1}{2}\frac{\partial^2 s'}{\partial y^2}\Delta y^2 + \frac{\partial^2 s'}{\partial y \partial u}\Delta y \Delta u + \frac{\partial^2 s'}{\partial y \partial n}\Delta y \Delta n + \frac{\partial^2 s'}{\partial y \partial n'}\Delta y \Delta n' \\ &+ \frac{1}{2}\frac{\partial^2 s'}{\partial u^2}\Delta u^2 + \frac{\partial^2 s'}{\partial u \partial n}\Delta u \Delta n + \frac{\partial^2 s'}{\partial u \partial n'}\Delta u \Delta n' + \frac{1}{2}\frac{\partial^2 s'}{\partial n^2}\Delta n^2 \\ &+ \frac{\partial^2 s'}{\partial n \partial n'}\Delta n \Delta n' + \frac{1}{2}\frac{\partial^2 s'}{\partial n'^2}\Delta n'^2\end{aligned} \tag{3.8}$$

1st-order terms At first only the derivatives of the linear terms, e.g. the 1st-order terms, are considered. When inserting the derivatives for Δs and $\Delta s'$, attached in Appendix, the following equations are obtained:

$$\Delta s_{1st} = -\frac{1}{u}\Delta y + \frac{y}{u^2}\Delta u \tag{3.9}$$

$$\Delta s'_{1st} = -\frac{nu}{n'u'^2}\Delta y + \frac{ny}{n'u'^2}\Delta u + \frac{yi}{n'u'^2}\Delta n - \frac{nyi}{n'^2u'^2}\Delta n' \tag{3.10}$$

Here, i is the paraxial incident angle of the marginal ray with $i = u + yc$ (see Section 2.1.2). To specify the axial color contribution AXC^S_{1st} of the refractive surface, the difference of the axial color aberration at the intermediate image after the surface $\Delta s'_{1st}$ and the axial color aberration at the intermediate image in front of the surface Δs_{1st} has to be considered. Since these axial color aberrations are longitudinal aberrations at a specific intermediate image, the axial magnification $\alpha = nu^2/n'u'^2$ between the considered intermediate image and the final image needs to be taken into account as a longitudinal scaling factor (see Section 2.4). Note that, in the case of intermediate images of surfaces, the axial magnification not only depends on the marginal ray angles but also on the refractive indices of the individual materials.
Following these considerations, the 1st-order axial color surface contribution AXC^S_{1st} is given by

$$AXC^S_{1st} = \Delta s'_{1st}(-n'u'^2) - \Delta s_{1st}(-nu^2) \tag{3.11}$$

Inserting and simplifying Equation (3.9) and (3.10) leads to the following relation:

$$\begin{aligned} AXC^S_{1st} = &\left(-\frac{nu}{n'u'^2}\Delta y + \frac{ny}{n'u'^2}\Delta u + \frac{yi}{n'u'^2}\Delta n - \frac{nyi}{n'^2u'^2}\Delta n'\right)(-n'u'^2) \\ &-\left(-\frac{1}{u}\Delta y + \frac{y}{u^2}\Delta u\right)(-nu^2) \end{aligned} \tag{3.12}$$

$$AXC^S_{1st} = niy\left(\frac{\Delta n'}{n'} - \frac{\Delta n}{n}\right) \tag{3.13}$$

This result agrees with the common Seidel theory of primary axial color, shown in Section 2.3.1.

2nd-order terms In analogous manner to the 1st-order terms, the nonlinear terms are obtained. Consequently, the 2nd-order axial color effects of an arbitrary surface equals to:

$$AXC^S_{2nd} = \Delta s'_{2nd}(-n'u'^2) - \Delta s_{2nd}(-nu^2) \tag{3.14}$$

Here, the following relations for the 2nd-order terms Δs_{2nd} and $\Delta s'_{2nd}$ are applied.

$$\Delta s_{2nd} = \frac{1}{2}\frac{\partial^2 s}{\partial y^2}\Delta y^2 + \frac{\partial^2 s}{\partial y \partial u}\Delta y \Delta u + \frac{1}{2}\frac{\partial^2 s}{\partial u^2}\Delta u^2 \tag{3.15}$$

$$\begin{aligned}\Delta s'_{2nd} = {} & \frac{1}{2}\frac{\partial^2 s'}{\partial y^2}\Delta y^2 + \frac{\partial^2 s'}{\partial y \partial u}\Delta y \Delta u + \frac{\partial^2 s'}{\partial y \partial n}\Delta y \Delta n + \frac{\partial^2 s'}{\partial y \partial n'}\Delta y \Delta n' \\ & + \frac{1}{2}\frac{\partial^2 s'}{\partial u^2}\Delta u^2 + \frac{\partial^2 s'}{\partial u \partial n}\Delta u \Delta n + \frac{\partial^2 s'}{\partial u \partial n'}\Delta u \Delta n' + \frac{1}{2}\frac{\partial^2 s'}{\partial n^2}\Delta n^2 \\ & + \frac{\partial^2 s'}{\partial n \partial n'}\Delta n \Delta n' + \frac{1}{2}\frac{\partial^2 s'}{\partial n'^2}\Delta n'^2\end{aligned} \tag{3.16}$$

Inserting the 2nd-order derivatives, attached at the appendix, a slightly more complex expression compared to the thin lens approach of [Nob14] is achieved. This is caused by the additional terms depending on Δn and $\Delta n'$. Following the idea of induced aberrations, illustrated in Section 3.1, some of the 2nd-order terms have to depend on the cumulative preexisting lower-order aberrations in the system before. Hence, in the case of a single refractive surface, there have to be some of the 2nd-order terms, depending on the 1st-order axial color aberration in front of the surface, which was already described by Equation (3.9). Multiplied by the magnification factor, Equation (3.17) shows the expression AXC_{1st} characterizing the preexisting 1st-order axial color aberration in front of the surface.

$$AXC_{1st} = \Delta s_{1st}(-nu^2) = \; nu\Delta y - ny\Delta u \tag{3.17}$$

Analyzing now the 2nd-order terms for a dependence on this expression, the 2nd-order axial color surface contribution is obtained after simplifying with common relations for ray tracing (Section 2.1.3):

$$\begin{aligned}AXC^S_{2nd} = {} & \frac{F}{nn'uu'}AXC^2_{1st} + \frac{u' + 2yc}{u'}\left(\frac{\Delta n'}{n'} - \frac{\Delta n}{n}\right)AXC_{1st} + \frac{n^2 i^2 y}{n'u'}\left(\frac{\Delta n'}{n'} - \frac{\Delta n}{n}\right)^2 \\ & - niy\left(\frac{\Delta n'^2}{n'^2} - \frac{\Delta n' \Delta n}{n'n}\right)\end{aligned} \tag{3.18}$$

This equation is one of the main results of this thesis.

3.2.2 Lens Contribution of Intrinsic and Induced Axial Color

Since induced aberrations are caused by the small differences in ray heights and ray angles due to the prior lower-order aberrations, especially the influence of the distance between two lens surfaces will be of greater interest. Furthermore, a derivation of a

2nd-order axial color thick lens contribution will be more instructive for an optical designer than a surface resolved contribution, as color correction is usually connected to changing glasses of lenses, not surfaces.

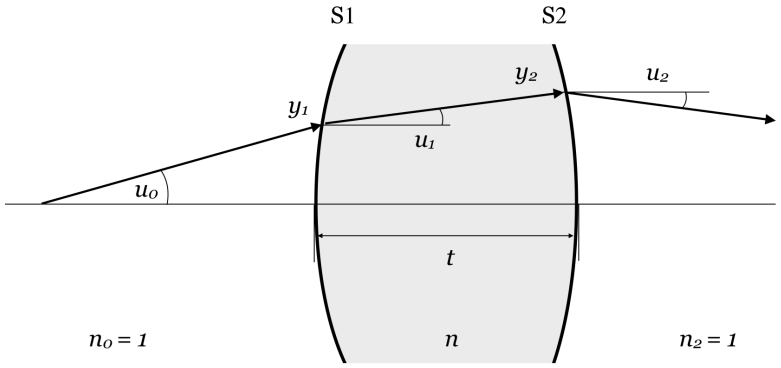

Figure 3-5: Refraction of the marginal ray at a thick lens. The marginal ray heights and angles are y_1 and u_1 as well as y_2 and u_2 at surface S1 and surface S2, respectively.

To find an analytical description for a lens in air with a thickness t and a refractive index of n, Equation (3.18) can be considered for the two surfaces of a thick lens applying a paraxial ray trace for the ray propagation within this lens. Figure 3-5 illustrates the relevant quantities for the thick lens approach. The preexisting 1st-order axial color for surface S1 is again AXC_{1st} and according to the Seidel surface coefficient for axial color C_1 (Section 2.3.1, Equation (2.46)) shows the preexisting axial color for surface S2 is:

$$AXC'_{1st} = AXC_{1st} + y_1 i_1 \frac{\Delta n}{n} \tag{3.19}$$

Considering now a certain thickness t for an individual lens in an optical system the 2nd-order axial color thick lens contribution AXC^{tL}_{2nd} can be calculated by the sum of both surface contributions.

$$AXC^{tL}_{2nd} = AXC^{S1}_{2nd} + AXC^{S2}_{2nd} \tag{3.20}$$

with a surface contribution AXC^{S1}_{2nd} of surface S1:

$$AXC^{S1}_{2nd} = \frac{F_1}{nu_0u_1} AXC^2_{1st} + \frac{u_1 + 2y_1c_1}{u_1} \frac{\Delta n}{n} AXC_{1st} + \frac{i_1^2 y_1}{nu_1} \left(\frac{\Delta n}{n}\right)^2 - i_1 y_1 \left(\frac{\Delta n^2}{n^2}\right) \tag{3.21}$$

and a second surface contribution AXC_{2nd}^{S2} of surface S2:

$$AXC_{2nd}^{S2} = \frac{F_2}{nu_1u_2}AXC_{1st}'^2 - \frac{u_2 + 2y_2c_2}{u_2}\frac{\Delta n}{n}AXC_{1st}' + \frac{n^2i_2^2y_2}{nu_2}\left(\frac{\Delta n}{n}\right)^2 \tag{3.22}$$

The indices 0, 1 and 2 are used for ray data according to Figure 3-5. Here, the lens' thickness t is represented in Equation (3.22) by the raytrace parameters $y_2(t), i_2(y_2)$ and $u_2(y_2)$. Inserting now Equations (3.21) and (3.22) into Equation (3.20) and rearranging as well as simplifying the terms, the following thick lens formula is achieved:

$$\begin{aligned} AXC_{2nd}^{tL} = \quad & \frac{F_L}{u_0u_2}AXC_{1st}^2 + \frac{2y_1(c_1 - c_2)\Delta n}{u_2}AXC_{1st} + \frac{y_1^3(c_1 - c_2)^2}{u_2}\Delta n \\ & + t\frac{(n-1)c_1c_2}{nu_0u_2}AXC_{1st}^2 - t\frac{\alpha_1\Delta n}{nu_2}AXC_{1st} + t\frac{\alpha_2}{nu_2}\Delta n^2 \end{aligned} \tag{3.23}$$

The coefficients α_1 and $\alpha_2(t)$ can be found in the appendix. Comparing this with Nobis' thin lens formula (2.52) shown in Section 2.5.2 and considering the relation $\Delta F_L = \Delta n(c_1 - c_2)$, a consistent relation to his results is obtained.

$$AXC_{2nd}^{tL} = \quad CHL_{2nd}^{L} + t\frac{(n-1)c_1c_2}{nu_0u_2}AXC_{1st}^2 - t\frac{a_1\Delta n}{nu_2}AXC_{1st} + t\frac{a_2(t)}{nu_2}\Delta n^2 \tag{3.24}$$

3.2.3 Discussion

A Taylor expansion of the surface resolved axial color considering derivatives up to 2nd-order results in Equation (3.18).

Induced and Intrinsic Terms There are four terms. The first two terms depend on the preexisting 1st-order axial color aberration in front of the surface. Hence, they are of induced character, since they vanish, if there is no preexisting axial color. The last two terms are pure dispersion depending terms. They show only dependencies on the chromatic variation of the refractive indices before and after the surface Δn and $\Delta n'$ without any additional dispersion-depending quantities. Hence, these terms are intrinsic terms of 2nd-order.
In detail, the first 2nd- order term $\frac{F}{nn'uu'}AXC_{1st}^2$ shows a quadratic dependence on the preexisting cumulative 1st-order axial color AXC_{1st} without any additional wavelength depending quantities. Hence, this term describes an induced 2nd-order contribution of an optical surface, which is not required to be made of a dispersive material. For that case, even a mirror with a specific refractive power F can show this induced axial color 2nd-order effect, if a relevant amount of prior summed up axial color aberration

is present.
The second term $\frac{u'+2yc}{u'}\left(\frac{\Delta n'}{n'} - \frac{\Delta n}{n}\right)AXC_{1st}$ of Equation (3.18) is characterized by its linear dependency on the preexisting axial color. This term is also an induced one, as it describes the interaction between the summed up 1st-order axial color with a dispersive refracting surface. For a mirror, this contribution vanishes.
In contrast to the first two terms, the third term $\frac{n^2 i^2 y}{n'u'}\left(\frac{\Delta n'}{n'} - \frac{\Delta n}{n}\right)^2$ is of intrinsic character, as it is caused by pure dispersive effects only. Hence, if there is no preexisting axial color, this 2nd-order term will still be non- zero, unless the surface is positioned at an intermediate image, where y equals to zero or in the case of normal incidence.
The character of the fourth term $niy\left(\frac{\Delta n'^2}{n'^2} - \frac{\Delta n' \Delta n}{n'n}\right)$ is similar to the third one. All of the considerations for the third term are also true for this last one. Additionally, it shows a dependence on the individual surface type. If it is a back surface in air, this term vanishes as $\Delta n'$ for air is zero. But for a cemented surface or front surface in air, the fourth term introduces a certain 2nd -order contribution to axial color.

Required Parameters Beneficial, due to the Seidel sum definition (2.46), the 1st-order axial color AXC_{1st} before an individual surface S_j inside an optical system can easily be calculated by summing up all of the 1st-order surface contributions up to surface $j-1$ by:

$$\begin{aligned} AXC_{1st} &= \sum_{a=1}^{j-1} AXC_{1st}^{S} \\ &= \sum_{a=1}^{j-1} n_a i_a y_a \left(\frac{\Delta n'}{n'} - \frac{\Delta n}{n}\right)_a \end{aligned} \tag{3.25}$$

Therefore, all terms in Equation (3.18) are determined by paraxial marginal ray data for the reference wavelength, only. Hence, one paraxial raytrace for the reference wavelength provides all required parameters for calculating the 2nd-order axial color effects. An additional raytrace for another wavelength is not necessary.

Lens Contribution Note that the results and the discussion of the first three 2nd-order surface contribution terms is very similar to the outcome of Nobis' thin lens resolved analysis for axial color [Nob14]. Comparing both results, the most noticeable fact is the additional intrinsic term in the new surface resolved description. But by completing the new surface contribution with its deduced thick lens contribution, derived in Equation (3.23), the derivation shows that for lenses the additional intrinsic term of 2nd-order cancels out. Therefore, the new surface based approach is completely consistent and describes a consequent enhancement of Nobis' approach. Consequently, the thick lens formula consists of four sums, the thin lens contribution and three thick-

ness depending terms. The latter one can again be divided in thickness depending induced terms $t\frac{(n-1)c_1c_2}{nu_0u_2}AXC_{1st}^2$ and $t\frac{a_1\Delta n}{nu_2}AXC_{1st}$, as well as one thickness depending intrinsic term $t\frac{a_2(t)}{nu_2}\Delta n^2$. According to the coefficient $a_2(t)$, given in the appendix, the intrinsic term includes linear as well as quadratic and cubic dependencies on t.

3.3 Induced Lateral Color

3.3.1 Surface Contribution of Intrinsic and Induced Lateral Color

In this section an equivalent approach for lateral color is introduced. Figure 3-6 illustrates the parameters and relations defining lateral color conditions at an arbitrary surface S in an optical system.

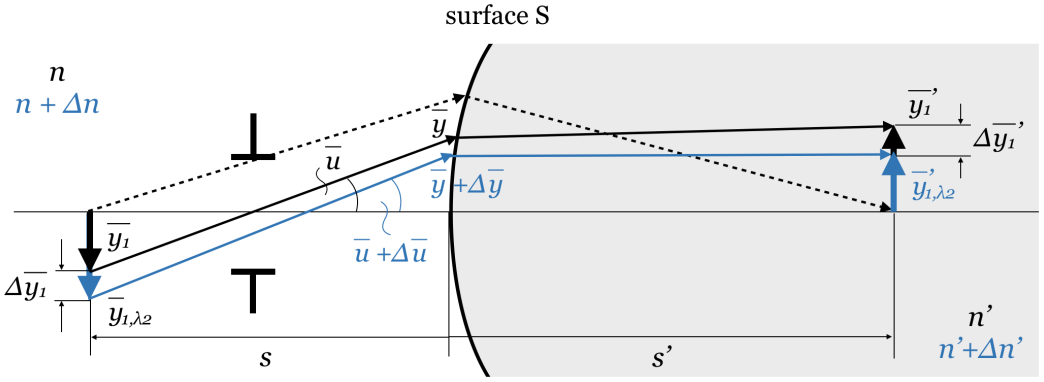

Figure 3-6: Refraction of two paraxial chief rays with different wavelengths (black and blue line) at an arbitrary surface S. The intermediate images show different lateral color aberrations $\Delta\bar{y}_1$ and $\Delta\bar{y}_1'$, whereby the image position is defined by the intersection length of the marginal ray (dashed line)

Considering a single refractive surface S with a curvature c hit by a paraxial chief and marginal ray of the reference wavelength $\lambda = \lambda_1$, the chief ray height at the surface is $\bar{y}$ and the marginal ray height is y. The chief and marginal ray angles before the surface are $\bar{u}$ and u, respectively, and the chief and marginal ray angles after the surface are $\bar{u}'$ and u', respectively. At the intermediate images in front and after the surface, the chief ray heights are $\bar{y}_1$ and $\bar{y}_1'$. Since the position of these intermediate images are fixed by the marginal ray's intersection lengths s and s', $\bar{y}_1$ and $\bar{y}_1'$ can be obtained by

$$\bar{y}_1(\bar{y}, \bar{u}) = \bar{y} + s\bar{u} \tag{3.26}$$

$$\bar{y}_1'(\bar{y}, \bar{u}') = \bar{y} + s'\bar{u}' \tag{3.27}$$

To define the chief ray angle after refraction $\bar{u}'$, the refractive power F of the surface defined by Equation (2.9), according to the paraxial raytrace relation of Equation (3.28), has to be considered:

$$\begin{aligned} n'\bar{u}' &= n\bar{u} - \bar{y}F \\ &= n\bar{u} - \bar{y}c(n'-n) \end{aligned} \tag{3.28}$$

Hence, the chief ray height at the intermediate image after refraction is:

$$\bar{y}_1'(\bar{y},\bar{u},n,n') = \bar{y} + s'\,\frac{n\bar{u} - \bar{y}c(n'-n)}{n'} \tag{3.29}$$

Considering now a second wavelength $\lambda_2 = \lambda_1 + \Delta\lambda$, the corresponding chief ray height at the surface is $\bar{y}_{\lambda 2} = \bar{y} + \Delta\bar{y}$ and the chief ray angle before the surface is $\bar{u}_{\lambda 2} = \bar{u} + \Delta\bar{u}$. At the intermediate images, the image heights for λ_2 are $\bar{y}_{1,\lambda 2} = \bar{y}_1 + \Delta\bar{y}_1$ and $\bar{y}'_{1,\lambda 2} = \bar{y}'_1 + \Delta\bar{y}'_1$. Similarly to this, also the refractive indices show again a wavelength depending character by their dispersive behavior with $n_2 = n + \Delta n$ and $n'_2 = n' + \Delta n'$. Note that, in case of lateral color considerations, the intersection lengths s and s' refer to the reference wavelength λ_1 and are not wavelength depending. Consequently, and according to the definition of lateral color aberration in Section 2.3.2, the lateral color aberration before and after the surface, $\Delta\bar{y}_1$ and $\Delta\bar{y}'_1$, within a wavelength range from λ_1 to λ_2 are given by

$$\begin{aligned} \Delta\bar{y}_1 &= \bar{y}_{1,\lambda 2} - \bar{y}_1 \\ &= \bar{y}_1(\bar{y} + \Delta\bar{y}, \bar{u} + \Delta\bar{u}) - \bar{y}_1(\bar{y},\bar{u}) \end{aligned} \tag{3.30}$$

$$\begin{aligned} \Delta\bar{y}'_1 &= \bar{y}'_{1,\lambda 2} - \bar{y}'_1 \\ &= \bar{y}'_1(\bar{y} + \Delta\bar{y}, \bar{u} + \Delta\bar{u}, n + \Delta n, n' + \Delta n') - \bar{y}_1(\bar{y},\bar{u},n,n') \end{aligned} \tag{3.31}$$

If the differences $\Delta\bar{y}, \Delta\bar{u}, \Delta n$ and $\Delta n'$ are small, again a Taylor series expansion up to 2nd- order can be applied and yields to the following expression for the chief ray height $\bar{y}_{1,\lambda 2} = \bar{y}_1(\bar{y} + \Delta\bar{y}, \bar{u} + \Delta\bar{u})$ at the intermediate image in front of the surface:

$$\bar{y}_{1,\lambda 2} = \bar{y}_1(\bar{y},\bar{u}) + \frac{\partial\bar{y}_1}{\partial\bar{y}}\Delta\bar{y} + \frac{\partial\bar{y}_1}{\partial\bar{u}}\Delta\bar{u} + \frac{1}{2}\frac{\partial^2\bar{y}_1}{\partial\bar{y}^2}\Delta\bar{y}^2 + \frac{\partial^2\bar{y}_1}{\partial\bar{y}\partial\bar{u}}\Delta\bar{y}\Delta\bar{u} + \frac{1}{2}\frac{\partial^2\bar{y}_1}{\partial\bar{u}^2}\Delta\bar{u}^2 \tag{3.32}$$

Inserting this into Equation (3.30) the lateral color before the refractive surface is

obtained by:

$$\Delta\bar{y}_1 = \frac{\partial\bar{y}_1}{\partial\bar{y}}\Delta\bar{y} + \frac{\partial\bar{y}_1}{\partial\bar{u}}\Delta\bar{u} + \frac{1}{2}\frac{\partial^2\bar{y}_1}{\partial\bar{y}^2}\Delta\bar{y}^2 + \frac{\partial^2\bar{y}_1}{\partial\bar{y}\partial\bar{u}}\Delta\bar{y}\Delta\bar{u} + \frac{1}{2}\frac{\partial^2\bar{y}_1}{\partial\bar{u}^2}\Delta\bar{u}^2 \tag{3.33}$$

Applying the same for $\bar{y}'_1$ and $\Delta\bar{y}'_1$ leads to the following result:

$$\begin{aligned}\Delta\bar{y}'_1 = \quad & \frac{\partial\bar{y}'_1}{\partial\bar{y}}\Delta\bar{y} + \frac{\partial\bar{y}'_1}{\partial\bar{u}}\Delta\bar{u} + \frac{\partial\bar{y}'_1}{\partial n}\Delta n + \frac{\partial\bar{y}'_1}{\partial n'}\Delta n' \\ & + \frac{1}{2}\frac{\partial^2\bar{y}'_1}{\partial\bar{y}^2}\Delta\bar{y}^2 + \frac{\partial^2\bar{y}'_1}{\partial\bar{y}\partial\bar{u}}\Delta\bar{y}\Delta\bar{u} + \frac{\partial^2\bar{y}'_1}{\partial\bar{y}\partial n}\Delta\bar{y}\Delta n + \frac{\partial^2\bar{y}'_1}{\partial\bar{y}\partial n'}\Delta\bar{y}\Delta n' \\ & + \frac{1}{2}\frac{\partial^2\bar{y}'_1}{\partial\bar{u}^2}\Delta\bar{u}^2 + \frac{\partial^2\bar{y}'_1}{\partial\bar{u}\partial n}\Delta\bar{u}\Delta n + \frac{\partial^2\bar{y}'_1}{\partial\bar{u}\partial n'}\Delta\bar{u}\Delta n' \\ & + \frac{1}{2}\frac{\partial^2\bar{y}'_1}{\partial n^2}\Delta n^2 + \frac{\partial^2\bar{y}'_1}{\partial n\partial n'}\Delta n\Delta n' \\ & + \frac{1}{2}\frac{\partial^2\bar{y}'_1}{\partial n'^2}\Delta n'^2\end{aligned} \tag{3.34}$$

1st-order terms At first again only the derivatives of the 1st-order terms, e.g. the linear terms, are considered. When inserting the derivatives for $\Delta\bar{y}_1$ and $\Delta\bar{y}'_1$, given at the appendix, the following equations are obtained:

$$\Delta\bar{y}_{1,1st} = \Delta\bar{y} + s\Delta\bar{u} = \Delta\bar{y} - \frac{y}{u}\Delta\bar{u} \tag{3.35}$$

$$\Delta\bar{y}'_{1,1st} = \Delta\bar{y} - \frac{s'c(n'-n)}{n'}\Delta\bar{y} + \frac{s'n}{n'}\Delta\bar{u} + \frac{s'\bar{i}}{n'}\Delta n - \frac{ns'\bar{i}}{n'^2}\Delta n' \tag{3.36}$$

Here, i is the incident angle of the chief ray with $\bar{i} = \bar{u} + \bar{y}c$. To describe now the lateral color surface contribution LAC^S_{1st} of the refractive surface, the difference between the lateral color aberration $\Delta\bar{y}'_{1,1st}$ at the intermediate image after the surface and the lateral color aberration $\Delta\bar{y}_{1,1st}$ at the intermediate image in front of the surface has to be considered. Since these lateral color aberrations are determined as transverse aberrations at a specific intermediate image, the magnification $\beta = (nu)/(n'u')$ between the considered intermediate image and the final image needs to be taken into account as a scaling factor (Section 2.4). Note again, in the case of intermediate images of surfaces, the magnification not only depends on the marginal ray angles but also on the refractive indices of the individual materials. Following these considerations, the 1st-order lateral color surface contribution LAC^S_{1st} is equal to:

$$LAC^S_{1st} = \Delta\bar{y}'_{1,1st}(n'u') - \Delta\bar{y}_{1,1st}(nu) \tag{3.37}$$

Now, inserting Equation (3.35) and (3.36) leads to the following relation:

$$LAC_{1st}^{S} = n'u'\Delta\bar{y} - u's'c(n'-n)\Delta\bar{y} + nu's'\Delta\bar{u} + u's'\bar{i}\Delta n - u'\frac{ns'\bar{i}}{n'}\Delta n' \\ - nu\Delta\bar{y} - nus\Delta\bar{u} \tag{3.38}$$

Considering now Equation (3.1) and (3.2) for the intersection lengths s and s' of the marginal ray, the 1st-order lateral color surface contribution LAC_{1st}^{S} is given by:

$$LAC_{1st}^{S} = n\bar{i}y\left(\frac{\Delta n'}{n'} - \frac{\Delta n}{n}\right) \tag{3.39}$$

This result agrees with the common Seidel theory of primary lateral color, shown in Section 2.3.2.

2nd-order terms In analogous manner to the 1st-order terms, the nonlinear terms are obtained. Hence, the 2nd-order lateral color effects of an arbitrary surface is equal to

$$LAC_{2nd}^{S} = \Delta\bar{y}'_{1,2nd}(n'u') - \Delta\bar{y}_{1,2nd}(nu) \tag{3.40}$$

with

$$\Delta\bar{y}_{1,2nd} = \frac{1}{2}\frac{\partial^2\bar{y}_1}{\partial\bar{y}^2}\Delta\bar{y}^2 + \frac{\partial^2\bar{y}_1}{\partial\bar{y}\partial\bar{u}}\Delta\bar{y}\Delta\bar{u} + \frac{1}{2}\frac{\partial^2\bar{y}_1}{\partial\bar{u}^2}\Delta\bar{u}^2 \tag{3.41}$$

and

$$\begin{aligned}\Delta\bar{y}'_{1,2nd} = \quad & \frac{1}{2}\frac{\partial^2\bar{y}'_1}{\partial\bar{y}^2}\Delta\bar{y}^2 + \frac{\partial^2\bar{y}'_1}{\partial\bar{y}\partial\bar{u}}\Delta\bar{y}\Delta\bar{u} + \frac{\partial^2\bar{y}'_1}{\partial\bar{y}\partial n}\Delta\bar{y}\Delta n + \frac{\partial^2\bar{y}'_1}{\partial\bar{y}\partial n'}\Delta\bar{y}\Delta n' \\ & + \frac{1}{2}\frac{\partial^2\bar{y}'_1}{\partial\bar{u}^2}\Delta\bar{u}^2 + \frac{\partial^2\bar{y}'_1}{\partial\bar{u}\partial n}\Delta\bar{u}\Delta n + \frac{\partial^2\bar{y}'_1}{\partial\bar{u}\partial n'}\Delta\bar{u}\Delta n' \\ & + \frac{1}{2}\frac{\partial^2\bar{y}'_1}{\partial n^2}\Delta n^2 + \frac{\partial^2\bar{y}'_1}{\partial n\partial n'}\Delta n\Delta n' \\ & + \frac{1}{2}\frac{\partial^2\bar{y}'_1}{\partial n'^2}\Delta n'^2\end{aligned} \tag{3.42}$$

In the case of lateral color, inserting the 2nd-order derivatives leads to a quite compact expression compared to the axial color one. This is caused by the six derivatives depending on ray differences only. They vanish, since the chief ray height, described in Equation (3.26) and (3.27), only depends linearly on those ray based quantities. Consequently, the following expression for a 2nd-order lateral color surface contribution

LAC^S_{2nd} is obtained:

$$\begin{aligned} LAC^S_{2nd} = \quad & s'u'c\Delta\bar{y}\Delta n - \frac{s'u'nc}{n'}\Delta\bar{y}\Delta n' + s'u'\Delta\bar{u}\Delta n - \frac{s'u'n}{n'}\Delta\bar{u}\Delta n' \\ & - \frac{s'u'\bar{i}}{n'}\Delta n\Delta n' + \frac{s'u'n\bar{i}}{n'^2}\Delta n'^2 \end{aligned} \tag{3.43}$$

If again Equations (3.1) and (3.2) for the intersection lengths s and s' of the marginal ray are considered, Equation (3.43) will simplify to:

$$\begin{aligned} LAC^S_{2nd} = \ & - yc\Delta\bar{y}\Delta n + \frac{nyc}{n'}\Delta\bar{y}\Delta n' - y\Delta\bar{u}\Delta n + \frac{ny}{n'}\Delta\bar{u}\Delta n' \\ & + \frac{y\bar{i}}{n'}\Delta n\Delta n' - \frac{yn\bar{i}}{n'^2}\Delta n'^2 \end{aligned} \tag{3.44}$$

Following now again the idea of induced aberrations, illustrated in the Section 3.1, some of the 2nd-order terms have to depend on the cumulative preexisting lower-order aberrations in the system before. Hence, in case of a single refractive surface, there have to be some of the 2nd-order terms depending on the 1st-order lateral color aberration in front of the surface. This 1st-order amount was already described by Equation (3.35). Multiplied by the magnification factor, the preexisting 1st-order lateral color aberration in front of the surface LAC_{1st} results in:

$$LAC_{1st} = \Delta\bar{y}_{1,1st}(nu) = \ nu\Delta\bar{y} - ny\Delta\bar{u} \tag{3.45}$$

Analyzing the 2nd-order terms for a dependence on LAC_{1st} and simplifying the terms with common relations for ray tracing (Section 2.1.3), a 2nd- order lateral color surface contribution LAC^S_{2nd} depending on the prior summed up 1st-order lateral color is obtained by:

$$LAC^S_{2nd} = LAC_{1st}\left(\frac{\Delta n'}{n'} - \frac{\Delta n}{n}\right) + ni\Delta\bar{y}\left(\frac{\Delta n'}{n'} - \frac{\Delta n}{n}\right) - n\bar{i}y\left(\frac{\Delta n'^2}{n'^2} - \frac{\Delta n\Delta n'}{nn'}\right) \tag{3.46}$$

Comparing this result to the 2nd-order axial color contribution in Equation (3.18), the second term of Equation (3.46) stands out, since there is neither a dependency on the preexisting lower-order aberration nor it is a pure dispersive depending term like the third one.

Hence, to find a clear characterization for the second term, an extended description specifying lateral color relations and parameters shown in Figure 3-7 has to be considered.

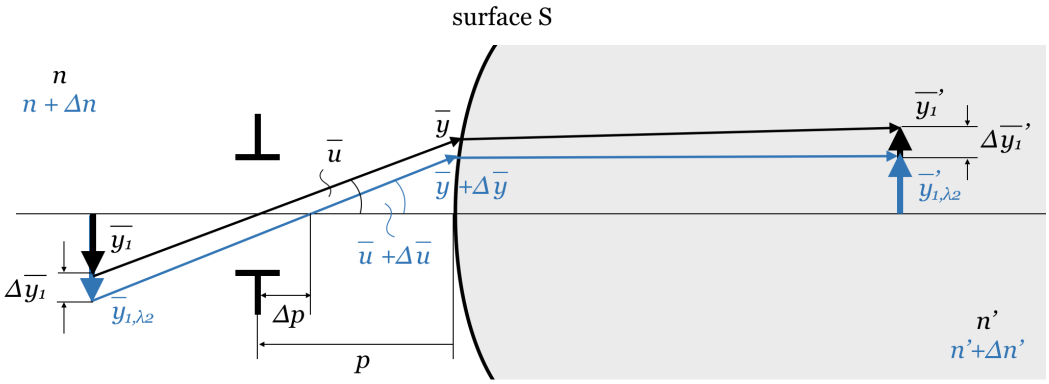

Figure 3-7: Refraction of two paraxial chief rays with different wavelengths (black and blue line) at an arbitrary surface S. The intermediate images show lateral color aberrations $\Delta\bar{y}_1$ and $\Delta\bar{y}'_1$, which also leads to a chromatic defocused image of the stop position Δp.

According to Figure 3-7 the lateral color aberration $\Delta\bar{y}_1$ not only causes a chromatical magnification variation at the intermediate images, it also determines a chromatically defocused image of the stop. This effect appears as Δp at the imaged stop position p and can be understood as the chief ray's axial color aberration. Or in other words, since the chief ray represents the marginal ray of the systems pupil imaging, this effect can be described as the axial color aberration of the pupil. Following this idea, all considerations for axial color aberration in Section 3.2 can be transformed for chief ray conditions in an adequate way. Consequently, the intersection lengths p and p' of the chief ray before and after the surface are gained by

$$p(\bar{y}, \bar{u}) = -\frac{\bar{y}}{\bar{u}} \tag{3.47}$$

$$p'(\bar{y}, \bar{u}, n, n') = -\frac{\bar{y}n'}{n\bar{u} - \bar{y}(n' - n)c} \tag{3.48}$$

Furthermore, the axial color aberration of the chief ray before and after a surface within a wavelength range from λ_1 to λ_2 can therefore be defined as

$$\begin{aligned} \Delta p &= p_{\lambda 2} - p \\ &= p(\bar{y} + \Delta\bar{y}, \bar{u} + \Delta\bar{u}) - p(\bar{y}, \bar{u}) \end{aligned} \tag{3.49}$$

$$\begin{aligned} \Delta p' &= p'_{\lambda 2} - p' \\ &= p'(\bar{y} + \Delta\bar{y}, \bar{u} + \Delta\bar{u}, n + \Delta n, n' + \Delta n') - p(\bar{y}, \bar{u}, n, n') \end{aligned} \tag{3.50}$$

Reviewing this, the calculations for the axial color of the pupil is equivalent to the calculation for axial color of the marginal ray only by exchanging y with $\bar{y}$ and u with $\bar{u}$. For this reason, the 1st-order axial color surface contribution $AXC^S_{p,1st}$ of the pupil,

describing the chromatically defocused imaged stop p is found by

$$AXC^{S}_{p,1st} = n\bar{i}\bar{y}\left(\frac{\Delta n'}{n'} - \frac{\Delta n}{n}\right) \tag{3.51}$$

Consequently, also the corresponding description of the chief ray's preexisting 1st-order axial color aberration $AXC_{p,1st}$ in front of the surface can be found by equation (3.52).

$$AXC_{p,1st} = \Delta p_{1st}(-n\bar{u}^2) = \; n\bar{u}\Delta\bar{y} - n\bar{y}\Delta\bar{u} \tag{3.52}$$

Combining Equation (3.45) and (3.52) reveals the eliminating of $\Delta\bar{u}$ within these two relations:

$$n\Delta\bar{u} = \frac{-AXC_{p,1st} + n\bar{u}\Delta\bar{y}}{\bar{y}} = \; \frac{-LAC_{1st} + nu\Delta\bar{y}}{y} \tag{3.53}$$

Reordering this leads to a new expression for $n\Delta\bar{y}$.

$$n\Delta\bar{y} = \frac{yAXC_{p,1st} - \bar{y}LAC_{1st}}{y\bar{u} - \bar{y}u} \tag{3.54}$$

Now, with this findings, the second term $ni\Delta\bar{y}(\Delta n'/n' - \Delta n/n)$ of Equation (3.46) and its single dependency on the chromatic difference of the chief ray height $\Delta\bar{y}$ can simply be rewritten by inserted (3.54) into Equation (3.46). This results in a new expression for 2nd-order lateral color surface contribution LAC^{S}_{2nd} with all terms depending either on preexisting lower-order aberration or pure dispersive effects:

$$\begin{aligned} LAC^{S}_{2nd} = \quad & LAC_{1st}\left(\frac{\Delta n'}{n'} - \frac{\Delta n}{n}\right) + \frac{iyAXC_{p,1st} - i\bar{y}LAC_{1st}}{y\bar{u} - \bar{y}u}\left(\frac{\Delta n'}{n'} - \frac{\Delta n}{n}\right) \\ & - n\bar{i}y\left(\frac{\Delta n'^2}{n'^2} - \frac{\Delta n\Delta n'}{nn'}\right) \end{aligned} \tag{3.55}$$

Rearranging and simplifying leads to a formula with only two terms left. Hence, the final description of 2nd-order lateral color surface contribution LAC^{S}_{2nd} is obtained by

$$LAC^{S}_{2nd} = \frac{y(iAXC_{p,1st} - \bar{i}LAC_{1st})}{y\bar{u} - \bar{y}u}\left(\frac{\Delta n'}{n'} - \frac{\Delta n}{n}\right) - n\bar{i}y\left(\frac{\Delta n'^2}{n'^2} - \frac{\Delta n\Delta n'}{nn'}\right) \tag{3.56}$$

This equation is the second main result of this thesis.

3.3.2 Lens Contribution of Intrinsic and Induced Lateral Color

Since all of the considerations for the surface resolved lateral color can also be used for a thin lens description analog to [Nob15], the equivalent thin lens contribution formula

of 2nd-order lateral color is obtained by Equation (3.57).

$$LAC_{2nd}^{L} = \frac{y\Delta F_L}{y\bar{u} - \bar{y}u}(yAXC_{p,1st} - \bar{y}LAC_{1st}) \tag{3.57}$$

In contrast, the parameters for a thick lens formula in air are shown in Figure 3-8.

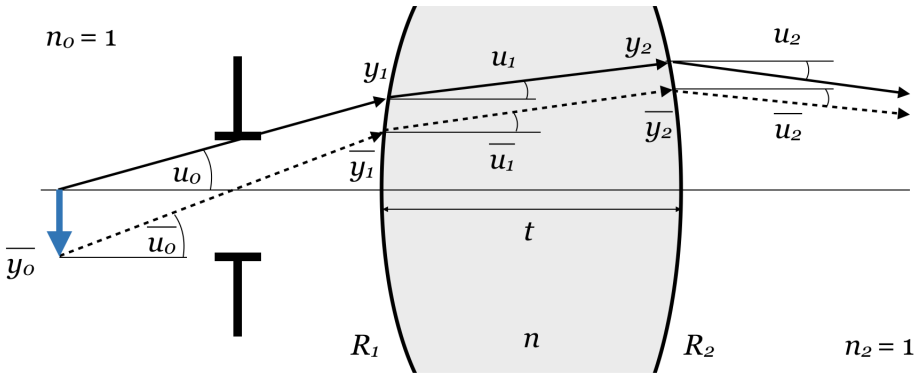

Figure 3-8: Refraction of the marginal ray and chief ray (dashed and solid line) at a thick lens with an refractive index of n. The marginal ray heights and angles are y_1 and u_1 as well as y_2 and u_2 at surface S1 and surface S2, respectively. The chief ray heights and angles are $\bar{y}_0$ and $\bar{u}_0$, $\bar{y}_1$ and $\bar{u}_1$ as well as $\bar{y}_2$ and $\bar{u}_2$ at the intermediate image, surface S1 and surface S2, respectively.

Considering a certain thickness t for an individual lens in an optical system, the 2nd-order lateral color thick lens contribution LAC_{2nd}^{tL} can be calculated by the sum of both surface contributions:

$$LAC_{2nd}^{tL} = LAC_{2nd}^{S1} + LAC_{2nd}^{S2}(t) \tag{3.58}$$

The surface contribution LAC_{2nd}^{S1} of surface S1 is

$$LAC_{2nd}^{S1} = \frac{y_1(i_1 AXC_{p,1st} - \bar{i}_1 LAC_{1st})}{y_1\bar{u}_0 - \bar{y}_1 u_0}\left(\frac{\Delta n}{n}\right) - n\bar{i}_1 y_1\left(\frac{\Delta n^2}{n^2}\right) \tag{3.59}$$

and the surface contribution LAC_{2nd}^{S2} of surface S2 is

$$LAC_{2nd}^{S2} = \frac{y_2(i_2 AXC_{p,1st} - \bar{i}_2 LAC_{1st})}{y_2\bar{u}_1 - \bar{y}_2 u_1}\left(\frac{-\Delta n}{n}\right) \tag{3.60}$$

Here, the preexisting 1st-order chromatic variation of magnification at the intermediate image in front of surface S1 is assumed to LAC_{1st}. According to the Seidel surface coefficient C_2 (Section 2.3.2), for surface S2 the preexisting 1st-order lateral color can

be calculated by:

$$LAC'_{1st} = \; LAC_{1st} + \bar{i}_1 y_1 \Delta n/n \tag{3.61}$$

Equivalent considerations have to be done for the chromatically defocused image of the stop. Here, the axial color of the imaged stop in front of surface S1 is considered to be $AXC_{p,1st}$. Following Equation (3.51) , the preexisting axial color of the chief ray for surface S2 can be obtained by:

$$AXC'_{p,1st} = \; AXC_{p,1st} + \bar{i}_1 \bar{y}_1 \Delta n/n \tag{3.62}$$

The influence of the lens' thickness is represented by $y_2(t), \bar{y}_2(t), i_2(t)$ and $\bar{i}_2(t)$. Inserting now Equation (3.59) and (3.60) into Equation (3.58) and rearranging as well as simplifying it, the following thick lens formula is achieved:

$$\begin{aligned} LAC^{tL}_{2nd} = \; & - \frac{y_1(c_1 - c_2)\Delta n}{y_1\bar{u}_0 - \bar{y}_1 u_0}\left(y_1 AXC_{p,1st} - \bar{y}_1 LAC_{1st}\right) \\ & + t\frac{\beta_1 \Delta n}{y_1\bar{u}_0 - \bar{y}_1 u_0} AXC_{p,1st} + t\frac{\beta_2 \Delta n}{y_1\bar{u}_0 - \bar{y}_1 u_0} LAC_{1st} \\ & + t\frac{\bar{i}_1 \Delta n^2(\beta_1\bar{y}_1 + \beta_2 y_1)}{n(y_1\bar{u}_0 - \bar{y}_1 u_0)} \end{aligned} \tag{3.63}$$

The coefficients β_1 and β_2 can be found in the appendix. Now, considering the relation $\Delta F_{tL} = \Delta n(c1_c2)$ and the definition of the Lagrange Invariant $H = n(y\bar{u} - \bar{y}u)$ of Section 2.1.3, the following final result for the thick lens formula is obtained:

$$LAC^{tL}_{2nd} = \; - LAC^{L}_{2nd} + t\beta_1 \frac{n\Delta n}{H} AXC_{p,1st} + t\beta_2 \frac{n\Delta n}{H} LAC_{1st} + t\frac{\bar{i}_1 \Delta n^2(\beta_1\bar{y}_1 + \beta_2 y_1)}{H} \tag{3.64}$$

3.3.3 Discussion

In case of 2nd-order lateral color surface contributions, Equation (3.56) was obtained by a Taylor expansion up to 2nd-order considering a differentiation with respect to dispersion. Here, the 2nd-order effects are expressed by two terms.

Induced and Intrinsic Terms The first term depends on the preexisting 1st-order lateral color aberration in front of the surface, expressed by the chromatic variation of magnification at the intermediate image LAC_{1st} supplemented with the chromatically defocused image of the stop $AXC_{p,1st}$. Considering the definition and characteristics of induced color aberrations, introduced in Section 3.1, this term describes clearly an

induced effect, as it would vanish, if there is no preexisting lateral color or axial color of the pupil. In contrast to this, the second term only shows dependencies on the chromatic variation of the refractive indices before and after the surface Δn and$\Delta n'$. Therefore, this term is an intrinsic term of 2nd-order.
Analyzing the two terms of Equation (3.56) in detail, a linear dependency of the first term on the preexisting lateral color described by $(iAXC_{p,1st} - \bar{i}LAC_{1st})$ is found. Furthermore, since also the dispersion factor $(\Delta n'/n' - \Delta n/n)$ is present, this term specifies the interaction between the preexisting summed up 1st-order lateral color effects with a dispersive acting surface. As it is the only induced term, a mirror cannot produce any induced lateral color effects.
Comparing the last term $-n\bar{i}y(\frac{\Delta n'^2}{n'^2} - \frac{\Delta n \Delta n'}{nn'})$ of Equation (3.56) with the last term $-niy(\frac{\Delta n'^2}{n'^2} - \frac{\Delta n' \Delta n}{n'n})$ of the 2nd-order axial color contribution, the calculation for the lateral color term is equivalent to the calculation for the axial color term only by exchanging i with $\bar{i}$. Hence, this term shows again a dependence on the individual surface type. If it is a back surface in air, this term vanishes, as $\Delta n'$ for air is zero. But if it is a cemented surface or a front surface in air, this term introduces a certain 2nd-order contribution to lateral color. Therefore, for the lens resolved approach this term vanishes analog to the fourth term of 2nd-order axial color.

Required Parameters Due to the additional consideration of the pupil axial color aberration effect, again the calculation of all required quantities by only one paraxial raytrace is enabled. Following the Seidel sum definition for lateral color (2.50) and the new found relation of (3.51), any preexisting 1st-order lateral color LAC_{1st} and 1st-order axial color of the pupil $AXC_{p,1st}$ before an individual surface S_j can easily be calculated by summing up all 1st-order surface contributions up to surface S_{j-1} by:

$$\begin{aligned} LAC_{1st} &= \sum_{a=1}^{j-1} LAC_{1st}^{S} \\ &= \sum_{a=1}^{j-1} n_a y_a \bar{i}_a \left(\frac{\Delta n'}{n'} - \frac{\Delta n}{n} \right)_a \end{aligned} \tag{3.65}$$

$$\begin{aligned} AXC_{p,1st} &= \sum_{a=1}^{j-1} AXC_{p,1st}^{S} \\ &= \sum_{a=1}^{j-1} n_a \bar{y}_a \bar{i}_a \left(\frac{\Delta n'}{n'} - \frac{\Delta n}{n} \right)_a \end{aligned} \tag{3.66}$$

Therefore, all terms in Equation (3.56) are determined by paraxial marginal and chief ray data for the reference wavelength only. Hence, a single paraxial raytrace for the reference wavelength provides all required parameters for calculating the 2nd-order lateral color effects. An additional raytrace for another wavelength is again not needed.

The Role of the Real Stop Furthermore, just as for 1st-order lateral color, the location of the real stop within an optical system influences the amount of 2nd-order, too. For 2nd-order lateral color this influence of the real stop position is represented by $AXC_{p,1st}$. For every surface in an optical system an intermediate image formed by the preceding optical elements can be determined. For lateral color, additionally the image of the real stop, seen from that intermediate image has to be considered. As long as the chief ray hits the optical axis at an image of the stop, a certain amount of $AXC_{p,1st}$ will be identified. But in case of the real stop position, the axial color of the chief ray $AXC_{p,1st}$ will be zero by definition at the location of the stop, as for every wavelength the chief ray will pass through the center of it. Hence, in optical systems with a front stop arrangement $AXC_{p,1st}$ sums up surface by surface. However, a setup with a real stop within the optical system shows a certain off-set of $AXC_{p,1st}$ in front of the first surface, which then sums up surface by surface to zero until the real stop is reached. Hence, for the front part of the system the summation $AXC_{p,1st}$ has to be done in the opposite direction starting at the real stop position.

Lens Contribution The considerations for the thick lens resulting in Equation (3.64) again confirms two facts. On the one hand the compensating effect of the intrinsic term in Equation (3.56) is shown, as there is no 2nd-order intrinsic term left in the equation, independent of the thickness t. This intrinsic term is canceling out by rearranging and simplifying Equation (3.58). On the other hand, the expected relation between the thin lens formula and the thick lens approach was shown again. In case of 2nd-order lateral color the thick lens formula consists of four summands, the thin lens contribution of Equation (3.57) and three thickness depending terms. Here, the latter one can again be divided in two thickness depending induced terms, $tb_1\frac{n\Delta n}{H}AXC_{p,1st}$ as well as $+tb_2\frac{n\Delta n}{H}LAC_{1st}$, and one thickness depending intrinsic term $t\frac{\bar{i}_1\Delta n^2(b_1\bar{y}_1+b_2y_1)}{H}$.

3.4 Induced Spherochromatism

3.4.1 Definition of Spherochromatism

In this section, the paraxial region of axial and lateral color is left by increasing the aberration's order of pupil dependency obtaining spherical aberration and its chromatic variation. In general, spherochromatism is defined as the chromatic variation of spherical aberration. Therefore, the analytical description of spherical aberration represents the initial point for this approach. There are several ways to obtain an exact expression for spherical aberration at an arbitrary surface in an optical system described in literature [Del52], [Ker95], [CK92]. An appropriate expression of [Del52]is shown in Equation (3.67). Additionally, Figure 3-9 illustrates the corresponding parameters defining the spherical aberration conditions.

$$SPH' = SPH\frac{nu\sin U}{n'u'\sin U'} + \frac{-4nir\sin(\frac{I-U}{2})\sin(\frac{I-I'}{2})}{n'u'\sin U'} \tag{3.67}$$

Here, a single refractive surface j with curvature c is hit by a paraxial and real marginal ray. The paraxial and the real ray heights at the surface are y and Y, respectively. The paraxial ray angle before the surface is determined by u, and the paraxial ray angle after the surface is determined by u'. Accordingly, the ray angles of the real ray before and after the surface are defined by U and U'. Furthermore, the equivalent incident angles are described by i for the paraxial ray and I for the real ray. Considering now the different intersection lengths s and S of the paraxial marginal ray and the real marginal ray, respectively, the longitudinal spherical aberration SPH before the surface is obtained by the difference $SPH = S - s$. Similarly, the longitudinal spherical aberration SPH' at the intermediate image after the surface is represented by the corresponding difference of the intersection lengths S' and s' of the real and paraxial ray after the surface. (Figure 3-9)

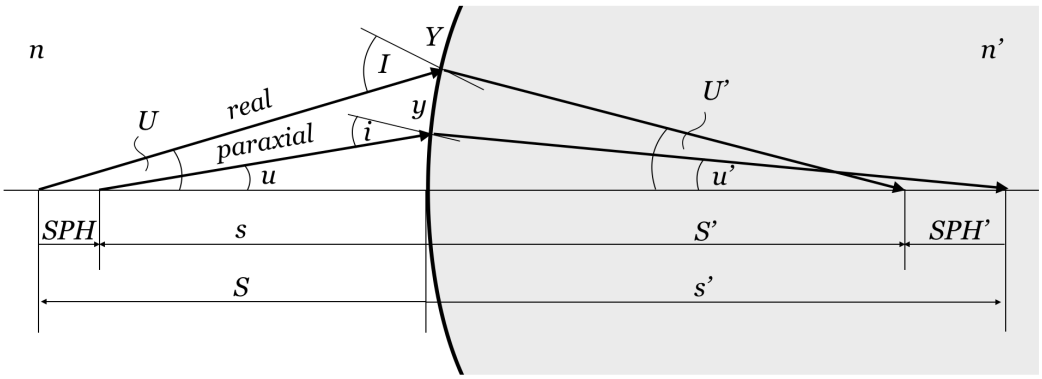

Figure 3-9: Parameters defining the spherical aberration conditions. Here, capital letters refer to real ray and small letter to the paraxial ray parameters.

Equation (3.67) now allows the exact calculation of *SPH'* depending on the spherical aberration in the preceding optical system *SPH* and the above described ray conditions at an arbitrary surface. The first term of Equation (3.67) represents the longitudinal spherical aberration, transferred from the preceding system, in which the factor in front of *SPH* describes the longitudinal magnification of the surface. However, the second term expresses the new longitudinal spherical aberration introduced by the surface itself. This term represents the relevant part for obtaining a single surface contribution formula.

Considering now the definition of spherochromatism, the chromatic variation of the above described parameters have to be included. Here, the first wavelength is assumed to be the reference wavelength $\lambda = \lambda_1$. For a second wavelength λ_2 small differences within the material's refractive index $\Delta n, \Delta n'$, in ray heights $\Delta y, \Delta Y$ and in ray angles $\Delta u, \Delta U$ for the paraxial as well as for the real marginal ray occur. Hence, for a second wavelength different spherical aberration values before and after the surface as well as the axial color between the two wavelengths affects the spherochromatism. This is shown in Figure 3-10.

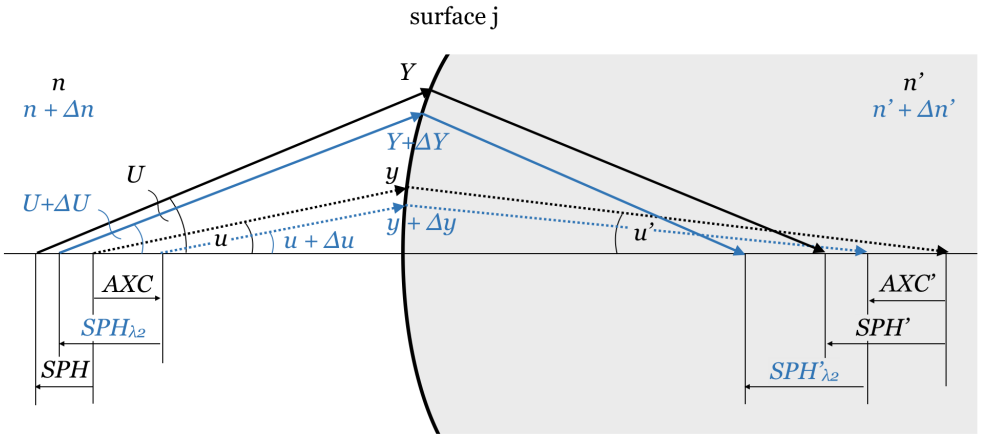

Figure 3-10: Quantities defining spherochromatism. Here, the solid black line parameters refer to the real ray path and dashed black line parameters to the paraxial ray path of the primary wavelength λ_1. The second wavelength λ_2 is represented by blue lines. Again, capital letters belong to the real rays and small letters to the paraxial rays.

In literature, no consistent procedure can be found how to deal with the axial color contribution. For example, Haferkorn [Haf86], Hofmann [Hof] and Smith [Smi04] include axial color to the spherochromatism amount, but e.g. Kingslake [Kin12], Zimmer [Zim67] and Malacara [MM17] remove the axial color for their definitions. Since this approach is following the Seidel idea, where a surface contribution for axial color is already existing and to ensurean independent evaluation of the spherical aberration effects, here the influence of the surface's axial color will be neglected. Hence, the longitudinal spherochromatism *GA*, named corresponding to its German expression

Gaußfehler, is defined as the difference of the longitudinal spherical aberration of different wavelengths:

$$GA = SPH_{\lambda_2} - SPH_{\lambda_1} \tag{3.68}$$

Figure 3-11 illustrates this definition for the case, shown in Figure 3-10. Please note that for spherochromatism GA and GA' the axial color contribution is neglected.

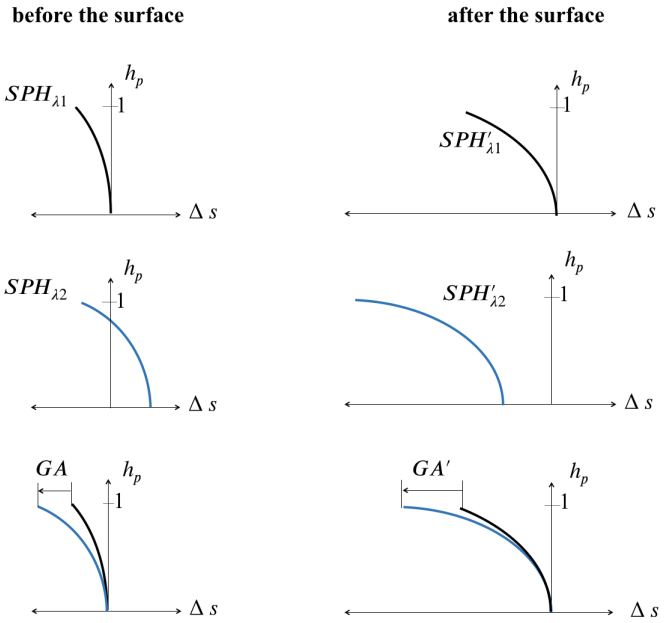

Figure 3-11: Longitudinal aberration plot corresponding to the relations, shown in Figure 3-10 for wavelength λ_1 and wavelength λ_1. Here, the intersection length s for λ_1 provides the reference. Δs describes the difference in z-direction to this reference and h_p characterizes the relative pupil height.

3.4.2 Surface Contribution of Intrinsic and Induced Spherochromatism

Following now Seidel's approach, where the primary monochromatic aberrations are obtained by paraxial approximation of the rays, a 3rd-order spherochromatism will be achieved by the chromatic variation of the paraxial rays, characterizing primary spherical aberration. As mentioned before, the second term of the exact Equation (3.67) represents the relevant term for defining an exact single surface contribution formula of spherical aberration SPH_j^{exact}:

$$SPH_j^{exact} = \frac{-4nir \sin(\frac{I-U}{2}) \sin(\frac{I-I'}{2})}{n'u' \sin U'} \tag{3.69}$$

Considering this expression, the primary surface contribution for spherical aberration is now obtained by assuming $\sin x = x$, by replacing the real ray data with their paraxial ray data with $U = u, u' = u', I = i,\ I' = i'$ and by taking the following paraxial relations (2.5) and (2.6) of Section 2.1.2 as well as (2.12) of Section 2.1.3 into account.

Equation (3.70) shows the result for primary longitudinal spherical aberration surface contribution SPH'_j. Here, S_I describes the Seidel coefficient for spherical aberration. The expression $\frac{1}{2n'u'^2}$ is the conversion factor for the longitudinal description of the wavefront aberration S_I.

$$\begin{aligned} SPH_j = & \ \frac{1}{2n'u'^2}\, n^2 i^2 y \left(\frac{u'}{n'} - \frac{u}{n}\right) \\ = & \ \frac{-S_I}{2n'u'^2} \end{aligned} \tag{3.70}$$

For a 3rd-order chromatic variation approach, the Seidel coefficient $S_I = -n^2 i^2 y(\frac{u'}{n'} - \frac{u}{n})$ represents the basic relation to investigate for different wavelengths. Hence, an expression depending only on ray heights, angles and the refractive index is required and can be obtained by applying the paraxial relation for the incident angle $i = u + yc$ and the raytrace equation $n'u' = nu - yc(n' - n)$:

$$S_I(u, y, n, n') = \ -\frac{y(n^2 - n'n)(u + yc)^2(nu + n'u + ycn)}{n'^2} \tag{3.71}$$

Considering now a second wavelength $\lambda_2 = \lambda_1 + \Delta\lambda$, the corresponding paraxial ray height at the surface is $y_2 = y + \Delta y$ and the corresponding ray angle before the surface is$u_2 = u + \Delta u$. Similarly to this, also the refractive indices show a wavelength depending, dispersive behavior, considered by $n_2 = n + \Delta n$ and $n'_2 = n' + \Delta n'$. Therefore,the chromatic variation ΔS_I of the Seidel coefficient, within a wavelength range from λ_2 to λ_1 represents the Seidel equivalent surface coefficient for spherochromatism G^S and can be defined by

$$\begin{aligned} G^S = & \ \Delta S_I = S_{I,\lambda_2} - S_{I,\lambda_1} \\ = & \ S_I(u + \Delta u,\ y + \Delta y,\ n + \Delta n,\ n' + \Delta n') - S_I(u, y, n, n') \end{aligned} \tag{3.72}$$

Equally to the Seidel coefficient S_I, also the here described spherochromatism coefficient G is expressed in effective wavefront aberration. Now, if the differences $\Delta u, \Delta y, \Delta n$ and $\Delta n'$ are small, a Taylor expansion of 1st-order yields to the following

expression for the Seidel coefficient S_{I,λ_2} of the second wavelength:

$$\begin{aligned} S_{I,\lambda_2} =&\ S_I(u+\Delta u,\ y+\Delta y,\ n+\Delta n,\ n'+\Delta n') \\ =&\ S_I(u,y,n,n') + \frac{\partial S_1}{\partial y}\Delta y + \frac{\partial S_1}{\partial u}\Delta u + \frac{\partial S_1}{\partial n}\Delta n' + \frac{\partial S_1}{\partial n'}\Delta n' \end{aligned} \tag{3.73}$$

Corresponding to Equation (3.72) the Seidel equivalent surface contribution of spherochromatism G^S is given by:

$$G^S = \frac{\partial S_1}{\partial y}\Delta y + \frac{\partial S_1}{\partial u}\Delta u + \frac{\partial S_1}{\partial n}\Delta n' + \frac{\partial S_1}{\partial n'}\Delta n' \tag{3.74}$$

The partial derivatives required for G^S can be found in the appendix. Considering those and the paraxial relations of mentioned before, an expression for the spherochromatism surface contribution G^S is obtained:

$$\begin{aligned} G^S = &\quad \Delta y(u-u')(-4n'i^2 - nu^2 + 3nuu') \\ &+ \Delta uy(u-u')(-4n'i + nu - 3nu') \\ &+ \Delta niy(i'2 - i'u + 2i'u' - u^2 + uu') \\ &+ \Delta n'i'^2 y(u'-i') \end{aligned} \tag{3.75}$$

Here, two terms depending on the dispersive behavior of the materials before and after the surface, represented by Δn and $\Delta n'$, can be found. But additionally, also both terms depending on the chromatic variation of the paraxial marginal ray angle Δu and the paraxial marginal ray height Δy remain after expansion. In contrast to the 1st-order derivatives of axial color and lateral color in Section 3.2.1 and 3.3.1, these terms do not cancel out for the chromatic variation of Seidel's spherical aberration coefficient.

Following now the idea of induced aberrations, some of the four terms in Equation (3.75) have to depend on the cumulative preexisting lower-order color aberrations of the system before. Since here the marginal ray's chromatic variation occurs, 1st-order axial color is investigated. For the preexisting axial color AXC in front of a surface, an expression, including the marginal ray's Δu and Δy, was already described in (3.17):

$$AXC_{1st} = nu\Delta y - ny\Delta u \tag{3.76}$$

Analyzing the spherochromatism terms of Equation (3.75) for a dependency on Equation (3.76), shows that G^S cannot be described with the help of axial color only. Hence, to specify all paraxial effects of a chromatically varying marginal ray, the approach has to be extended. Figure 3-12, shows the additional considerations.

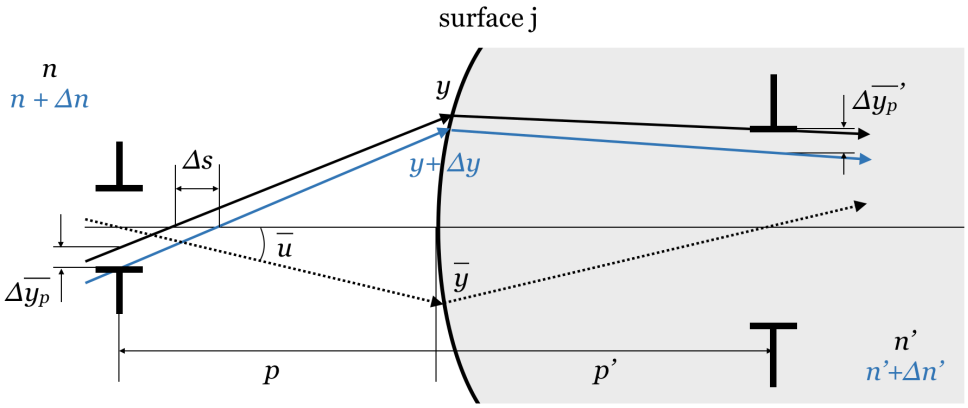

Figure 3-12: Extended considerations on a chromatically varying marginal ray. Here, the solid line parameters again refer to the marginal ray of the primary wavelength λ_1 and the blue line parameters to the marginal ray of the second wavelength λ_2. Additionally, the chief ray of λ_1 is plotted as a dotted line. The intersection length s of the marginal ray characterizes the intermediate image for λ_1. At this image, an axial color aberration Δs is present. The position of the imaged stop in front of the surface is defined by the intersection length p of the chief ray. Here, a chromatic varying stop size characterized by $\Delta\bar{y}_p$ is present. The same considerations are applied for the primed quantities after the surface.

The relations shown in Figure 3-12 describe the consequent extension of the very similar approach of Section 3.3.1. In contrast to this, here the influence of a chromatically varying marginal ray on the imaged stop is considered. According to Figure 3-12, the color variation of the marginal ray not only causes a chromatic difference in image position, which is described by the axial color amount Δs at the intermediate image, it also generates a chromatically varying imaged stop size Δy_p. Since the marginal ray represents the chief ray of the systems pupil imaging, this effect can be understood as a lateral color aberration at the imaged stop position p. Hence, this extended consideration on a chromatically varying marginal ray, allows a description of all chromatic effects by two individual quantities, the axial color at the intermediate image and the lateral color of the pupil image.

For the axial color, the common used Seidel surface contribution formula C_1 (Section 2.3.1, Equation (2.46)) as well as Equation (3.76) can be applied. For the lateral color of the stop image, the considerations for 2nd-order lateral color derived in Section 3.3.1 can be adopted, but have to be transformed for the above explained marginal ray conditions in an adequate way. Therefore, the ray heights of the marginal ray at the imaged stop position, y_p and $\Delta y'_p$, before and after the surface are obtained by:

$$y_p(y,u) = y + pu \tag{3.77}$$

$$y'_p(y,u,n,n') = y + p' \, \frac{nu - yc(n'-n)}{n'} \tag{3.78}$$

Here, the imaged stop positions p and p' can be understood as the intersection lengths of the chief ray, which is characterized by its ray height $\bar{y}$ and its ray angle $\bar{u}$. (3-12) Hence, they are found by:

$$p(y,u) = -\frac{\bar{y}}{u} \tag{3.79}$$

$$p'(y,u,n,n') = -\frac{\bar{y}n'}{n\bar{u} - \bar{y}c(n'-n)} \tag{3.80}$$

Now, the lateral color aberration of the imaged stop before and after a surface, Δy_p and $\Delta y'_p$, within a wavelength range from λ_1 to λ_2, is defined by the difference of the two stop sizes for λ_1 and λ_2. Here, again the chromatic variation in ray angle Δu, ray height Δy and for the material's refractive index, and Δn and and $\Delta n'$, are included:

$$\begin{aligned}\Delta y_p &= y_{p,\lambda 2} - y_{p,\lambda 1} \\ &= y_p(y+\Delta y, u+\Delta u) - y_p(y,u)\end{aligned} \tag{3.81}$$

$$\begin{aligned}\Delta y'_p &= y'_{p,\lambda 2} - \bar{y}'_{p,\lambda 1} \\ &= y'_p(y+\Delta y, u+\Delta u, n+\Delta n, n'+\Delta n') - y'_p(y,u,n,n')\end{aligned} \tag{3.82}$$

Reviewing this, the calculations for the lateral color of pupil image is equivalent to the calculation for the lateral color of the object, only by exchanging $\bar{y}$ with$y$ and $\bar{y}$ with u.For this reason, the surface contribution for the lateral color of the imaged stop LAC_p^S as well as the corresponding expression for the preexisting amount in front of a surface LAC_p, can easily be obtained by the same exchange of ray data. For LAC_p^S, this exchange is applied to Seidel's well-known surface contribution formula for lateral color C_2 (Section 2.3.2, Equation (2.50)). The result is shown in Equation (3.83).

$$LAC_{p,1st}^S = ni\bar{y}\left(\frac{\Delta n'}{n'} - \frac{\Delta n}{n}\right) \tag{3.83}$$

Furthermore, after exchanging the chief ray data with the marginal ray data of Equation (3.45) to obtain LAC_p, the relation shown in (3.84), depending on Δu and Δy is found:

$$LAC_{p,1st} = n\bar{u}\Delta y - n\bar{y}\Delta u \tag{3.84}$$

Coming back to the Seidel equivalent spherochromatism coefficient $G^S(\Delta y, \Delta u, \Delta n, \Delta n')$, derived in Equation(3.75), the remaining dependency on the chromatic variation of the paraxial marginal ray angle Δu and ray heightΔy can be expressed by combining Equation (3.76) and (3.84). This is carried out by rearranging the formulas for AXC_{1st} and

$LAC_{p,1st}$ in the following way.

$$\Delta y = \frac{AXC_{1st} + ny\Delta u}{nu} = \frac{LAC_{p,1st} + n\bar{y}\Delta u}{n\bar{u}} \tag{3.85}$$

$$\Delta u = \frac{-AXC_{1st} + nu\Delta y}{ny} = \frac{-LAC_{p,1st} + n\bar{u}\Delta y}{n\bar{y}} \tag{3.86}$$

Considering these relations,Δu and Δy can be rewritten as shown in Equation (3.87) and (3.88) . Please again note, AXC_{1st} represents the cumulative summed up 1st-order axial color Seidel coefficients in front of the surface, $LAC_{p,1st}$ the summed up 1st-order lateral color of the imaged stop in front of the surface and H the Lagrange Invariant with $H = n\bar{u}y - nu\bar{y}$.

$$\Delta u = \frac{uLAC_{p,1st} - \bar{u}AXC_{1st}}{n\bar{u}y - nu\bar{y}} = \frac{uLAC_{p,1st} - \bar{u}AXC_{1st}}{H} \tag{3.87}$$

$$\Delta y = \frac{yLAC_{p,1st} - \bar{y}AXC_{1st}}{n\bar{u}y - nu\bar{y}} = \frac{yLAC_{p,1st} - \bar{y}AXC_{1st}}{H} \tag{3.88}$$

These two Equations now represent the missing relations to allow all terms of G^S to depend either on preexisting lower-order color aberration or pure dispersive effects. Hence, inserting them into Equation (3.75) results in a new expression for a 3rd-order Seidel equivalent spherochromatism surface contribution G^S:

$$\begin{aligned} G^S = \quad & (\bar{y}AXC_{1st} - yLAC_{p,1st})\frac{4in}{H}(u - u')(i + u') \\ & - AXC_{1st}(u - u')(u' - 3u - 4i') \\ & - \Delta niy\big((u' - u)^2 - (i' + u')^2 + u(i' + u')\big) \\ & - \Delta n' i'^2 y(i' + u') \end{aligned} \tag{3.89}$$

This equation is the third main result of this thesis.

3.4.3 Thin Lens Contribution of Intrinsic and Induced Spherochromatism

To analyze the effect of spherochromatism in compound systems, also a contribution formula for a thin lens in air is investigated. For spherochromatism, this lens contribution can again be derived by the sum of both thin lens' surface contributions:

$$G^L = G^{S1} + G^{S2} \tag{3.90}$$

Here, the surface contribution G^{S1} of the this lens' first surface S1 equals to Equation (3.91), considering $n = 0$ and $\Delta n = 0$, since the lens is assumed to be in air. The two material characterizing quantities of the thin lens' glass are the refractive index $n' = n_L$ and its dispersive quantity $\Delta n' = \Delta n'_L$.

$$\begin{aligned} G^{S1} = \quad & (\bar{y}AXC^{S1}_{1st} - yLAC^{S1}_{p,1st})\frac{4i_0}{H}(u_0 - u'_0)(i_0 + u'_0) \\ & - AXC^{S1}_{1st}(u_0 - u'_0)(u'_0 - 3u_0 - 4i'_0) \\ & - \Delta n' i'^2 y(i' + u') \end{aligned} \tag{3.91}$$

AXC^{S1}_{1st} and $LAC^{S1}_{p,1st}$ are the prior summed up 1st-order color aberrations in front of the thin lens.
Consequently, the second surface contribution G^{S2} of the thin lens' second surface S2 is obtained by:

$$\begin{aligned} G^{S2} = \quad & (\bar{y}AXC^{S2}_{1st} - yLAC^{S2}_{p,1st})\frac{4i_1 n_L}{H}(u_1 - u'_1)(i_1 + u'_1) \\ & - AXC^{S2}_{1st}(u_1 - u'_1)(u'_1 - 3u_1 - 4i'_1) \\ & - \Delta n i_1 y\big((u'_1 - u_1)^2 - (i'_1 + u'_1)^2 + u_1(i'_1 + u'_1)\big) \end{aligned} \tag{3.92}$$

Please note, the ray heights y and $\bar{y}$ do not differ from surfaces S1 to surface S2, since a negligible thickness is assumed. Concerning the incident and emergent angles as well as the ray angle before and after the surfaces, the index 0 refer to the angles in front of surface S1 and the index 1 to the angles in front of surface S2. Now, considering the paraxial relations (2.5) and (2.6) of Section 2.1.2 as well as the ray trace Equation (2.12) of Section 2.1.3, the different angles at surface S2 can simply be calculated from the given angles at surface S1. As a result of this and referring to the Seidel axial color surface contribution C_1 (Section 2.3.1, Equation (2.46)) and Equation (3.83) for the surface contribution of $LAC_{p,1st}$, the prior summed up axial color at the second surface is equal to $AXC^{S2}_{1st} = AXC_{1st} - n_L i_1 y \Delta n_L / n_L$ and the prior summed up lateral color of the pupil at the second surface is equal to $LAC^{S2}_{p,1st} = LAC_{p,1st} - n_L i_1 \bar{y} \Delta n_L / n_L$. With those considerations and by inserting Equation (3.92) and (3.91) into Equation (3.90), the final thin lens spherochromatism formula is obtained by:

$$G^L = (\bar{y}AXC_{1st} - yLAC_{p,1st})\frac{4yF}{Hn_L}\gamma_1 + AXC_{1st}\frac{yF}{n_L}\gamma_2 + \Delta n_L \frac{y^2}{n_L^2}(c_1 - c_2)\gamma_3 \tag{3.93}$$

Here, F is the refractive power of the thin lens shown in Section 2.1.4 by Equation (2.22).The coefficients $\gamma_1(i_0, u_0, i'_1, n_L)$,$\gamma_2(i_0, u_0, i'_1, n_L)$ and $\gamma_3(i_0, u_0, i'_1, n_L)$ can be found in the appendix.

3.4.4 Discussion

The final equation for a 3rd-order Seidel equivalent spherochromatism surface contribution is shown in Equation 65. It was obtained by a Taylor expansion of Seidel's spherical aberration coefficient S_I up to 1st–order concerning its dependency on wavelength variation. Equally to the Seidel coefficient S_I , also the new found spherochromatism coefficient G is given as an effective wavefront aberration.

Induced and Intrinsic Terms Here, G is expressed by four terms. The first two terms depend on prior summed up 1st-order color effects, caused by the chromatic variation of the marginal ray. In case of the first term, this is expressed by the factor $(\bar{y}AXC_{1st} - yLAC_{p,1st})$, including both, the prior summed up lateral color of the pupil $LAC_{p,1st}$ and the prior summed up axial color AXC_{1st}. In case of the second term, again the presence of the prior summed up axial color AXC_{1st} indicates its dependency on the chromatic variation of the marginal ray. Hence, these two terms show clearly induced characteristics, as they would vanish, if there is no preexisting axial color or lateral color of the imaged stop. In contrast to this, the third and fourth term show only dependencies on the chromatic variation of the refractive indices before and after the surface Δn and $\Delta n'$. Therefore, these terms are of intrinsic character, as they would still be valid without any prior element in front of the investigated surface.

Required Parameters The extended considerations by including also the color aberrations of the imaged stop besides the axial color, enables the calculation of all required quantities by only one paraxial raytrace through the optical system. Due to Equations 64 and the well-known Seidel sum for axial color C_1 (Section 2.3.1, Equation (2.46), the 1st-order color aberrations AXC_{1st}. and $LAC_{p,1st}$ before an individual surface j can easily be calculated by summing up all of their surface contributions up to surface $j-1$ by:

$$\begin{aligned} AXC_{1st} &= C_1 \\ &= \sum_{a=1}^{j-1} n_a i_a y_a \left(\frac{\Delta n'}{n'} - \frac{\Delta n}{n} \right)_a \end{aligned} \tag{3.94}$$

$$\begin{aligned} LAC_{p,1st} &= \sum_{a=1}^{j-1} LAC^S_{p,1st} \\ &= \sum_{a=1}^{j-1} n_a i_a \bar{y}_a \left(\frac{\Delta n'}{n'} - \frac{\Delta n}{n} \right)_a \end{aligned} \tag{3.95}$$

Therefore, all terms of Equation (3.89) are determined by the marginal and chief ray data for the reference wavelength only. Hence, a single paraxial raytrace for the reference wavelength provides all required parameters for calculating the 3rd -order spherochromatism. An additional raytrace for another wavelength is not needed.

The Role of the Real Stop Just as known for higher-order spherical aberration [Haf86], the location of the real stop within an optical system influences the amount of 3rd- order spherochromatism, too. For spherochromatism this influence of the real stop position is represented by $LAC_{p,1st}$. For every surface in an optical system an intermediate image formed by the preceding optical elements can be determined. For spherochromatism, additionally the image of the real stop, seen from that intermediate image has to be considered. As long as the chief ray hits the optical axis at an image of the stop, a certain amount of $LAC_{p,1st}$ will be identified. But in case of the real stop position, the lateral color of the marginal ray $LAC_{p,1st}$ will be zero by definition, as for every wavelength the marginal ray will pass the stop at the rim. Hence, in optical systems with a front stop arrangement $LAC_{p,1st}$ sums up surface by surface. However, a setup with a real stop within the optical system shows a certain off-set of $LAC_{p,1st}$ in front of the first surface, which then sums up surface by surface to be zero until the real stop is reached.

Longitudinal Spherochromatism Contribution Since the contribution of G was derived from Seidel's spherical aberration coefficient S_I, also Equation (3.89) and all of the previous expressions of G give the spherochromatism surface contribution in terms of wavefront aberrations. Please note, likewise the Seidel aberrations, this is essentially a wavefront aberration. E.g.,the scaling factor of 1/8 relates Seidel's spherical aberration coefficient to the actual wavefront aberration coefficient (Section 2.2.3).
Obtaining an expression for the longitudinal contribution of spherochromatism, requires a comparable longitudinal conversion calculation like for Seidel coefficients. But in case of spherochromatism, this is not only a simple conversion factor, since the image space condition of the second wavelength also has to be considered. Hence, to gain this longitudinal spherochromatism surface contribution GA, taking the image space conditions of an arbitrary surface k into account, the following relation is initially valid:

$$GA = \frac{S_{I,\lambda_2}}{2n'_{k,\lambda_2}u'^2_{k,\lambda_2}} - \frac{S_{I,\lambda_1}}{2n'_k u'^2_k} \tag{3.96}$$

Here, the expression $\frac{1}{2n'_k u'^2_k}$ is the common used conversion factor for the longitudinal description of Seidel's spherical aberration coefficient S_I of the primary wavelength. This was already shown in Equation (3.70). Including now the second wavelength, the

spherical aberration coefficient as well as the conversion factor has to be adapted. To obtain the spherical aberration coefficient S_{I,λ_2} of the second wavelength, the following simple relation according to Equation (3.72) can be considered:

$$S_{I,\lambda_2} = G + S_{I,\lambda_1} \tag{3.97}$$

For adapting the conversion factor for the second wavelength, not only the different refractive index of the k-th image space n'_{k,λ_2} but also the different marginal ray angle u'_{k,λ_2} of the second wavelength has to be taken into account. Beneficially, again the new relation found in Equation (3.86) can also be applied for this in the following way:

$$u'_{k,\lambda_2} = u'_k + \Delta u'_k \tag{3.98}$$

with

$$u'_{k,\lambda_2} = \frac{u_k LAC_{p,1st} - \bar{u}_k AXC_{1st}}{H} \tag{3.99}$$

Since the axial color AXC_{1st} and the lateral color of the imaged stop $LAC_{p,1st}$, present at the k-th image space, can be summed up applying Equation (3.94) and (3.95) , again all required parameters also for a longitudinal description of 3rd-order spherochromatism GA can be calculated with paraxial ray data of primary wavelength only. Therefore, this approach now fulfills all conditions to be approved as an expansion of Seidel's monochromatic and primary color surface contributions by a new spherochromatism contribution.

Lens Contribution Additionally, the considerations for a thin lens contribution resulting in Equation (3.93) completes this approach. The AXC_{1st} and $LAC_{p,1st}$, are the prior summed up 1st-order color aberrations in front of the investigated lens, calculated according to their thin lens formulas. For the pupil's lateral color $LAC_{p,1st}$ again only the marginal and chief ray heights, y with $\bar{y}$ have to be exchanged within the well-known thin lens contribution C_2^L for lateral color of the object imaging (Section 2.3.2, Equation (2.51)). Equation (3.100) and (3.101) show those thin lens formulas for the summed up 1st-order color aberrations of the j-th lens in a compound system.

$$AXC_{1st}^L = C_1^L = \sum_{a=1}^{j-1} y_a^2 \Delta n_{L,a} (c_1 - c_2)_a \tag{3.100}$$

$$LAC_{p,1st}^L = C_2^L = \sum_{a=1}^{j-1} y_a \bar{y}_a \Delta n_{L,a} (c_1 - c_2)_a \tag{3.101}$$

Please note, in case of thin lenses, the lateral color of the pupil image is equal the lateral color of the object imaging. Similar to the surface contribution formula of Equation (3.89) the first and the second term of Equation (3.93) are of induced character, since they are depending on the preexisting axial color and lateral color of pupil. The third term, however, represents the intrinsic part.

3.5 Induced Chromatic Variation of 3rd-order Seidel Aberrations

Based on the above shown approaches for paraxial axial color and lateral color as well as for Spherochromatism, the analysis of the other Seidel aberrations regarding their 3rd-order chromatic variation will be shown in this Section.
Hence, by increasing the aberration order of field dependency, primary coma, astigmatism, field curvature and distortion are obtained. Their Seidel expressions are shown in Equations (3.102) to (3.105).

$$S_{II} = -\sum \bar{A} A y \, \Delta\left(\frac{u}{n}\right) \qquad \text{Coma} \tag{3.102}$$

$$S_{III} = -\sum \bar{A}^2 y \, \Delta\left(\frac{u}{n}\right) \qquad \text{Astigmatism} \tag{3.103}$$

$$S_{IV} = -\sum H^2 c \, \Delta\left(\frac{1}{n}\right) \qquad \text{Field curvature} \tag{3.104}$$

$$S_V = -\sum \frac{\bar{A}}{A}(S_{III} + S_{IV}) \qquad \text{Distortion} \tag{3.105}$$

Here, $A = ni$ and $\bar{A} = n\bar{i}$ are the refraction invariants at the chosen surface for the marginal ray and the chief ray, respectively, and H is again the Lagrange invariant $H = n(u\bar{y} - \bar{u}y) = n'(u'\bar{y} - \bar{u}'y)$. Clearly, these primary monochromatic aberrations are of zero-order in color, since they do not depend on dispersive effects. However, by differentiation with respect to dispersion, like successfully shown for Spherochromatism, the chromatic variations of the monochromatic aberrations are found.
Now, since all of these Seidel aberration depend on marginal ray data, y and u, as well as on chief ray data, $\bar{y}$ and $\bar{u}$, also their chromatic variations $\Delta y, \Delta u, \Delta\bar{y}$ and $\Delta\bar{u}$ will occur within this differentiation. Based on the findings in Sections 3.2, 3.3 and 3.4 there are existing descriptions for $\Delta y, \Delta u$ and $\Delta\bar{y}$ found in Equation (3.87), (3.88) and (3.54). Therefore, to obtain the fourth expression for $\Delta\bar{u}$, the same considerations as before can be applied. Consequently, combining Equation (3.45) and (3.52), enables the eliminating of $\Delta\bar{y}$ within these two relations. This is carried out by rearranging

the formulas for $AXC_{p,1st}$ and LAC_{1st} in the following way:

$$\Delta\bar{y} = \frac{AXC_{p,1st} + n\bar{y}\Delta\bar{u}}{n\bar{u}} = \frac{LAC_{1st} + ny\Delta\bar{u}}{nu} \tag{3.106}$$

Reordering this leads to the expression for the chromatic variation of the chief ray angle $\Delta\bar{u}$. The Equation is shown in (3.110), together with the prior derived expressions for $\Delta y, \Delta u$ and $\Delta\bar{y}$. Please note, in order to simplify the following equations, the indices are reduced by "1st", but still mean 1st-order color aberrations in any case.

$$\Delta y = \frac{yLAC_p - \bar{y}AXC}{H} \tag{3.107}$$

$$\Delta u = \frac{uLAC_p - \bar{u}AXC}{H} \tag{3.108}$$

$$\Delta\bar{y} = \frac{yAXC_p - \bar{y}LAC}{H} \tag{3.109}$$

$$\Delta\bar{u} = \frac{uAXC_p - \bar{u}LAC}{H} \tag{3.110}$$

These four equations represent the main idea of the discussed approach within this thesis. They explain how and why the paraxial marginal ray and chief ray varies in angle and in ray height on the way through the optical system, caused by the influence of dispersion. The direct relation to prior summed paraxial color aberrations, AXC and LAC, and pupil color aberrations, AXC_p and LAC_p, found within this approach, now enables the calculation of the chromatic variations of all aberrations described by marginal and chief ray data and additionally the differentiation of intrinsic and induced parts.

Considering these expressions for the four Seidel aberration Coma, Astigmatism, Field Curvature and Distortion, the following final results are obtained after a differentiation with respect to dispersion. Here, $cS_{II}, cS_{III}, cS_{IV}$ and cS_V describe the chromatic variations of 3rd-order Coma, Astigmatism, Field Curvature and Distortion, respectively. Again, the distinction between intrinsic and induced terms is possible by finding induced terms to depend on the prior summed up lower-order color aberrations AXC, AXC_p, LAC and LAC_p.

$$
\begin{aligned}
cS_{II} = \quad & AXC\left(\frac{cH(n+2n')}{nn'}+\frac{3n\bar{y}(i'+u)(\bar{i}u'-i\bar{u})}{H}+3i(\bar{i}-2\bar{u})+6\bar{i}'u'+u\bar{u}-4u'\bar{u}'\right)\\
& +AXC_p\frac{niy(i+u')(u-u')}{H}\\
& -(LAC-3LAC_p)(u-u')\left(\frac{ni\bar{y}(i+u')}{H}+(i'+u)\right)\\
& -\Delta n(i\bar{y}+\frac{H}{n})\left(i'^2-i'(u-2u')+u(u'-u)\right)\\
& +\Delta n'i'^2\bar{y}(i'+u')+\Delta n'i'\frac{H}{n}(i'-u+2u')+\Delta n'\frac{H(u-u')(u-2u')}{n'}
\end{aligned}
\tag{3.111}
$$

$$
\begin{aligned}
cS_{III} = \quad & \frac{AXC\bar{i}^2\left(H\left(n'^2-n^2\right)+2nn'\bar{y}(n'u-nu')\right)}{Hn'^2}\\
& +\frac{AXC_p(u'-u)2n\bar{i}y(i+u')}{H}\\
& +\frac{(LAC-LAC_p)(\bar{u}-\bar{u}')2n\bar{i}y(i+u')}{H}\\
& +\frac{\Delta n\bar{i}^2y(in'-u(n+2n')+u'(3n+n'))}{n'}\\
& +\frac{\Delta n'\bar{i}^2y\left(n'(u(n+n')-in')-u'\left(2n^2+nn'+n'^2\right)+n^2u\right)}{n'^2}
\end{aligned}
\tag{3.112}
$$

$$
cS_{IV} = \quad -(LAC-LAC_p)\frac{2cH(n-n')}{nn'}-\Delta n\frac{cH^2(n'-2n)}{n^2n'}-\Delta n'\frac{cH^2}{n'^2}
\tag{3.113}
$$

$$
\begin{aligned}
cS_V = \quad & (AXC\bar{i}+3iLAC-iLAC_p)\frac{\bar{y}n(\bar{i}+\bar{u}')(\bar{u}-\bar{u}')}{H}\\
& +AXC_p\left(\frac{3ni\bar{y}(\bar{u}'(i-u+u')-i\bar{u})}{H}-u(3\bar{u}+\bar{u}')+u'(\bar{u}+3\bar{u}')\right)\\
& +\Delta ni\bar{y}\left(\bar{i}^2-3\bar{i}\bar{u}+4\bar{i}\bar{u}'+\bar{u}^2-4\bar{u}\bar{u}'+3\bar{u}'^2\right)\\
& +\Delta n\frac{2H\bar{u}'(\bar{u}'^2+\bar{i}-\bar{u})}{n}\\
& -\Delta n'\bar{y}\left(i\bar{i}^2+4\bar{u}'(i(\bar{i}-2\bar{u})+u\bar{u})-3i\bar{i}\bar{u}+\bar{u}'^2(5i-5u+2u')+3i\bar{u}^2-u\bar{u}^2\right)\\
& +\Delta n'\frac{H(n'\bar{u}'(-2\bar{i}+\bar{u}+\bar{u}')+n(\bar{u}+\bar{u}')(\bar{u}-2\bar{u}'))}{nn'}
\end{aligned}
\tag{3.114}
$$

4 Application of the New Theory

4.1 Classical Design Examples

In this Section some of the classical design examples for induced color aberrations are investigated. All of them are kept very simple in design, since those are best for understanding the characteristics and possible influences of 2nd-order induced and intrinsic color aberrations. Particularly, the catadioptric system in 4.1.4 and the split achromat in 4.1.5 are often-cited examples for induced color effects. But an exact analytical analysis and therefore also a deeper understanding of them was missing. Here, the new surface contribution formulas, found in this thesis, can now be applied and explain how these designs work.

4.1.1 8f-imaging System

As a first example a simple 8f-system composed of two lenses, each in a 4f-arrangement, is analyzed. Figure 4-1 illustrates the paraxial conditions for axial and lateral color aberration.
The primary wavelength is $\lambda = 587\,\text{nm}$ and a wavelength range from $\lambda_1 = 486\,\text{nm}$ to $\lambda_2 = 656\,\text{nm}$ is assumed. The object height is $y = 1\,\text{mm}$. Note that the stop position of the system is located after lens 2. Two cases shall be analyzed. Case (1) is described by two, equiconvex lenses consisting of a 3 mm thick, low dispersive crown glass BK7, each with a focal length of $f' = 50\,\text{mm}$. In case (2) lens 1 now consists of SF6, a high dispersive flint glass and the center thickness of lens 2 is 12 mm. To analyze these designs for intrinsic and induced color aberration, only a ray trace of the primary wavelength $\lambda = 587\,\text{nm}$ is required.

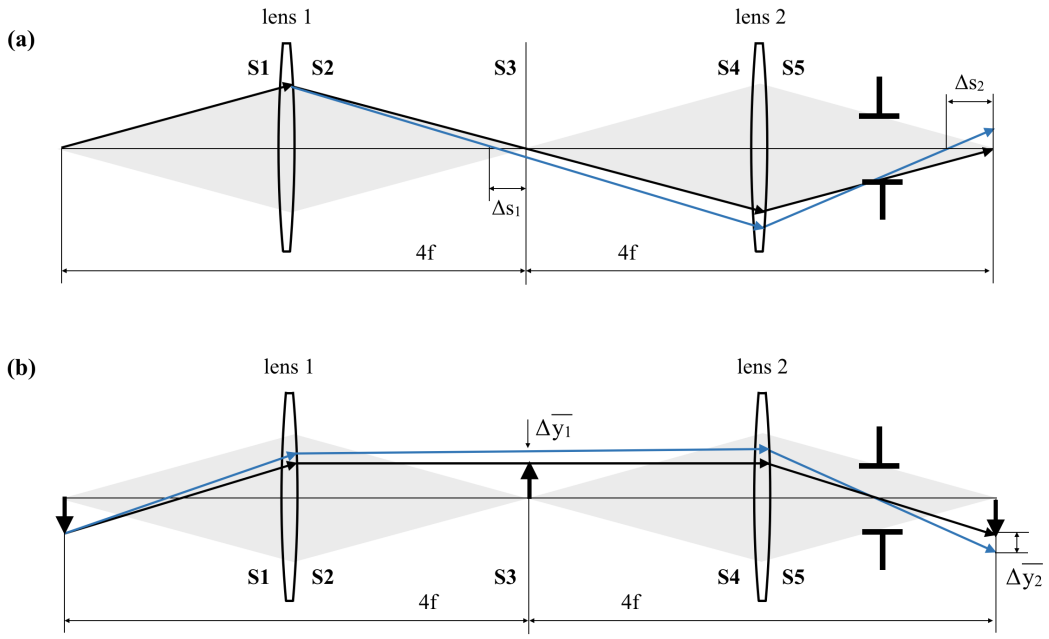

Figure 4-1: Example design composed of two lenses, each in a 4f- arrangement. (a) shows the marginal raytrace for two different wavelengths (dashed and dotted line), illustrating the axial color parameters and (b) shows the chief raytrace of two different wavelengths (solid and dotted line) illustrating the lateral color parameters.

Considering the equations for 1st- and 2nd-order axial color of Equation (3.18) twice, at first for $\lambda_1 = 486\,\text{nm}$ and secondly for $\lambda_2 = 656\,\text{nm}$, and adding up these contributions, a differentiation between intrinsic and induced parts for a wavelength range from 486 nm to 656 nm according to Table 4.1 and Table 4.2 is achieved.

Table 4.1: Axial color contributions for the example system for case (1). The wavelength range is $\lambda_1 = 486\,\text{nm}$ to $\lambda_2 = 656\,\text{nm}$.

Surf.	**prior** ***AXC***	**1st** ***AXC*** **[mm]**	**2nd** ***AXC*** **[mm]**	**lens int [mm]**	**lens ind [mm]**	**thickn.** ***AXC*** **[mm]**
S1	0.000	1.449	−0.870	−0.034	0.000	0.0002
S2	0.004	1.459	0.836			
S3	0.008					
S4	0.008	1.508	−7.779	−0.036	−0.135	0.002
S5	0.012	1.518	7.609			
S6	0.016					
sum	**contrib.**	5.934	−0.205	−0.070	−0.135	0.002
sum	**1st+2nd**	5.729				
sum	**system**	5.747				

Table 4.2: Axial color contributions for the example system for case (2). The wavelength range is $\lambda_1 = 486\,\text{nm}$ to $\lambda_2 = 656\,\text{nm}$.

Surf.	**prior** $\boldsymbol{AXC}$	**1st** $\boldsymbol{AXC}$ **[mm]**	**2nd** $\boldsymbol{AXC}$ **[mm]**	**lens int [mm]**	**lens ind [mm]**	**thickn.** $\boldsymbol{AXC}$ **[mm]**
S1	0.000	3.261	−6.515	−0.217	0.000	0.001
S2	0.010	3.284	6.298			
S3	0.020					
S4	0.020	1.368	−7.369	−0.031	−0.548	0.025
S5	0.024	1.397	6.790			
S6	0.028					
sum	**contrib.**	9.310	−0.795	−0.248	−0.548	0.026
sum	**1st+2nd**	8.515				
sum	**system**	8.658				

Assuming then the same considerations for lateral color (Equation (3.56)) and taking additionally the rear sided stop position into account, the results of Table 4.3 and Table 4.4 are obtained.

Table 4.3: Lateral color contributions for the example system for case (1). The wavelength range is $\lambda_1 = 486\,\text{nm}$ to $\lambda_2 = 656\,\text{nm}$.

Surf.	**prior** $\boldsymbol{iAXC_p}$ $\boldsymbol{10^{-3}}$	**prior** $\boldsymbol{\bar{i}LAC}$ $\boldsymbol{10^{-3}}$	**1st** $\boldsymbol{LAC}$ **[mm]**	**2nd** $\boldsymbol{LAC}$ **[mm]**	**lens int [mm]**	**lens ind [mm]**	**thickn.** $\boldsymbol{LAC}$ **[µm]**
S1	−0.113	0.000	−27.53	0.499	0.003	0.888	0.003
S2	0.033	−0.033	−17.77	0.392			
S3	0.003	−0.013					
S4	0.009	0.008	1.72	0.001	0.000	−0.172	0.005
S5	−0.005	−0.034	11.67	−0.173			
S6	0.000	−0.023					
sum	**contrib.**		−31.92	0.719	0.003	0.715	0.008
sum	**1st+2nd**		−31.20				
sum	**system**		−31.23				

Table 4.4: Lateral color contributions for the example system for case (2). The wavelength range is $\lambda_1 = 486\,\text{nm}$ to $\lambda_2 = 656\,\text{nm}$.

Surf.	prior $iAXC_p$ 10^{-3}	prior $\bar{i}LAC$ 10^{-3}	1st LAC [mm]	2nd LAC [mm]	lens int [mm]	lens ind [mm]	thickn. LAC [µm]
S1	−0.191	0.000	−67.05	3.086	0.019	5.189	0.018
S2	0.041	−0.046	−36.15	2.122			
S3	0.004	−0.026					
S4	0.011	0.033	2.86	−0.096	−0.001	−0.577	0.055
S5	−0.006	−0.086	11.49	−0.483			
S6	0.000	−0.072					
sum	**contrib.**		−88.85	4.63	0.02	4.61	0.07
sum	**1st+2nd**		−84.23				
sum	**system**		−84.68				

Comparing case (1) and case (2) shows clearly the influence of preexisting 1st-order color aberrations, expressed by the prior 1st-order parameters AXC, AXC_p and AXC_p according to Equation (3.25), (3.65) and (3.66). In case (1), due to the low dispersive BK7 lens, small 1st- order axial color aberrations are summed up until the light hits lens 2. Hence, the induced contributions equal only 2.4% of the overall sum for axial color of the 8f-system. In contrast to this, in case (2) the high dispersive flint glass SF6 produces large 1st-order axial color aberrations Δs_1 at the intermediate image in front of lens 2(Figure 4-1). This induces larger 2nd-order terms at the second lens compared to case (1). Here, they reach up to 6.5% of the overall aberration. It should also be noted that the individual 2nd-order surface contributions are partly of same order of magnitude as the 1st-order ones and also at some points larger. The lens contributions, however, in all cases show the expected lower order of magnitude. The same basic conclusions as for axial color are also true for lateral color. Since the induced lateral color aberrations show a linear dependency on $(iAXC_{p,1st} - \bar{i}LAC_{1st})$, the 1st-order parameters $iAXC_p$ and $\bar{i}LAC$ are plotted in Table 4.3 and Table 4.4 as reference. Here, additionally the influence of the rear sided stop location at surface S6 has to be considered. Hence, in Table 4.3 and Table 4.4 non-zero off-set values for prior $iAXC_{p,1st}$ are present, which then sum up surface by surface and become zero at surface S6, since the real stop position is located here. These non-zero off-set conditions are also the reason for the large induced contributions of lens 1 compared to lens 2. In this regard, Table 4.3 shows an eight times larger induced contribution of lens 1 and Table 4.4 illustrates even a factor of ten between lens 1 and 2.
Additionally the increased thickness of lens 2 in case (2) leads to a rise of thickness

depending terms by a factor of twelve for 2nd-order axial color and by a factor of eleven for 2nd-order lateral color compared to case (1).
In summary, although this is a very simple design example composed of only two lenses, very large 2nd-order effects dominated by the induced parts in both cases and for both color aberration are present. The reason for this effect can be found in the widely separated lenses. Hence, the introduced color aberration of lens 1 leads to large differences in ray angles and ray heights at the second lens for the different wavelengths. Consequently, in optical systems like this, where single, non achromized lenses are widely separated from each other, induced color aberration parts can reach up to 9.3% or even more of the overall aberration (Table 4.3 and Table 4.2). Without considering those contributions here, a 1st-order prediction would show an error of 7.5% compared to the real design value. But by considering the 2nd-order effects the error reduces to only 1.6%.

4.1.2 Thick Meniscus

As a second example, a single meniscus lens, focusing light from infinity, is analyzed for axial color. Figure 4-2 illustrates this lens setup.

Figure 4-2: Thick meniscus lens with same radii of $R = 15\,\text{mm}$ and a thickness of $t = 10\,\text{mm}$.

Both radii of the lens are supposed to have the same value of $R = 1/c_1 = 1/c_2 = 15\,\text{mm}$. The center thickness is 10 mm. Assuming F2 as a glass material for the meniscus lens, the resulting sums of intrinsic and induced surface contributions are shown in Table 4.5.
Note, for such a meniscus lens the thin lens formula for 2nd-order axial color contributions by Nobis [Nob14] is no longer valid, since the thin lens approach would result in a 2nd-order contribution of zero for the meniscus lens. Instead of that, the new surface approach applied in Table 4.5, shows the first surface already inducing a relevant amount of 2nd-order axial color at the second surface. In combination with the thickness of the lens, a significant amount of 2nd-order intrinsic and induced effects are present.

Table 4.5: Induced and intrinsic axial color contributions of a meniscus lens for a wavelength range from 486 nm (F-line) to 587 nm (d-line).

Surf.	**R [mm]**	**t [mm]**	**glass**	**1st *AXC* [mm]**	**2nd *AXC* [mm]**	**surf. int [mm]**	**surf. ind [mm]**
STOP		10		0	0	0	0
S2	15	10	F2	4.455	−0.087	−0.087	0
S3	15	70.62		−1.946	0.016	−0.054	0.069
sum	**contrib.**			2.508	−0.071	−0.140	0.069
sum	**1st+2nd**		2.437				
sum	**system**		2.439				

4.1.3 Schupmann Achromat

The third example shows an one-glass dialyte lens, presented in Figure 4-3. Dialytes enable color correction at a virtual image plane with two widely air spaced lenses, consisting of the same glass material [Kin12]. Figure 4-3(a) shows this classical two-lens setup.

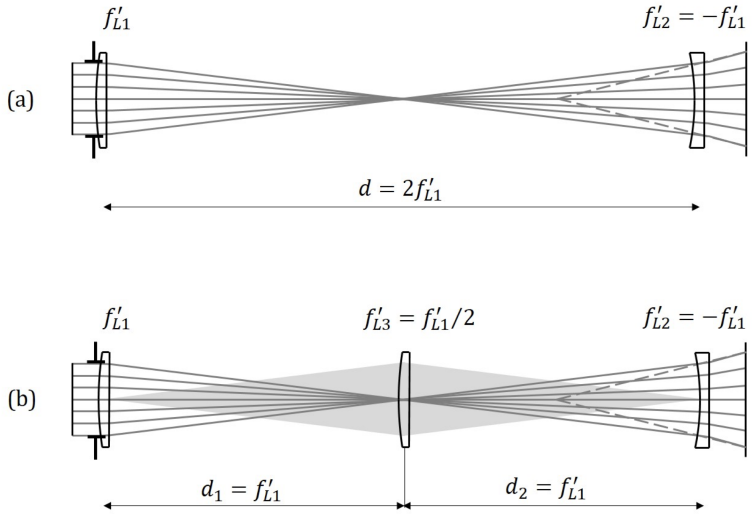

Figure 4-3: (a) Schupmann achromatic design, where a positive lens with f'_{L1} and negative lens with $f'_{L2} = -f'_{L1}$ are set up together, separated by an airspace of $d = 2f'_{L1}$. (b) Schupmann design improved by a third lens with $f'_{L3} = 1/2f'_{L1}$, positioned exactly at the intermediate image between the two lenses.

In case of the Schupmann Achromat, a positive lens L1 with a focal length f'_{L1} and a negative lens L2 with a focal length of $f'_{L2} = -f'_{L1}$ are set up together separated by an airspace $d = 2f'_{L1}1$. According to 1st-order theory, such a design is perfectly corrected for axial color. This is a result of the same dispersive behavior of both lenses, since they are made of the same glass. The 1st-order axial color introduced by lens L1 is exactly canceled out by the 1st-order axial color contribution of lens L2, as they have

equal but opposite power and are operating at identical marginal ray heights. However, for secondary color, a significant amount of color aberration is left, which cannot be explained with this 1st-order approach. Nobis showed in [Nob14] how 2nd-order color aberration, including induced aberration parts, leads to this amount of secondary color. Furthermore, he also proved with his approach that an additional third lens L3, with $f'_{L3} = 1/2 f'_{L1}$ positioned exactly at the intermediate image between the two lenses, can almost perfectly correct the secondary color of the system by introducing additional induced axial color amounts. This design setup is shown in Figure 4-3(b). Now, Figure 4-4 gives the longitudinal aberration plot for the classical two- lenses and the improved three-lenses Schupmann design, assuming $f'_{L1} = -f'_{L2} = 2f'_{L3} = 50\,\text{mm}$ and N-BK7 to be the glass material. The entrance pupil diameter is chosen to be 7 mm and the lenses are assumed to be thin lenses with either a plano-convex or plano-concave shape.

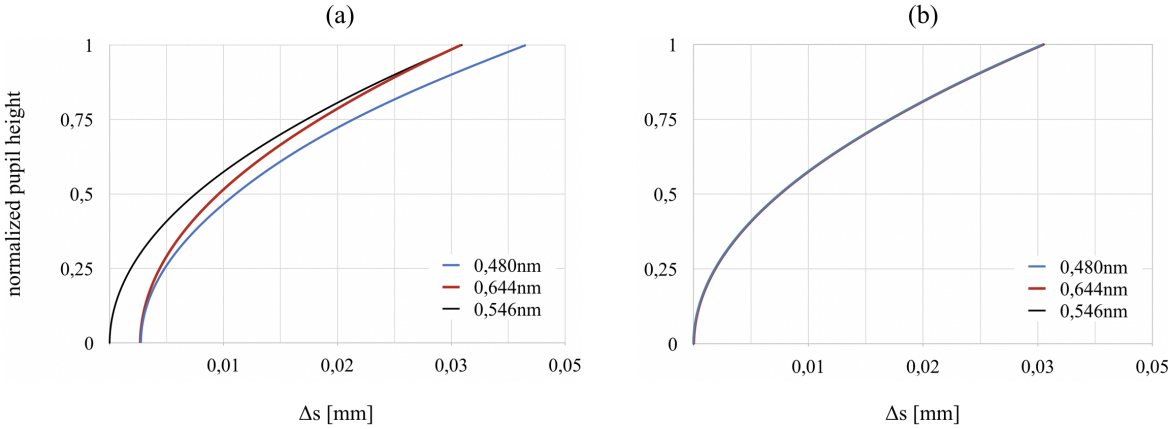

Figure 4-4: Longitudinal aberration plots for (a) the two-lenses N-BK7 Schupmann design and (b) the same Schupmann design improved by a third N-BK7 thin lens with positioned exactly at the intermediate image between the two lenses.

These longitudinal aberration plots clearly show that not only secondary color is corrected, but also spherochromatism is completely vanishing by inserting the additional third lens.

Now, according to the thin lens formula derived in Equation (3.93), the total spherochromatism amount G^L_{tot} for the classical two-lens Schupmann Achromat is obtained by the sum of both thin lens contributions G^{L1} and G^{L2}:

$$G^L_{tot} = G^{L1} + G^{L2} \tag{4.1}$$

Considering the induced terms of G^{L1} to be zero, since no prior axial and lateral color was summed up previously, G^L_{tot} is determined by adding up the intrinsic part G^{L1}_{int} of lens L1 and the induced as well as the intrinsic part of lens L2, G^{L2}_{int} and G^{L2}_{ind}

respectively:

$$G^L_{tot} = G^{L1}_{int} + G^{L2}_{int} + G^{L2}_{ind} \tag{4.2}$$

Assuming now $\lambda_1 = 546\,\text{nm}$ to be the primary wavelength and $\lambda_2 = 480\,\text{nm}$ as the second wavelength, Table 4.6 represents those results.

Table 4.6: G^L coefficients of the two-lens Schupmann design for the prior summed up 1st-order color aberrations AXC^L and LAC^L_p and the intrinsic and induced parts of G^L

Lens	$\boldsymbol{y}$ **[mm]**	$\boldsymbol{\bar{y}}$ **[mm]**	**prior** $\boldsymbol{AXC^L}$ $\boldsymbol{10^{-4}}$ **[mm]**	**prior** $\boldsymbol{LAC^L_p}$ $\boldsymbol{10^{-4}}$ **[mm]**	$\boldsymbol{G^L}$ $\boldsymbol{10^{-4}}$ **[mm]**	**int** $\boldsymbol{G^L}$ $\boldsymbol{10^{-4}}$ **[mm]**	**ind** $\boldsymbol{G^L}$ $\boldsymbol{10^{-4}}$ **[mm]**
L1	3.5	0	0	0	−0.03	−0.03	0
L2	3.5	2	9.7	0	0.45	0.11	0.34
sum					0.42	0.08	0.34

Similar to Nobis' axial color study of the Schupmann design [Nob15], the analysis, shown in Table 4.6, indicates a dominating amount of induced aberration parts for spherochromatism also. Lens L2 introduces more than 80% of the total spherochromatism amount by its induced aberration parts. Since the prior summed up lateral color of the imaged stop is equal to zero for that lens, the whole induced amount is caused by the 1st-order axial color of lens L1.
If now the third lens L3 is insert into the system, its spherochromatism contribution, represented by G^{L3}_{int} and G^{L3}_{ind}, has to be added to the total spherochromatism amount G^L_{tot} :

$$G^L_{tot} = G^{L1}_{int} + G^{L2}_{int} + G^{L2}_{ind} + G^{L3}_{int} + G^{L3}_{ind} \tag{4.3}$$

Here, the position of lens L3 at the intermediate image, where the marginal ray height y is zero, causes some special conditions. First of all, according to Equation (3.93) this position leads to a zero spherochromatism contribution of lens L3 for the induced as well as for the intrinsic case, since in all terms of Equation (3.93) the marginal ray height y occurs as a constant factor. Hence, the terms G^{L3}_{int} and G^{L3}_{ind} of Equation (4.3) vanishes and the total amount of spherochromatism in the three-lens system again only depends on the contributions of L1 and L2.
Furthermore, the special position of L3 enables also the same marginal ray propagation like for the two-lens design. For this reason, the ray heights and ray angles at lens L1 and lens L2 are still the same as before, which causes a conservation of both intrinsic

contributions of L1 and L2. Therefore, the total intrinsic sum of the two-lens design is kept and its value of $0.08 \times 10^{-4}\,\mathrm{mm}$ can be insert into Equation (4.3):

$$G_{tot}^{L} = 0.08 \times 10^{-4}\,\mathrm{mm} + G_{ind}^{L2} \tag{4.4}$$

Now, Equation (4.4) clearly shows that only the induced parts of lens L2 are left for correcting the system's spherochromatism. These two induced terms are shown in Equation (4.5).

$$G_{ind}^{L2} = (\bar{y}AXC_{1st}^{L2} - yLAC_{p,1st}^{L2})\frac{4yF}{Hn_L}\gamma_1 + AXC_{1st}^{L2}\frac{yF}{n_L}\gamma_2 \tag{4.5}$$

Due to the fact that the marginal ray height y at the position of L3 equals to zero and considering then Equation (3.100) and (3.101) for the prior summed up 1st-order color aberrations, neither an additional axial color contribution nor an additional lateral color contribution of lens L3 is introduced to the system. With that, the prior summed up color aberrations in front of lens L2 are also maintained and still show the values of $AXC_{1st}^{L2} = 9.7 \times 10^{-4}\,\mathrm{mm}$ and $LAC_{p,1st}^{L2} = 0\,\mathrm{mm}$ like for the two-lens chase. Considering all of these simplifications, the only left parameter, which is changed by inserting the third lens L3, is the chief ray height $\bar{y}_{L2}$ at lens L2. By inserting all of the maintained values into Equation (4.5), the following simple relation is gained.

$$G_{ind}^{L2} = -0.08 \times 10^{-4}\,\mathrm{mm} + 0.21 \times 10^{-4}\,\mathrm{mm}\ \ \bar{y}_{L2} \tag{4.6}$$

Finally, it is easy to see that the remaining overall spherochromatism G_{tot}^{L} of the three-lens system, shown in Equation (4.4), can only be corrected completely, if the chief ray height $\bar{y}_{L2}$ at lens L2 becomes zero. Since this condition is perfectly fulfilled, if the focal length of L3 is exactly $f'_{L3} = 1/2 f'_{L1}$, for the first time the above shown derivation can prove analytical that not only secondary color is corrected, but also spherochromatism is completely vanishing by inserting the additional third lens with half of the focal length of L1 and L2 at the intermediate image. (Figure 4-3 and 4-4)

4.1.4 Catadioptric System

Since the probably most impressive example on induced color aberrations is the simple design, focusing light, coming from infinity, by two elements, a positive spherical lens and a collecting spherical mirror, this kind of system dealing with spherochromatism is now investigated. The design is illustrated in Figure 4-5. Here, the biconvex lens is

made of the high dispersive flint glass NSF6 with an center thickness of 2 mm and radii of $R_1 = -R_2 = 50\,\text{mm}$. The distance to the mirror equals 16mm and the mirror's radius is $R_M = -30\,\text{mm}$. A stop is placed 6 mm in front of the lens and shows a diameter of 10 mm. Furthermore, the light is coming from infinity within a field of view of $\pm 1\,\text{deg}$. For the described case, the primary wavelength is chosen to be $\lambda_1 = 587\,\text{nm}$ with a second wavelength, which is $\lambda_2 = 656\,\text{nm}$.

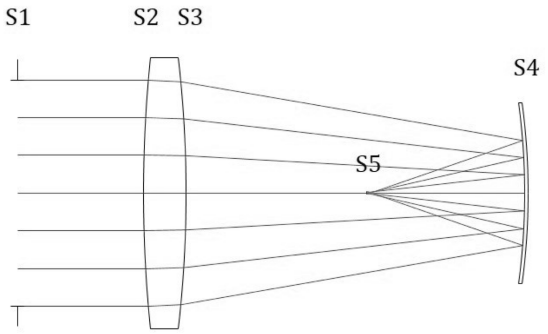

Figure 4-5: Thick meniscus lens with same radii of $R = 15\,\text{mm}$ and a thickness of $t = 10\,\text{mm}$.

Table 4.7 summarizes the Seidel results for the spherical aberration coefficient S_I, gained by two single paraxial ray traces for λ_1 and λ_2. Additionally, the resulting differences are calculated and plotted in the third column. Therefore, the first three columns describe, how spherochromatism contributions where identified in the past. Now, the fourth column represents the 3rd-order spherochromatism values G obtained by Equation (3.89) of this thesis. Hence, for this values, only the ray trace data of the primary wavelength were used and no additional raytrace for the second wavelength was needed. Comparing the results, shows the very high accuracy of G. Please note, the only reason for the remaining error are the small differences in ray heights and ray angles caused by higher order effects of axial and lateral color.

Table 4.7: Seidel wavefront aberration coefficient S_I by two single ray traces and the comparison to the spherochromatic coefficient G.

Surf.	$\boldsymbol{S_{I,\lambda 1}}$ **[mm]**	$\boldsymbol{S_{I,\lambda 2}}$ **[mm]**	$\boldsymbol{S_{I,\lambda 2} - S_{I,\lambda 1}}$ **[mm]**	**G [mm]**
S1	0	0	0	0
S2	−0.001 24	−0.001 23	0.000 01	0.000 01
S3	−0.044 03	−0.042 86	0.001 17	0.001 18
S4	−0.021 01	−0.021 39	−0.000 38	−0.000 38
sum	−0.066 28	−0.065 49	0.000 79	0.000 80

Table 4.8 and Table 4.9 now illustrate the main advantage of Equation (3.89). Besides the above shown benefit of G by following the basic idea of Seidel's approach, as it

ensures the calculation by tracing only the paraxial rays for the primary wavelength, this formula furthermore allows the differentiation of intrinsic and induced parts. These parts considering Equation (3.89) are shown in Table 4.8. In addition, also the prior summed up amounts of AXC_{1st} and $LAC_{p,1st}$ in front of the different surfaces, according to Equation (3.94) and (3.94), are given. For this design example, each of the three system surfaces show a different distribution of intrinsic and induced parts. The first surface of the lens does not exhibit any induced spherochromatism contribution. The whole amount is of intrinsic character. This is caused since it represents the first optical surface of the system, where no 1st-order color aberrations like AXC_{1st} and $LAC_{p,1st}$ could sum up before. Hence, the two terms of Equation (3.89), depending on this, also become zero and only the intrinsic terms, depending on the dispersive behavior of the surface are left. In contrast to this, surface S3 shows both, an intrinsic part of spherochromatism and an induced part. Here, the prior axial color and lateral color of the imaged stop, introduced by surface S2, causes the induced amount of S3. Moreover, also the intrinsic parts are present, since surface S3 is again a lens surface suffering from dispersion. Finally, the mirror surface S4 is the most interesting one. Table 4.7 already showed that S4 is suffering from a chromatic variation of spherical aberration, although this is the mirror surface of the system. Due to the fact that mirrors inherently do not have dispersive characteristics, the input of the mirror surface S4 on spherochromatism was not explainable by any common used 3rd-order theory before. Table 4.8 now gives the reason for this. Since the lens is the only dispersive element in the system, the mirror's spherochromatic behavior is completely caused in front of it by the lens' prior introduced 1st-order lateral color of the imaged stop as well as its axial color aberration. No intrinsic parts are present for S4.

Table 4.8: Wavefront aberration coefficients of the mirror design example for the prior summed up chromatic aberrations AXC_{1st} and $LAC_{p,1st}$ and the intrinsic and induced parts of G.

Surf.	**prior** $\boldsymbol{AXC}$ **[mm]**	**prior** $\boldsymbol{LAC_p}$ **[mm]**	**total** $\boldsymbol{G}$ **[mm]**	**int** $\boldsymbol{G}$ **[mm]**	**ind** $\boldsymbol{G}$ **[mm]**
STOP	0	0	0	0	0
S2	0	0	0.000 01	0.000 01	0
S3	−0.0025	−0.000 05	0.001 18	0.000 91	0.000 27
S4	−0.0089	−0.000 21	−0.000 38	0	−0.000 38
sum			0.000 80	0.000 91	−0.000 11

As an addition, Table 4.9 shows the equivalent longitudinal values of the spherochromatism contributions. Here, the adapted conversion relation of Equation (3.96) was applied. Please note, for the marginal ray angle $u'_{S4_{\lambda}2}$ of the second wavelength, the

calculation according to Equation (3.94) and (3.95), also has to be adapted individually for identifying the intrinsic and induced parts. For example, when determining the intrinsic amounts of G, the AXC_{1st} and $LAC_{p,1st}$ contributions in front of the surface have to be neglected, when calculating the image space sum of AXC_{1st} and $LAC_{p,1st}$ by (3.94) and (3.95), since by definition of the intrinsic parts, all of the color contributions in front of the surface are ignored. Following then the characteristics of induced aberrations, the difference between the total longitudinal amount at the image and the intrinsic longitudinal amount at the image equals the longitudinal induced sum of spherochromatism in image space.
To finally compare the spherochromatism results to the exact longitudinal value of 0.004 58 mm, determined by a real raytrace, Table 4.9 additionally shows the difference between the 3rd-order approximation and the exact value in the last row. Here, again the results are in very good agreement with the actual ray trace results. The main reason for the remaining error of ca. 10% is the 3rd-order approximation of the spherical aberration. The exact value of spherochromatism includes terms of higher-order, which are not considered here. Therefore, for other design examples, where also higher-order spherical aberration is present, such errors may become larger. But for systems with small 5th-order contributions on spherical aberration, the accuracy is as high as shown here.

Table 4.9: Conversation of Seidel's spherical aberration coefficients and of the spherochromatism coefficient G into longitudinal aberrations SPH and GA

Surf.	$\boldsymbol{SPH_{\lambda 2} - SPH_{\lambda 1}}$ **[mm]**	**total** $\boldsymbol{GA}$ **[mm]**	**int** $\boldsymbol{GA}$ **[mm]**	**ind** $\boldsymbol{GA}$ **[mm]**
STOP	0	0	0	0
S2	0.000 01	0.000 01	0.000 01	0
S3	0.006 04	0.006 09	0.004 64	0.001 45
S4	−0.001 77	−0.001 77	0	−0.001 77
sum	0.004 28	0.004 33	0.004 65	−0.000 32
error	−0.000 31	0.000 25		

4.1.5 Split Achromat

The last example to gain a deeper analytical understanding for a simple, but still less analytically discussed lens system is the split achromat.
Figure 4-6 (a) shows a classical achromatic design of two lenses made of NBK7 (crown glass) and NSF5 (flint glass). The focal length is set to be $f' = 100$ mm and the entrance pupil diameter is 20 mm. In literature, the example of a split achromat, exhibited in Figure 4-6 (b), is often showed for correcting spherochromatism, since

the main aberration left for a classical, unsplit achromat is the chromatic variation of spherical aberration [KT02] [Kin12]. The longitudinal aberration plot in Figure 4-7 (a) demonstrates this conditions. Here, spherical aberration of the primary wavelength $\lambda_2 = 587\,\text{nm}$ as well as axial color between $\lambda_1 = 486\,\text{nm}$ and $\lambda_3 = 656\,\text{nm}$ is corrected. But for zonal and maximum pupil height spherical aberration of those two outer wavelengths separate widely and causes still a large on axial spot size. However, the longitudinal aberration plot of the split achromat, shown in 4-7 (b), indicates an additional corrected spherochromatism for the maximal pupil height.
The reason for this are the different numbers of degrees of freedom within the systems. By assuming thin lenses and if the glass combination of the achromat is fixed, the unsplit achromat offers only three degrees of freedom. Those are the three radii of the system. Requiring a certain focal length of $f' = 100\,\text{mm}$, only two additional conditions can be solved. Hence, in case of the achromat shown in 4-6 (a), these conditions are the correction of spherical aberration SPH of the primary wavelength and the correction of axial color AXC.

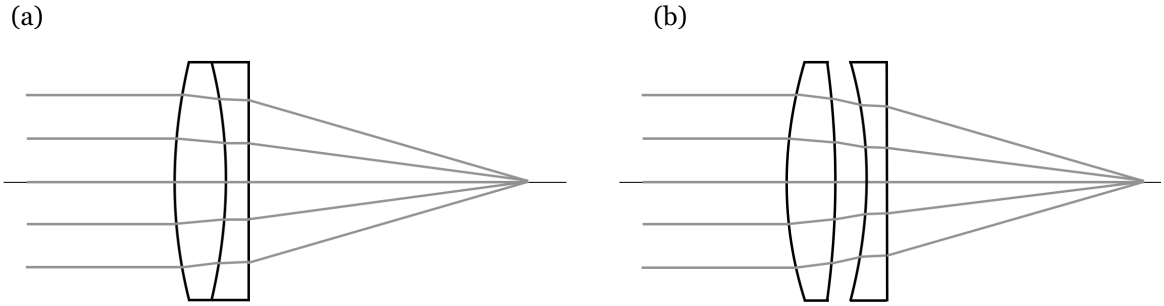

Figure 4-6: (a) a classical unsplit achromat and (b) a split achromat with a air space between the lenses.

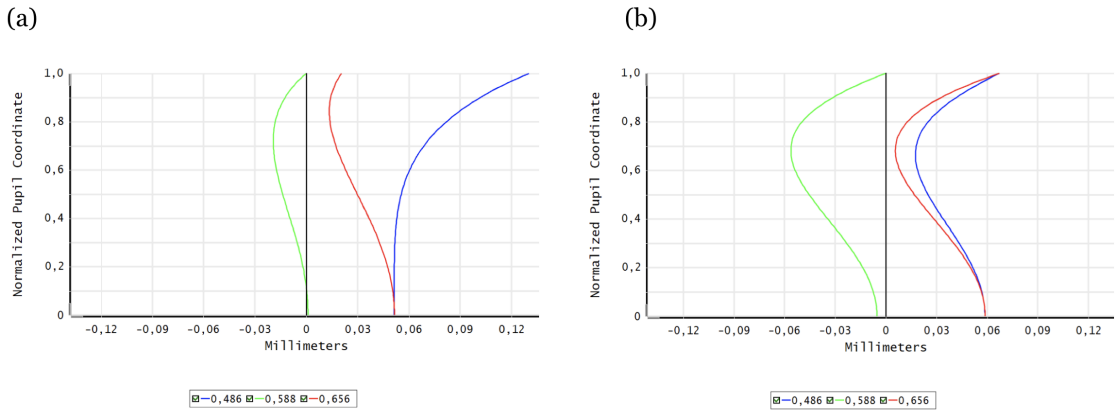

Figure 4-7: Longitudinal aberration plots for (a) the classical unsplit achromat and (b) the split achromat with a air space between the lenses. The first, positive lens is made of NBK7 and the second, negative lens of NSF5.

In case of spherical aberration, the longitudinal aberration plot also illustrates the

existence and the need of higher order spherical aberration for correction. This can be proven, since its longitudinal dependency on pupil height is not only of lowest, quadratic character. For large pupil heights, higher order spherical aberration terms enable the reversal of the graph and therefore the correction of spherical aberration for maximum pupil height. Consequently, only the sum of 3rd- and higher-order spherical aberration leads to a corrected overall spherical aberration. In literature, Buchdahl [Buc54] and Rimmer [Rim63] derived a 5th-order surface contributions for monochromatic aberrations, assuming the same ray based approach like Seidel. Here, 5th-order spherical aberration is named $B5$ and will be applied here. Its explicit formula given by Buchdahl and Rimmer can be found in the appendix.
Therefore, regarding the unsplit achromat, the three condition, which can be solved, are:

$$f' = 100mm \tag{4.7}$$

$$AXC = \sum_{S1}^{S3} C_1 = \sum_{S1}^{S3} niy\left(\frac{\Delta n'}{n'} - \frac{\Delta n}{n}\right) = 0 \tag{4.8}$$

$$SPH = \sum_{S1}^{S3} S_I + B5 = \sum_{S1}^{S3} n^2 i^2 y\, \Delta\left(\frac{u}{n}\right) + \sum_{S1}^{S3} B5 = 0 \tag{4.9}$$

By applying paraxial relations (Section 2.1) and solving this system of equations for the given glass combination of NBK7 and NSF5, an achromat with the following radii $R1, R2$ and $R3$, axial color as well as spherical aberration contributions is obtained. (Table 4.10)

Table 4.10: Numerical solution for three variable radii $R1, R2$ and $R3$ of the unsplit achromat. The Seidel contributions for axial color AXC and 3rd-order spherical aberration S_I as well as the Buchdahl-Rimmer 5th-order contributions $B5$ are given.

Surf.	$\boldsymbol{R}$ **[mm]**	**Glass**	$\boldsymbol{AXC}$ **[mm]**	$\boldsymbol{S1}$ **[mm]**	$\boldsymbol{B5}$ **[mm]**
S1	54.864	NBK7	−0.009 68	0.013 60	−0.000 26
S2	−48.365	NSF5	0.029 20	−0.031 26	0.002 11
S3	−176.850		−0.019 52	0.019 08	−0.000 43
sum			0.000	0.0142	−0.0142

Here, the perfect correction of 1st-order axial color AXC and spherical aberration SPH, including 3rd-order and 5th-order contributions, are shown.
Comparing those results with optimized values by a damped least squares algorithm, the exact radii would be $R1 = 54.480\,\text{mm}, R2 = -48.668\,\text{mm}$ and $R3 = -180.963\,\text{mm}$ to fulfill the conditions of $f' = 100\,\text{mm}$, a corrected axial color and a corrected spherical

aberration. Compared to the values of the Table 4.10, there are only small differences left, which verifies the above described approach. Furthermore, these differences indicates an additional, but small presents of even higher spherical aberration orders.
Now, due to the new surface resolved spherochromatism formula found in Section 3.4, the same approach can be followed for the first time also for a split achromat. The advantage of the split achromat design is the larger number of degrees of freedom by introducing the additional air space. Hence, two more variables within the system are generated, the size of the air space and the extra fourth radius. Regarding the additional correction of spherochromatism G, only one extra variable is required. A second one could be assumed to minimize also zonal spherical aberration by introducing even higher order spherical aberration terms. But this will not be investigated here. Consequently, one radius given from the unsplit achromat can be fixed and the remaining three radii as well as the air space are set to be variable. Therefore, in case of the split achromat, these four conditions, now including spherochromatism G, have to be solved:

$$f' = 100mm \tag{4.10}$$

$$AXC = \sum_{S1}^{S3} C_1 = \sum_{S1}^{S3} niy\left(\frac{\Delta n'}{n'} - \frac{\Delta n}{n}\right) = 0 \tag{4.11}$$

$$SPH = \sum_{S1}^{S3} S_I + B5 = \sum_{S1}^{S3} n^2 i^2 y\, \Delta\left(\frac{u}{n}\right) + \sum_{S1}^{S3} B5 = 0 \tag{4.12}$$

$$\begin{aligned} G = \sum_{S1}^{S3} & (\bar{y} AXC_{1st} - yLAC_{p,1st}) \frac{4in}{H}(u-u')(i+u') \\ & - AXC_{1st}(u-u')(u'-3u-4i') \\ & - \Delta niy\big((u'-u)^2 - (i'+u')^2 + u(i'+u')\big) \\ & - \Delta n' i'^2 y(i'+u') = 0 \end{aligned} \tag{4.13}$$

The numerical results, found by solving this system of four equations assuming the given glass combination of NBK7 and NSF5, can be found in Table 4.11. The four variables are $R2, R3$, $R4$ and the size of air space t in between both lenses. $R1$ is kept as $R1 = 54.480\,\mathrm{mm}$.
For the first time, the results shown in Table 4.11 analytically confirm the well-known and often discussed possibility to correct also Spherochromatism, besides axial color and spherical aberration, by applying an additional air space between both lenses of an achromat.
Although, the longitudinal plots of Figure 4-7(b) may constitute the need of considera-

tions for even higher-order Spherochromatism, again a comparison to optimized values by a damped least squares algorithm approves the here applied approach. The exact radii found by this are $R1 = 54.480\,\text{mm}$, $R2 = -38.972\,\text{mm}$, $R3 = -32.522\,\text{mm}$ as well as $R4 = -103.775\,\text{mm}$ and the optimized air space is $t = 4.505\,\text{mm}$. The differences to the values of Table 4.11 are still small, which indicates a present but still almost negligible influence of higher orders. Hence, the main correction effects are excepted to be caused by 3rd-order spherochromatism.

Table 4.11: Numerical solution for three variable radii $R2, R3$, $R4$ and a variable air space thickness t of the split achromat. The Seidel contribution for axial color AXC and 3rd-order spherical aberration S_I as well as the Buchdahl-Rimmer 5th-order contributions $B5$ and the Spherochromatism contributions G are given.

S	$\boldsymbol{R}$ **[mm]**	$\boldsymbol{t}$ **[mm]**	**Glass**	$\boldsymbol{AXC}$ **[mm]**	$\boldsymbol{S_I}$ **[mm]**	$\boldsymbol{B5}$ **[mm]**	$\boldsymbol{G}$ **[mm]**
S1	54.48	0	NBK7	−0.0098	0.0139	−0.0003	0.0001
S2	−36.06	5.612		−0.0274	0.5234	−0.0948	0.0171
S3	−28.50	0	NSF5	0.0586	−0.5758	0.0861	−0.0171
S4	−87.93	100		−0.0215	0.0300	0.0006	0.0001
sum				0.000	−0.0085	−0.0084	0.000

Furthermore, the new surface contributions also enables an deeper understanding, why and how the correction is possible. The main contributions on spherochromatism are clearly found at both inner surfaces, S2 and S3. Here, S3 exactly cancels out the contribution of S2. Furthermore, these are those two radii, which are directly in contact with the additional variable air space between the two lenses. The first and the last surface, S1 and S4, almost do not contribute at all.

Following that finding, a complementary investigation for the other three design versions, where $R2, R3$ and $R4$ are kept, showed that solutions also can be found for a fixed $R2$ and $R4$, but by fixing $R3$ there is no existing solution solving the system of the four equations. Therefore, to complete the understanding on why and how the correction of spherochromatism works within this design, Table 4.12 shows the separation of induced and intrinsic spherochromatism contributions for the same case like Table 4.11.

Emphasizing the dominating role of S3, the analysis of Table 4.12 also shows the induced part to be the main contributor for surface S3. Hence, to understand how the additional air space can correct spherochromatism, the three variable radii R2, R3 and R4 are again assumed to solve the conditions of the focal length to be $f' = 100\,\text{mm}$, a corrected axial color and a corrected spherical aberration like for the unsplit case. Now, the thickness t of the air space is left to enable the correction of spherochroma-

tism G. Since this is only possible due to induced effects of surface S3, the optimum thickness t of the airspace is strongly connected to the prior introduced lower order color aberration of the system before and the radius $R3$ of surface S3. Following that and considering the results of Table 4.12, the single, exact solution for t only is found, if the induced part of S3, caused by the prior introduced color aberration of the first lens, plus the intrinsic part of S3, caused by the radius $R3$, exactly cancels out the spherochromatism contributions introduced by the first lens.

Table 4.12: Numerical solution for three variable radii $R2, R3$, $R4$ and a variable air space thickness t of the split achromat. The spherochromatism contributions G and its intrinsic as well as its induced parts are given.

S	$\boldsymbol{R}$ **[mm]**	$\boldsymbol{t}$ **[mm]**	**Glass**	$\boldsymbol{G}$ **[mm]**	**int** $\boldsymbol{G}$ **[mm]**	**ind** $\boldsymbol{G}$ **[mm]**
S1	54.80	0	NBK7	0.0001	0.0001	0.0000
S2	−36.06	5.612		0.0171	0.0136	0.0035
S3	−28.50	0	NSF5	−0.0171	−0.0064	−0.0107
S4	−87.93	100		0.0001	0.0016	−0.0015
sum				0.000	0.009	−0.009

4.2 Complex Design Example - A Microscope Objective Lens

Compared to the classical and to same extend academic design examples of Section 4.1, now a more complex microscope objective lens is investigated. Although the simple design examples are best for understanding the characteristics and possible influence of 2nd-order induced and intrinsic color aberrations, a more complex design example shows a higher relevance for the practical work of an optical designer. Here, very often systems of many lenses within compact arrangements and a multitude of possible glass combinations are present. Especially for those systems, a surface resolved analysis can be the key method to find out the inner workings of the optical system and to understand why the present left aberrations arise at the final image plane.

4.2.1 Design Specifications

Microscope objectives represent a special kind of optical systems. They are essentially diffraction-limited optical devices with small object fields, but extremely high numerical apertures in object space. Therefore, microscope lenses are usually characterized

by their magnification factor and their object sided numerical aperture. The here investigated system was described in the patent DE102008006826A1 [BSW]. It is a 40x objective lens with a numerical aperture of NA=1.3 and oil immersion. A lens drawing is shown in Figure 4-8.

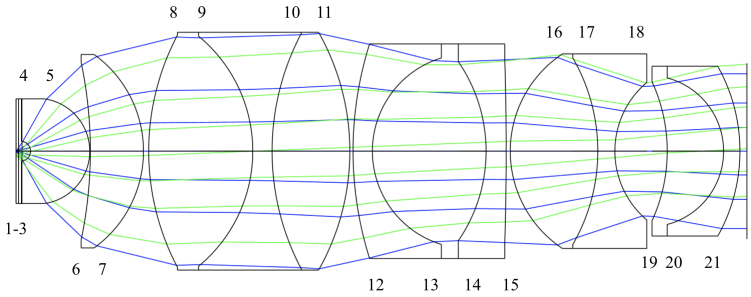

Figure 4-8: Lens drawing of the microscopic lens. [BSW]

The patent claims the system to be especially optimized for correcting axial color within a wide wavelength range from 425 nm to 800 nm. The plot shown in Figure 4-9 was taken from the patent and represents its axial color aberration within this wavelength range. Instead of paraxial focus variations, the patent refers to wavefront aberrations analysis for different wavelengths. The defocus of the best image plane can be approximated by the so-called Nijboer-Zernike wavefront aberration coefficient A_{02} [Gro05]. Here, the Nijboer Zernike wavefront aberration coefficient A_{02} for defocus is plotted over wavelength. Following the Marechal criteria for this index A_{02}, all deviations within ± 0.447 would guarantee a diffraction limited imaging, as long as no other aberrations are present [Gro05]. Hence, for this design a wavelength range from about 475 nm up to 700 nm could be diffraction limited imaged on axis.

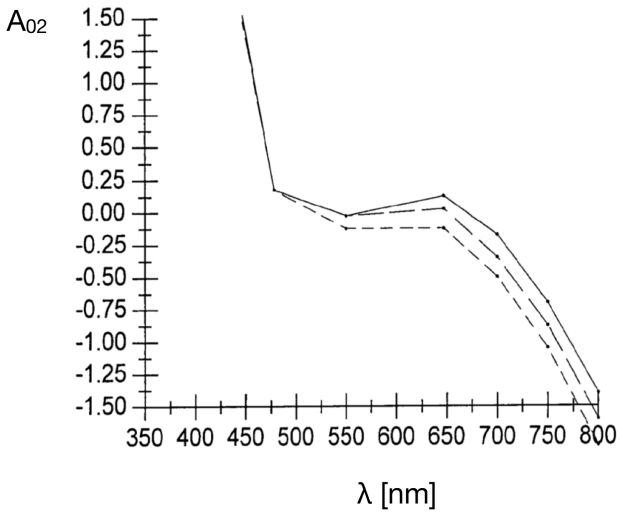

Figure 4-9: Axial color aberration represented by the Zernike wavefront aberration coefficient for defocus A_{02} from 425 nm to 800 nm. [BSW]

Please note, for this plot, a tube lens with a focal length of 164.5 mm, also mentioned in the patent, was positioned in a distance of 126.5 mm. The tube lens parameters were taken from [War19] and also include an additional 80 mm NBK7 glass block. This combination of microscope objective lens and tube lens enables the magnification of 40x. Although, the patent claims a numerical aperture of NA=1.3, a detailed analysis of the system showed that this microscope lens performs well and almost diffraction limited for a reasonable object field of 0.5 mm and a numerical aperture of NA=1.0 within a wavelength range of 450 nm to 700 nm. A lens drawing of the total design is shown in Figure 4-10 and the summary of the most important performance plots is represented by Figure 4-11.

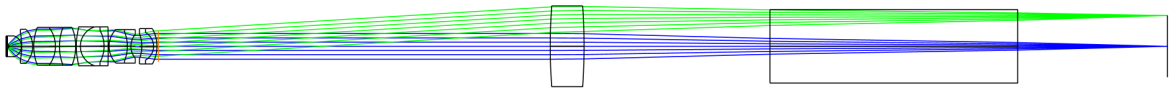

Figure 4-10: Lens drawing of the microscopic lens described in [BSW] combined with a standard tube lens package, described in [War19].

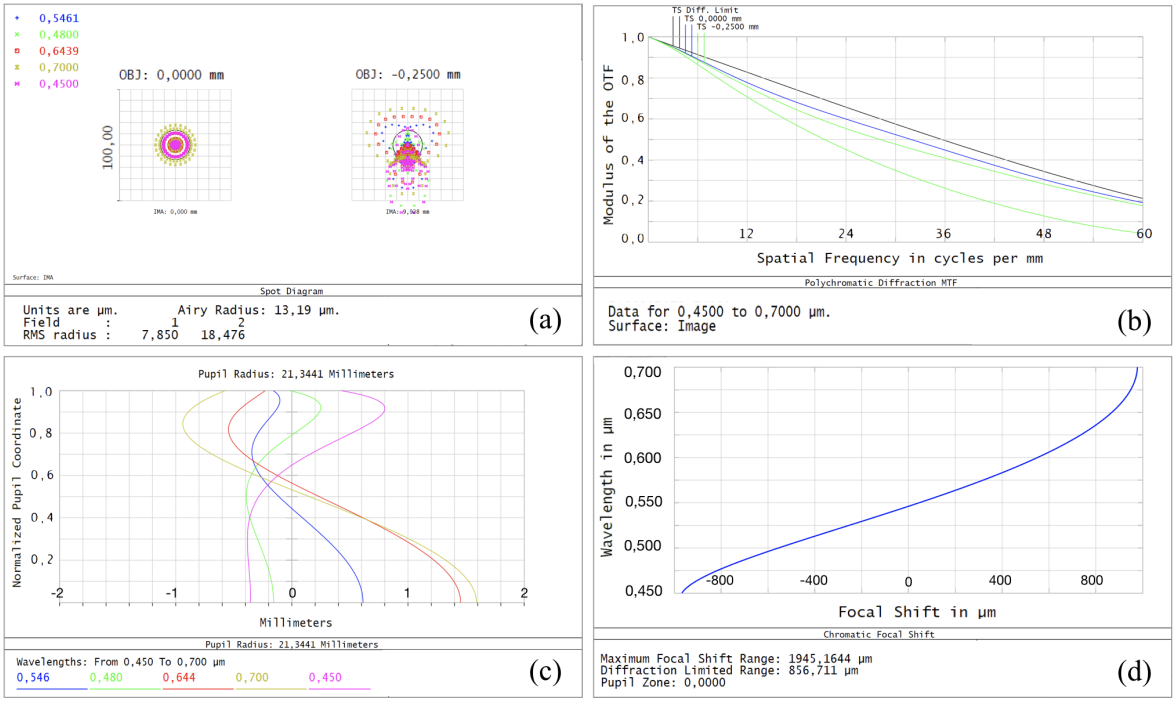

Figure 4-11: Optical Performance plots of the microscopic lens at $NA = 1.0$ (a) Spot diagram, (b) polychromatic MTF, (c) Longitudinal aberration plot and (d) paraxial chromatic focus shift

4.2.2 Design Analysis

The spot diagram in Figure 4-11(a) and the polychromatic MTF plot in Figure 4-11(b) confirm the very high optical performance of the lens. Especially the on axis field point shows an almost perfectly corrected spot. The root mean square (RMS) spot radius is 7.85 µm and therefore less than the Airy disc radius of 13.9 µm (for 546 nm), in which the diffraction limited resolution is guaranteed. The RMS field point spot size is 18.5 µm. Hence, also a very high resolution over the whole field was achieved. This behavior is again verified by the polychromatic MTF plot, where both field points are very close to the theoretical resolution limit.

The most significant plot for the design is the longitudinal aberration diagram. Here, the idea of correction can be seen. Since microscopic lenses are characterized by their high numerical apertures and small object fields, the most critical aberrations are axial color, spherical aberration and spherochromatism. In most cases, the only way to correct spherical aberration for such a high aperture system is to find the best interaction between 3rd-order and 5th- or even higher order spherical aberration parts. For the patent design, it can be seen that up to a numerical aperture of NA=0.5 a parabolic behavior and therefore a 3rd-order behavior is dominant for all wavelengths. For aperture rays higher than NA=0.5 a first or even a second inflection point is present. At these inflection points higher-order aberration become dominant and enable a balancing of the lower order aberration parts. It should be noted, since higher order aberrations always lead to increased sensitivities of the design, its presence and its amounts should always be reduced as best as possible by ensuring a high correction of 3rd-order aberrations up to a high NA, like it was done here. By means of the work of Buchdahl [Buc54], Rimmer [Rim63], Hoffman [Hof93] and Sasian [Sas10] the here present balancing of 3rd-, 5th- and 7th-order spherical aberration amounts, can completely be analyzed surface by surface through the design.

Now, within a considerable wavelength range like for the patent case, not only spherical aberration but also axial color and spherochromatism become performance critical aberrations. This was especially addressed within the patent. Here, the available analyzing tools for an optical designer are more limited and sometimes even less helpful to understand the system's way of color correction. For instance, usually first of all the chromatic focus shift plot, shown in Figure 4-11(d), and a Seidel analysis for axial color are investigated. In case of the microscope objective lens, the Seidel diagrams for axial color of the outer wavelength 450 nm to 700 nm and of secondary color from 450 nm to 546 nm are shown in Figures 4-12 and 4-13, respectively.

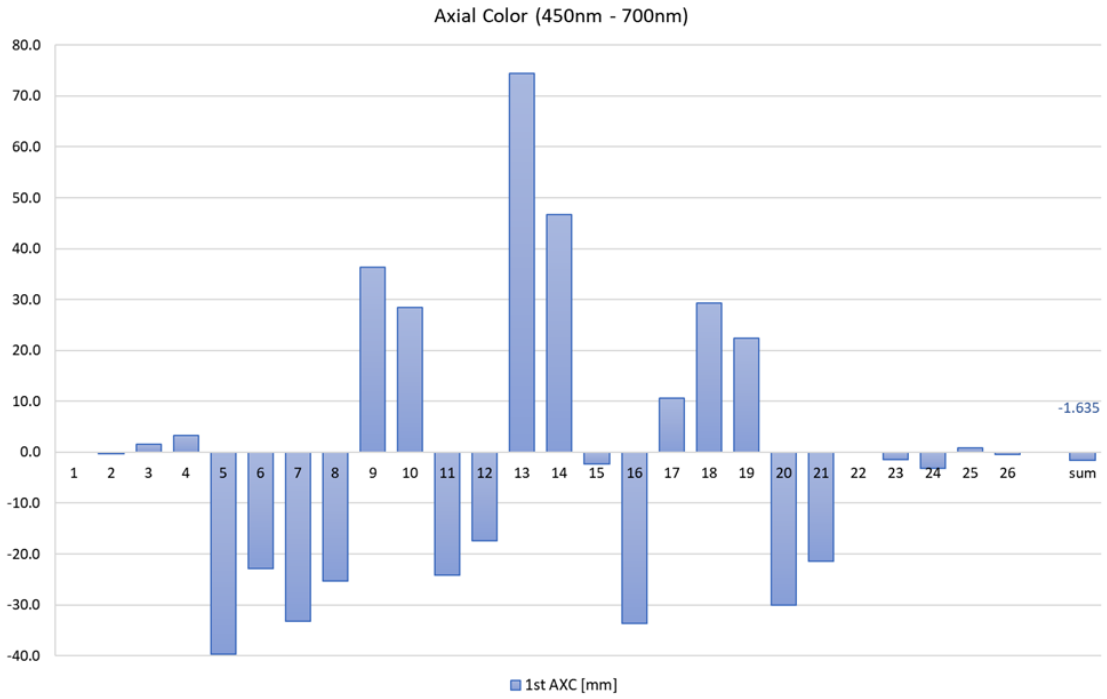

Figure 4-12: Longitudinal Seidel surface coefficients of axial color (1st AXC) for 450 nm and 700 nm. Surface numbers 1 to 3 are immersion surfaces. Surface numbers from 4 to 21 and 23 to 26 are the microscopic lens surfaces and the tube lens with glass block, respectively. The last bar shows the sum over the total system and its exact values above.

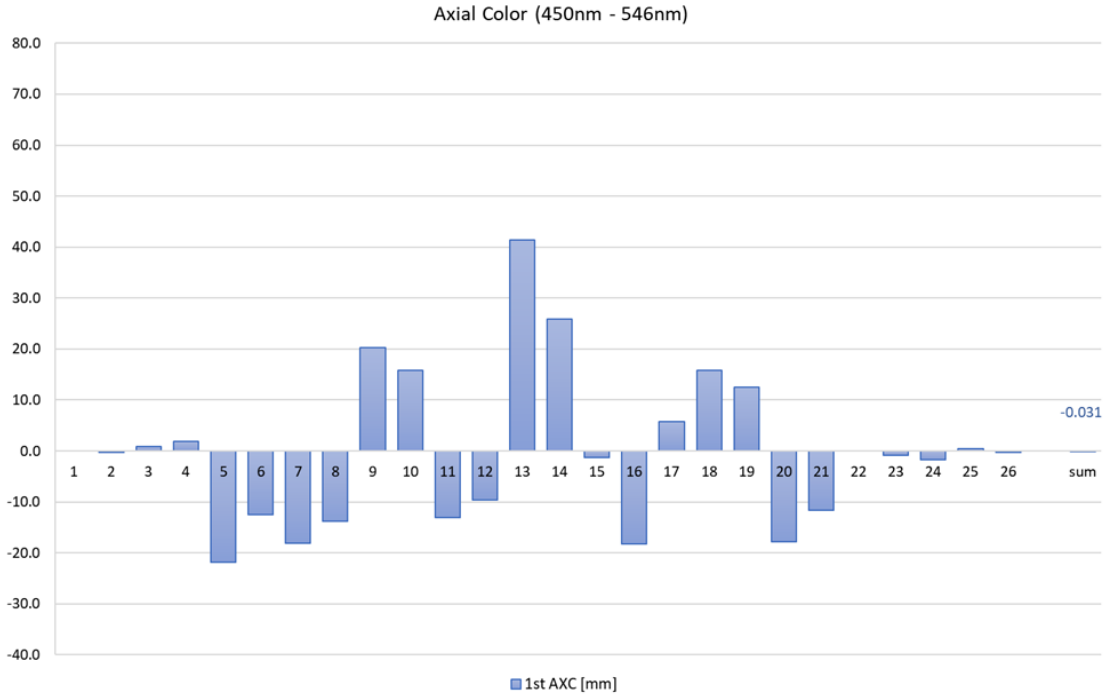

Figure 4-13: Longitudinal Seidel surface coefficients of axial color (1st AXC) for 450 nm and 546 nm. Surface numbers are the same as in Figure 4-12.

Here, a first misleading result can be found. By comparing the results of the chromatic focus shift plot to the longitudinal Seidel coefficients, a large deviation of the final axial color amounts can be found. Since the focus shift plot is based on a paraxial raytrace, its values are expected to be reproduced by the Seidel analysis. But in case of the microscopic lens, the Seidel analysis gives a total amount of $-1.635\,\text{mm}$ instead of $-1.945\,\text{mm}$ for 450 nm to 700 nm and even only $-0.031\,\text{mm}$ instead of $-0.968\,\text{mm}$ for 450 nm to 546 nm. Hence, for this design the standard Seidel analysis is not a reliable analyzing tool.
Furthermore, by investigating the paraxial chromatic focus shift plot of Figure 4-11(d) in detail, its result moreover does not meet the exceptions for a diffraction limited design and the corresponding axial color plot of the patent in Figure 4-9. Similar to the Airy disk diameter for the spot size, the Rayleigh length describes the longitudinal range within a diffraction limited imaging is possible [Gro05]. Since the Rayleigh length for the microscopic design amounts 0.87 mm, only a very narrow wavelength range of 510 nm up to 580 nm would be diffraction limited following the chromatic focus shift diagram. Therefore, the interpretation of this plot strongly deviates from the statement of the axial color aberration diagram of the patent, shown in Figure 4-9, which indicates a diffraction limited imaging from about 475 nm up to 700 nm. In consequence, this way of analyzing, by only considering the paraxial focus shift, seems to be not enough, since it contradicts the Rayleigh length criteria as well as the statement of the axial color plot taken from the patent.

4.2.3 Improved Analysis by the New Theory

Now, to overcome these misleading results of the two standard analyzing tools a lens designer can work with, the new surface contribution formulas, found in this thesis, have to be applied. They provide more reasonable results and give an additional deeper understanding on how this microscopic lens design works.
At first, the 1st-order Seidel coefficient results of Figure 4-12 and 4-13 for the longitudinal axial color contributions can be extended by their 2nd-order axial color amounts. For this purpose, the surface contribution formula (3.18) of Section 3.2 converted to its longitudinal description by the conversion factor $1/2nu'^2$ gives the following, new axial color surface contribution plots.
Comparing these results to the real, raytrace based axial color plot, this extension of the standard 1st-order Seidel analysis tool with their 2nd-order contributions now provides a reliable surface resolved analysis for axial color.

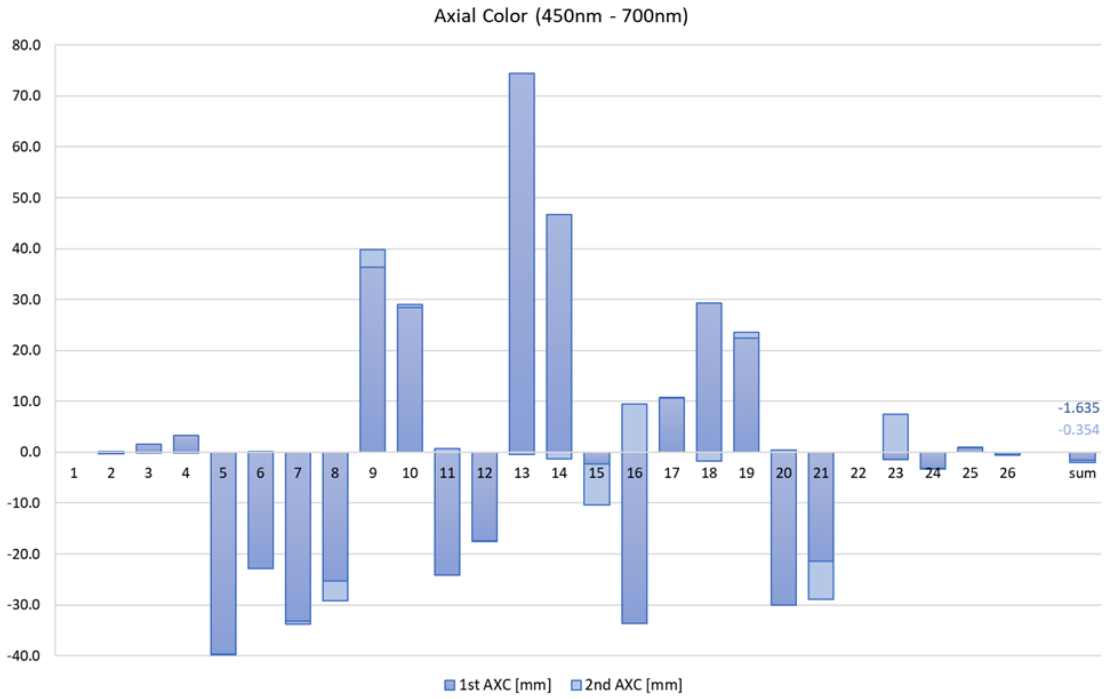

Figure 4-14: Longitudinal Seidel surface coefficients of axial color including 1st- and 2nd-order contributions for 450 nm and 700 nm. Surface numbers 1 to 3 are immersion surfaces. Surface numbers from 4 to 21 and 23 to 26 are the microscopic lens surfaces and the tube lens with glass block, respectively. The last bar shows the sum over the total system and its exact values above.

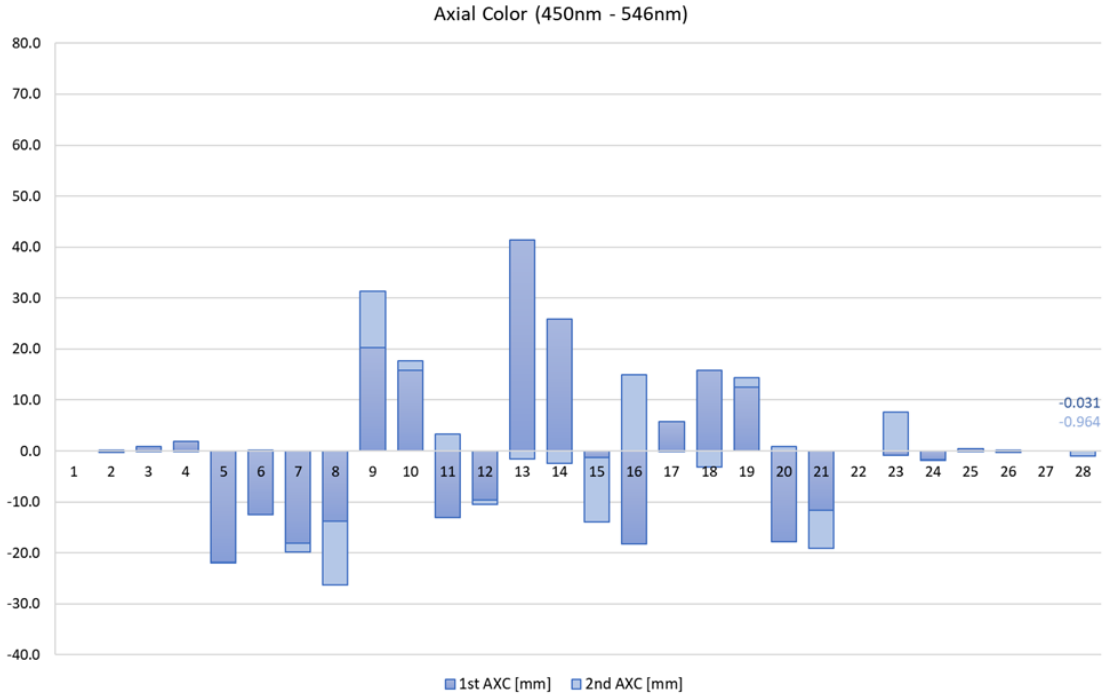

Figure 4-15: Longitudinal Seidel surface coefficients of axial color including 1st- and 2nd-order for 450 nm to 546 nm. Surface numbers are the same as in Figure 4-14.

Considering the plots of Figure 4-14 and 4-15 , the new surface coefficient analysis now gives a total amount of $-1.989\,\mathrm{mm}$ for $450\,\mathrm{nm}$ to $700\,\mathrm{nm}$ (instead of $-1.945\,\mathrm{mm}$ by raytrace) and $-0.995\,\mathrm{mm}$ for $450\,\mathrm{nm}$ to $546\,\mathrm{nm}$ (instead of $-0.968\,\mathrm{mm}$ by raytrace). This reduces the error of the total axial color amount at the image plane for both plots to less than 3%.
Furthermore, a larger influence of the 2nd-order terms on secondary spectrum than on the outer wavelengths is in evidence. This effect was already described by Wynne [Wyn78], Rogers [Rog13b] and Nobis [Nob15]. It is due to the fact that the 2nd-order color aberration parts introduce an additional bowing to the chromatic focal shift, which is essentially expressed as secondary color and can now be quantitatively recovered in Figure 4-15. In case of the microscopic lens, the 2nd-order parts account more than 96% of the final axial color value.
However, the most significant effect, when adding the 2nd-order terms to the 1st-order terms, is found in how the single surface contributions, their relation to each other and their relative input to the overall correction of axial color change. For instance, if only 1st-order Seidel contributions would be considered, surface 16 is the second largest negative contributor for secondary color and plays an important role for the overall correction. But by introducing 2nd-order parts, the contribution of surface 16 is almost completely canceled out. In contrast to this, the influence of surface 8 changes from one of the weakest negative contributors to the strongest one, since it is almost doubled by the 2nd-order part. Similar to these two examples, also the surfaces 9 and 15 suffer from comparable changes. Please note, besides the impact to the microscopic lens also the tube lens (surfaces 23-24) is affected by 2nd-order terms. Instead of being almost neglectable according to 1st-order, the tube lens does show a relevant contribution to the overall color correction. This kind of color correction concept is characteristic for the here shown microscope system designed by the company ZEISS and would not be visible without 2nd-order.
Hence, the new extended analyzing tool reproduces the values of raytrace based chromatic focus shift plot correctly, shows the right single surface contributions, how they are balanced by a strong negative front and rear group with a mainly positive acting middle group, and gives the correct relative input to the overall color correction at the final image plane.

Now, the second misleading result of the standard analyzing tools is addressed. Here, the inconsistency of the paraxial chromatic focus shift plot compared to the Rayleigh length criteria and the proven diffraction limited imaging over the total wavelength range has to be solved. Since the axial color plot, taken from the patent 4-9, confirms the high performance of the system, the differences between both plots were investigated. Following that, the reason for the contradiction can be found in the definition

of the Zernike polynomials. The advantage of describing wavefront aberrations with several Zernike polynomials is that here the highest order is always balanced by the lower orders by definition. Hence, e.g. for defocus, which was plotted in the patent, the A_{02} coefficient describes the best defocus considering also the present spherical aberration within the system. Transferring that considerations, the paraxial chromatic focal shift plot is not wrong, but it is simply not enough to understand and to explain, how the microscopic design can be diffraction limited for all wavelengths. In order to achieve this, it is essential to evaluate not only the pure paraxial chromatic defocus, but also its balancing by the chromatic variation of spherical aberration. This additional information about spherochromatism contributions can now be provided by the new surface contribution formula (3.89), described in Section 3.4.2.
It should be noted, that in general, 3rd-order Seidel aberrations coefficients cannot be calculated from the corresponding Zernike coefficients. Only in case if there are no higher aberrations than 3rd-order, a correlation between Seidel and Zernike coefficients can be found [Gro05]. Hence, to ensure no higher aberration orders are present and therefore a correlation to the Zernike coefficient can be found, this analysis operates with a maximum numerical aperture of NA=0.5. The corresponding pupil height is marked in Figure 4-16.

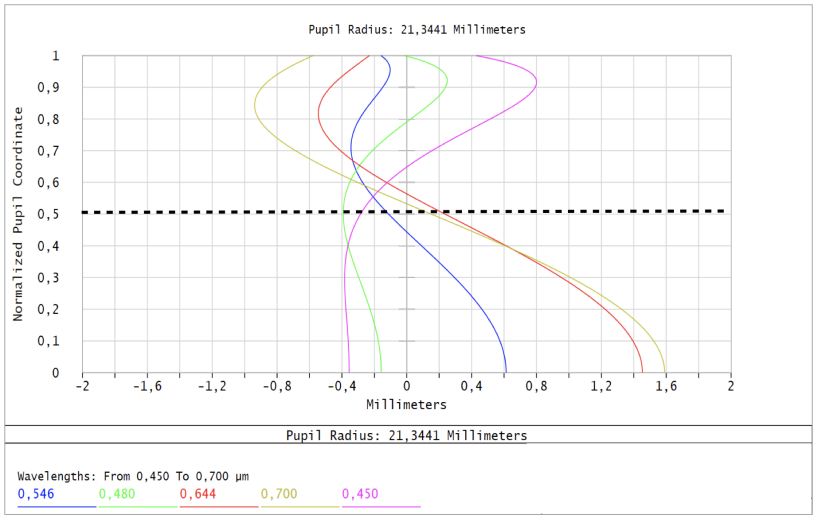

Figure 4-16: Longitudinal aberration plot of the microscopic lens.

Figure 4-17 and Figure 4-18 now show the surface resolved diagrams including 1st-order and 2nd-order axial color coefficients as well as the spherochromatism coefficients GA for the outer wavelengths 450 nm to 700 nm as well as for secondary color from 450 nm to 546 nm.

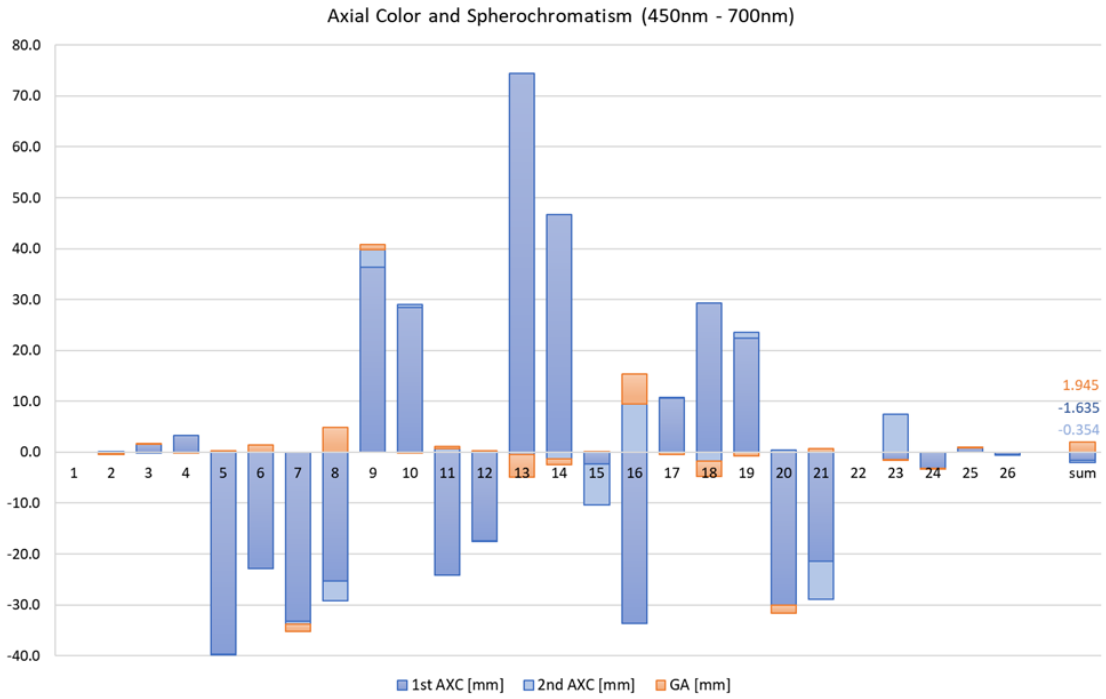

Figure 4-17: Longitudinal surface coefficients including axial color (1st- and 2nd-order) and spherochromatism (GA) for 450 nm to 700 nm. Surface numbers 1 and 3 are immersion surfaces. Surface numbers from 4 to 21 and 23 to 26 are the microscopic lens surfaces and the tube lens with glass block, respectively.

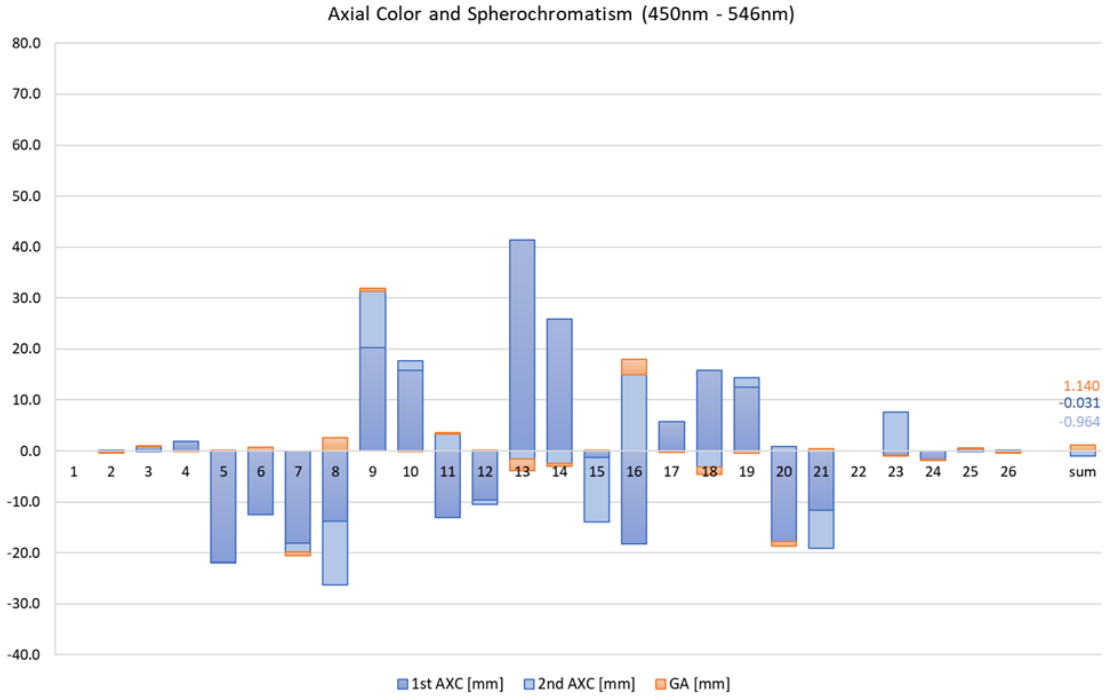

Figure 4-18: Longitudinal surface coefficients including axial color (1st- and 2nd-order) and spherochromatism (GA)for 450 nm and 546 nm. Surface numbers are the same as in Figure 4-17.

These two new plots illustrate descriptively the compensation and balancing effects of axial color and spherochromatism through the whole optical system and at the final image plane. Although the single surface contributions of spherochromatism are much smaller than the axial color ones, they finally reach a relevant amount at the image plane. This is caused by their signs, since for almost all surfaces the spherochromatism parts show the opposite sign than the axial color ones. In both cases, adding up the spherochromatism contributions leads to an total sum of 1.945 mm for 450 nm to 700 nm and 1.140 mm for secondary color, which balances the corresponding large axial color values of -1.989 mm and -0.995 mm to a final color contribution smaller than the Rayleigh length.

Although this new way of analyzing the on axis chromatic errors can only be applied within an numerical aperture, where no higher aberrations than 3rd-order are present, this analyzing tool finally explains how the microscopic lens works. Only the combination of axial color and spherochromatism enables the diffraction limited imaging. The new plots demonstrate descriptively how they are balanced and where the dominating surfaces and lenses are. Comparing this to the misleading standard Seidel surface coefficient plot, these extended analysis now enables the optical designer to understand the microscopic system and to find the best surfaces or lenses to even improve the design. For example, as stated before, since higher order aberrations always lead to increased sensitivities of the system, its present and its amounts should always be reduced as best as possible by ensuring a high correction of 3rd-order aberrations up to a high NA. This design goal now can directly be addressed by optimizing the system to compensate the here plotted axial color and spherochromatism for a even larger numerical apertures, e.g. NA=0.6.

Finally, to complete the detailed analysis of the microscopic lens, the new found surface description not only allows to analyze the relation between 1st- order and 2nd-order axial color as well as spherochromatism, it also enables the designer to distinguish between intrinsic and induced aberration parts. The corresponding diagrams for secondary color are shown in Figure 4-19 and 4-20 for axial color and spherochromatism, respectively.

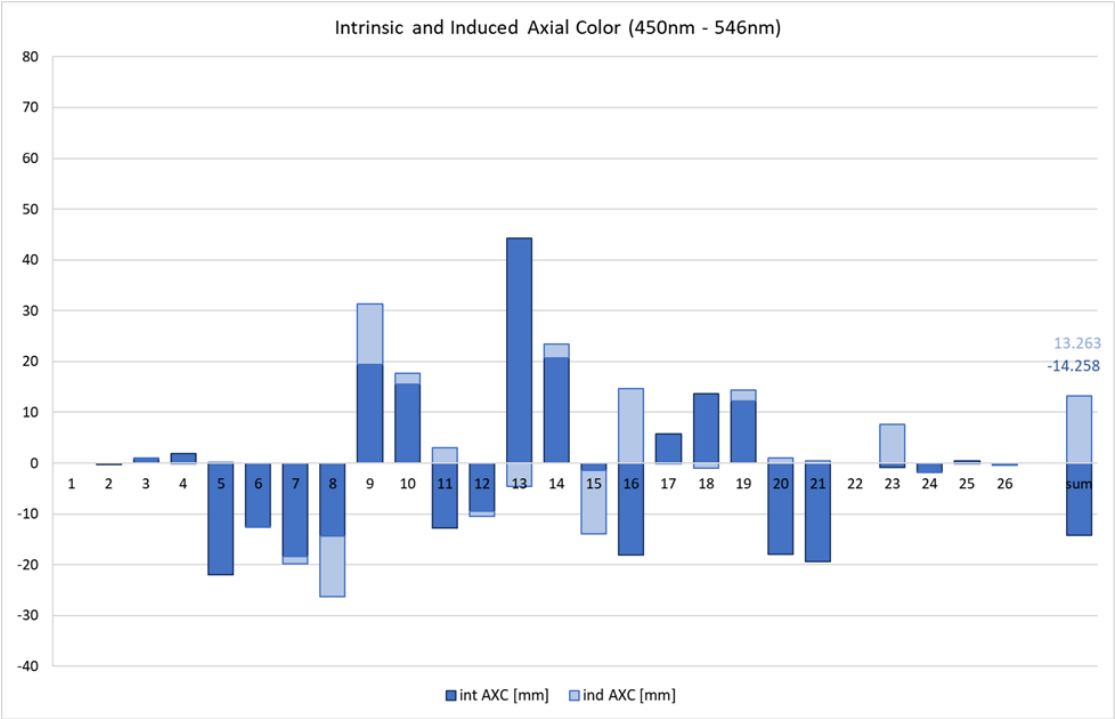

Figure 4-19: Longitudinal surface coefficients of axial color, distinguishing between intrinsic and induced aberration parts. Surface numbers 1 and 3 are immersion surfaces. Surface numbers from 4 to 21 and 23 to 26 are the microscopic lens surfaces and the tube lens with glass block, respectively.

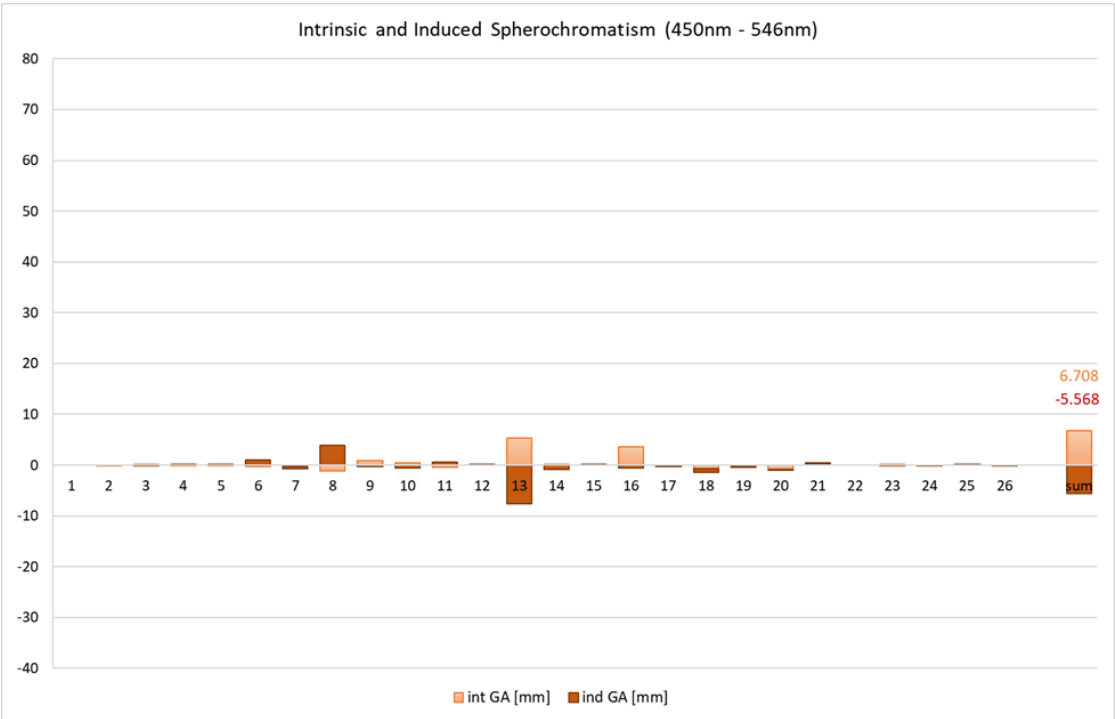

Figure 4-20: Longitudinal surface coefficients of spherochromatism, distinguishing between intrinsic and induced aberration parts. Surface numbers are the same as in Figure 4-19.

The here shown diagrams demonstrate clearly the high influence of induced aberrations on the performance of the microscope lens. Especially for axial color, some induced parts reach out almost the same amounts as the intrinsic ones or as for surface 15 and 23 also exceed them. The most impact of induced axial color aberrations can be found within the middle part of the microscopic objective from surface 8 to 16. Since the first three lenses of the objective essentially correct spherical aberration, implying high refractive glasses and meniscus shaped lenses, a large amount of 1st-order axial color sum up within this front group. This introduced 1st-order axial color generates the prominent induced color aberration amounts within the middle group. However, the induced parts of the tube lens is not directly a consequence of a very large 1st-order axial color summed before in the microscopic objective, but it is mainly caused by the huge distance between the microscope and tube lens. Hence, although the prior summed axial in front of the tube lens is relatively small, the separation of wavelength at the first surface of the tube becomes comparable large to the separation at surface 8, which is the first surface of the middle group. Figure 4-21 shows, how the wavelengths are separated at surface 8 and the tube lens.

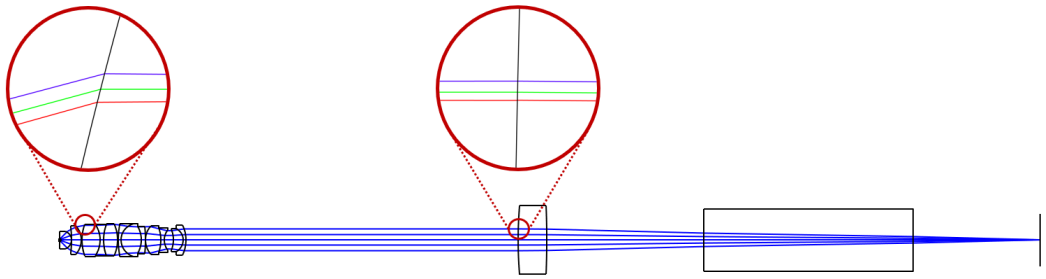

Figure 4-21: Separation of the different wavelengths at the first surface of the middle group of the microscopic lens as well as at the first surface of the tube lens.

Regarding spherochromatism, the influences of the induced aberrations are comparable small to the axial color ones. Mainly, surface 8 and surface 13 show a relevant amount. The reason for surface 8 can again be found in the large prior summed up 1st-order axial color. However, surface 13 shows no noticeable amount for induced axial color, but for spherochromatism this is the strongest contributor for induced and intrinsic parts. The explanation is found in the large incident angles i at this surface, which can also be seen in Figure 4-8. Here, surface 13 is the cemented surface of the second triplet, which is extremely bent. Since the induced as well as the intrinsic terms are linear depending on i, this extremely bent cemented surface is the key surface for spherochromatism and has to be observed very carefully during an optimization process.
Finally, at the image plane, for both aberrations, axial color and spherochromatism, the intrinsic and the induced parts are well balanced. Therefore, the overall diffraction limited performance can again be seen here.

5 Summary

The major focus of this work was devoted to the investigation of higher-order color aberrations and their induced and intrinsic aberration parts. In analogous manner to the monochromatic aberrations, lower-order aberrations, picked up surface by surface in the preceding optical system, generate induced aberrations of higher order. However, contrary to monochromatic aberrations, induced influences of color aberrations are already observable in the paraxial regime, since even paraxial rays are affected by dispersion.

Consequently, at first a new classification of aberration orders was introduced in thesis, since, in case of color aberrations, different orders do not refer to the ray dependency on field and pupil coordinates only. This work extended the aberration theory to higher-order effects regarding the ray dependency on dispersion.

Following that, a new analytical approach was described, investigating the influence of dispersion, starting at the paraxial parameters of the intersection length and the image height up to its impact on 3rd-order monochromatic aberrations. Based on the cumulative characteristics of induced aberrations, a surface and lens resolved descriptions was required. In Section 3.2, 3.3, 3.4 and 3.5 a complex analytical analysis showed, that the influence of dispersion can always be identified by the small chromatic differences in ray heights (Δy and $\Delta\bar{y}$) and ray angles (Δu and $\Delta\bar{u}$) of the marginal and chief ray within the optical system. In overcoming the analytical gap for induced color aberrations discussed in Section 2.5, the essential analytical finding of this thesis were four equations, (3.107), (3.108), (3.109) and (3.110), representing the direct relation of the marginal and chief ray variations to prior summed up 1st-order color aberrations, AXC and LAC, and pupil color aberrations, AXC_p and LAC_p. Considering these relations, the calculation of 2nd-order axial and lateral color as well as of the chromatic variations of spherical aberration, coma, astigmatism, field curvature and distortion, distinguishing between intrinsic and induced aberration parts, were enabled.

These new surface coefficient formulas provides the optical designer a new analysis tool to get a deeper understanding of how and why induced color aberration occur. Hence, in the second part of this work, at first five classical and academic examples for induced color aberrations were discussed. All of them are kept very simple in design, since those are best for understanding the characteristics and possible influences of 2nd-

order induced and intrinsic color aberrations. Particularly, the catadioptric system in 4.1.4 and the split achromat in 4.1.5 are often-cited examples for induced color effects. However, an exact analytical analysis and therefore also a deeper understanding of them was missing. Here, the new surface contribution formulas, found in this thesis, were applied and explained how these designs work.

Finally, since a more complex design example represents a higher relevance for the practical work of an optical designer, the final system example was a complex microscope objective lens. Here, a system of many lenses within a compact arrangement and a multitude of different glass combinations was presented. A detailed design analysis showed, that by considering the available standard analysis tools for color aberrations, like Seidel's surface coefficients and a chromatic focus shift plot, misleading results occurred. Only, by extending those standard tools with the new 2nd-order axial color surface coefficients and by adding up the balancing parts of spherochromatism, the present diffraction limited imaging can be explained. The new surface coefficient plots demonstrated descriptively how the intrinsic and induced 1st-order and 2nd-order axial color as well as spherochromatism parts were balanced and where the dominating surfaces and lenses were. Comparing this to the misleading standard Seidel surface coefficient plot, these extended analysis enabled the optical designer to understand the microscopic system and to find the best surfaces or lenses to even improve the design.

A Appendix

A.1 Induced Axial Color

1st-order derivatives for axial color:

$$\frac{\partial s}{\partial y} = -\frac{1}{u}$$

$$\frac{\partial s}{\partial u} = \frac{y}{u^2}$$

$$\frac{\partial s'}{\partial y} = -\frac{nu}{n'u'^2}$$

$$\frac{\partial s'}{\partial u} = \frac{ny}{n'u'^2}$$

$$\frac{\partial s'}{\partial n} = \frac{yi}{n'u'^2}$$

$$\frac{\partial s'}{\partial n'} = -\frac{nyi}{n'^2u'^2}$$

2nd-order derivatives for axial color:

$$\frac{\partial^2 s}{\partial y^2} = 0$$

$$\frac{\partial^2 s}{\partial u^2} = -\frac{2y}{u^3}$$

$$\frac{\partial^2 s'}{\partial y^2} = -\frac{nuc(n'-n)}{n'^2u'^3}$$

$$\frac{\partial^2 s'}{\partial u^2} = -\frac{n^2y}{n'^2u'^3u}$$

$$\frac{\partial^2 s'}{\partial n^2} = -\frac{yi^2}{n'^2u'^3}$$

$$\frac{\partial^2 s'}{\partial n'^2} = -\frac{y^2nic}{n'^3u'^3}$$

$$\frac{\partial^2 s}{\partial y \partial u} = \frac{1}{u^2}$$

$$\frac{\partial^2 s'}{\partial y \partial u} = \frac{n(n'-n)yc + n^2 u}{n'^2 u'^3}$$

$$\frac{\partial^2 s'}{\partial y \partial n} = \frac{u(n'-n)yc + nu^2 + 2nuyc}{n'^2 u'^3}$$

$$\frac{\partial^2 s'}{\partial y \partial n'} = -\frac{-n^2u^2 + nu(n'-n)yc - 2n'nuyc}{n'^3 u'^3}$$

$$\frac{\partial^2 s'}{\partial u \partial n} = \frac{-y^2(n'-n)c - nyu - 2ny^2 c}{n'^2 u' 3u}$$

$$\frac{\partial^2 s'}{\partial u \partial n'} = \frac{nu'y + 2ny^2 c}{n'^2 u'^3}$$

$$\frac{\partial^2 s'}{\partial n \partial n'} = \frac{nyi^2 + n'y^2 ic}{n'^3 u'^3}$$

Equation (3.23). Coefficients α_1 and α_2 of the thick lens formula for axial color:

$$\alpha_1 = 2u_1 c_2 + 2y_1 c_1 F_2$$

$$\alpha_2 = nu_1^3 - c_2 u_1^2 y_1 - c_1^2 y_1^3 F_2 + 3c_2^2 n u_1 y_1^2 - 2c_1 c_2 u_1 y_1^2 + 3c_2 n u_1^2 y_1 + 3c_2^2 t n u_1^2 y_1 + 2c_2 t n u_1^3 + c_2^2 t^2 n u_1^3$$

A.2 Induced Lateral Color

1st-order derivatives for lateral color:

$$\frac{\partial \bar{y}_1}{\partial \bar{y}} = 1$$

$$\frac{\partial \bar{y}_1}{\partial \bar{u}} = s$$

$$\frac{\partial \bar{y}'_1}{\partial \bar{y}} = 1 - \frac{s'(n'-n)c}{n'}$$

$$\frac{\partial \bar{y}'_1}{\partial \bar{u}} = -\frac{s'n}{n'}$$

$$\frac{\partial \bar{y}'_1}{\partial n} = \frac{s'\bar{i}}{n'}$$

$$\frac{\partial \bar{y}'_1}{\partial n'} = -\frac{ns'\bar{i}}{n'^2}$$

2nd-order derivatives for lateral color:

$$\frac{\partial^2 \bar{y}_1}{\partial \bar{y}^2} = \frac{\partial^2 \bar{y}_1}{\partial \bar{y} \partial \bar{u}} = \frac{\partial^2 \bar{y}_1}{\partial \bar{u}^2} = \frac{\partial^2 \bar{y}'_1}{\partial \bar{y}^2} = \frac{\partial^2 \bar{y}'_1}{\partial \bar{y} \partial \bar{u}} = \frac{\partial^2 \bar{y}'_1}{\partial \bar{u}^2} = \frac{\partial^2 \bar{y}'_1}{\partial n^2} = 0$$

$$\frac{\partial^2 \bar{y}'_1}{\partial \bar{y} \partial n} = \frac{s'c}{n'}$$

$$\frac{\partial^2 \bar{y}'_1}{\partial \bar{y} \partial n'} = -\frac{s'nc}{n'^2}$$

$$\frac{\partial^2 \bar{y}'_1}{\partial \bar{u} \partial n} = \frac{s'}{n'}$$

$$\frac{\partial^2 \bar{y}'_1}{\partial \bar{u} \partial n'} = -\frac{s'n}{n'^2}$$

$$\frac{\partial^2 \bar{y}'_1}{\partial n \partial n'} = -\frac{s'\bar{i}}{n'^2}$$

$$\frac{\partial^2 \bar{y}'_1}{\partial n'^2} = \frac{2s'n\bar{i}}{n'^3}$$

Equation (3.64). Coefficients β_1 and β_2 of the thick lens formula for lateral color

$$\beta_1 = 2y_1u_1c_2 + u_1^2 + tu_1^2c_2$$

$$\beta_2 = -y_1\bar{u}_1c_2 - u_1\bar{u}_1 - \bar{y}_1u_1c_2 - tu_1\bar{u}_1c_2$$

A.3 Induced Spherochromatism

1st-order derivatives for spherochromatism:

$$\frac{\partial S_1}{\partial y} = -\frac{in(n-n')((u-2i)^2 + (4i-3u)u')}{n'}$$

$$\frac{\partial \bar{S}_1}{\partial u} = (u-u')(4i'n' - nu + 3nu')y$$

$$\frac{\partial \bar{S}_1}{\partial n} = i(i'u - i'^2 + u^2 - (2i'+u)u')y$$

$$\frac{\partial \bar{S}_1}{\partial n'} = i'^2(i'+u')y$$

Equation (3.93). Coefficients γ_1,γ_2 and γ_3 of the thin lens formula for spherochromatism:

$$\gamma_1 = i_0^2 + i_1' n_L (i_1' + u_0) + i_0 (i_1' + n_L u_0)$$

$$\gamma_2 = i_1' + 3 i_1' n_L + i_0 (3 + n_L) + 2 n_L u_0$$

$$\gamma_3 = i_0^2 (n_L - 2) + i_0 n_L (2 i_1' n_L - 3 i_1' - u_0) + i_1' n_L (2 i_1' - 3 i_1' n_L + u_0 - 2 n_L u_0)$$

Bibliography

[Ber+15] A. Berner et al. “Chromatic Variation of Aberration: The Role of Induced Aberrations and Raytrace Direction”. In: vol. 9626. 2015.

[Ber+18] A. Berner et al. “3rd-Order Spherochromatism Surface Contribution and Its Intrinsic and Induced Aberration Parts”. In: *J. Opt. Soc. Am. A* 35.8 (Aug. 2018), pp. 1368–1378.

[BNG17] A. Berner, T. Nobis, and H. Gross. “Induced Axial and Lateral Color Surface Contributions”. In: *J. Opt. Soc. Am. A* 34.5 (May 2017), pp. 685–695.

[BSW] M. Brehm, R. Shi, and R. Wartmann. “Mikroskopobjektiv”. DE102008006826A1.

[Buc54] H.A. Buchdahl. *Optical Aberration Coefficients*. Oxford University Press, 1954.

[CK92] A.E. Conrady and R. Kingslake. *Applied Optics and Optical Design*. Applied Optics and Optical Design Bd. 1. Dover Publications, 1992. ISBN: 978-0-486-67007-2.

[Con14] A.E. Conrady. *Applied Optics and Optical Design, Part Two*. Dover Books on Physics. Dover Publications, 2014. ISBN: 978-0-486-16262-1.

[Del52] E. Delano. “A General Contribution Formula for Tangential Rays”. In: *J. Opt. Soc. Am.* 42.9 (Sept. 1952), pp. 631–633.

[Gro+07] H. Gross et al. *Handbook of Optical Systems, Aberration Theory and Correction of Optical Systems*. Handbook of Optical Systems. Wiley, 2007. ISBN: 978-3-527-40379-0.

[Gro05] H. Gross. *Handbook of Optical Systems, Fundamentals of Technical Optics*. Handbook of Optical Systems. Wiley, 2005. ISBN: 978-3-527-40377-6.

[Haf86] H. Haferkorn. *Bewertung Optischer Systeme*. Optisches Instrument. VEB Deutscher Verlag der Wissenschaften, 1986. ISBN: 978-3-326-00000-8.

[Hof] C. Hofmann. “Die Bewertung Optischer Systeme”. In: *Fortschritte der Physik* 27.11-12 (), pp. 595–639.

[Hof93] J. M. Hoffman. *Induced Aberrations in Optical Systems*. The University of Arizona., 1993.

[Hop50] H.H. Hopkins. *Wave Theory of Aberrations*. Monographs on the Physics and Chemistry of Materials. Clarendon Press, 1950.

[Ker95] A. Kerber. *Beiträge Zur Dioptrik*. Vol. Erstes Heft. Selbstverlag, Leipzig, 1895.

[Kin12] R. Kingslake. *Lens Design Fundamentals*. Elsevier Science, 2012. ISBN: 978-0-08-051009-5.

[KT02] M.J. Kidger and V.V. Tuchin. *Fundamental Optical Design*. Press Monographs. Society of Photo Optical, 2002. ISBN: 978-0-8194-3915-4.

[Mcc55] E. L. Mccarthy. "Optical System with Corrected Secondary Spectrum". In: (Jan. 1955). US Patent 2,698,555.

[MM17] D. Malacara-Hernández and Z. Malacara-Hernández. *Handbook of Optical Design*. CRC Press, 2017. ISBN: 978-1-351-83292-2.

[Nak15] H. Nakajima. *Optical Design Using Excel: Practical Calculations for Laser Optical Systems*. Wiley, 2015. ISBN: 978-1-118-93914-7.

[Nob14] T. Nobis. "A Lens-Resolved Approach for Analyzing and Correcting Secondary Axial Color". In: *Classical Optics 2014*. Classical Optics 2014. Optical Society of America, 2014, ITu1A.1.

[Nob15] T. Nobis. "Second-Order Axial Color of Thin Lenses in Air". In: *J. Opt. Soc. Am. A* 32.10 (Oct. 2015), pp. 1857–1869.

[Rim63] M.P. Rimmer. *Optical Aberration Coefficients*. 1963.

[Rog13a] J. R. Rogers. "Secondary Color Correction and Tolerance Sensitivity: What Can You Get Away With?" In: vol. 8844. 2013.

[Rog13b] J. R. Rogers. "The Importance of Induced Aberrations in the Correction of Secondary Color". In: *Advanced Optical Technologies* 2.1 (2013), p. 41. ISSN: 21928584.

[Sas10] J. Sasián. "Theory of Sixth-Order Wave Aberrations". In: *Appl. Opt.* 49.16 (June 2010), pp. D69–D95.

[Sei56] L. Seidel. "Zur Dioptrik. Ueber Die Entwicklung Der Glieder 3ter Ordnung, Welche Den Weg Eines Ausserhalb Der Ebene Der Axe Gelegenen Lichtstrahles Durch Ein System Brechender Medien Bestimmen, von Herrn Dr. L. Seidel". In: *Astronomische Nachrichten* 43.19 (1856), pp. 289–304.

[Sli84] G. G. Sliusarev. "Aberration and Optical Design Theory". In: *Bristol, England, Adam Hilger, Ltd., 1984, 672 p. Translation.* (1984).

[Smi04] W. Smith. *Modern Lens Design*. Electronic Engineering. Mcgraw-hill, 2004. ISBN: 978-0-07-143830-8.

[Smi66] W. J. Smith. *Modern Optical Engineering*. McGraw-Hill, 1966.

[War19] R. Wartmann. "Apochromatisches Mikroskopobjektiv Und Mikroskop". DE 102017218169B3. Mar. 2019.

[Wel86] W. T. Welford. *Aberrations of Optical Systems*. Series in Optics and Optoelectronics. Taylor & Francis, 1986. ISBN: 978-0-85274-564-9.

[Wyn77] C. G. Wynne. "Secondary Spectrum Correction with Normal Glasses". In: *Optics Communications* 21.3 (June 1977), pp. 419–424. ISSN: 0030-4018.

[Wyn78] C. G. Wynne. "A Comprehensive First-Order Theory of Chromatic Aberration. Secondary Spectrum Correction without Special Glasses". In: *Optica Acta: International Journal of Optics* 25.8 (1978), pp. 627–636.

[Zim67] H.-G. Zimmer. *Geometrische Optik*. Springer Verlag, Berlin, Heidelberg,New York, 1967.

List of Figures

2-1 Paraxial approximation of imaging, assuming all rays starting at one point of the object plane OP perfectly meeting at an image point of the conjugated image plane IP. 8
2-2 Refraction at an optical surface, assuming rotational symmetry along z-axis. 10
2-3 Paraxial ray transfer at an arbitrary surface j of an optical system to surface $j+1$. 12
2-4 Refraction of the marginal ray (solid line) and the chief ray (dashed line) at a thick lens. 14
2-5 Real imaging of an optical system, considering real optics with finite ray heights and ray angles. 15
2-6 Definition of wavefronts as a surface of constant optical path length measured from a point at the object plane. 16
2-7 Wavefront aberration defined as the deviation of the wavefront to a reference sphere (dotted line). This is determined by the paraxial image point O' as center and the intersection point of the chief ray with the optical axis. 17
2-8 Definition of field vector $\vec{F}$ at the object plane and pupil vector $\vec{P}$ at the pupil plane of an optical system. 18
2-9 Transverse ray aberration $\Delta y'$ in the y-z-plane of an optical system. . . 20
2-10 Lens example with three surfaces, forming a real intermediate image in each space in between the surfaces. 22
2-11 Variation of the refractive index n with wavelength for BK7 24
2-12 Abbe diagram of the manufacturer Schott 26
2-13 Partial Dispersion of the manufacturer Schott 26
2-14 Axial color aberration $\Delta s'$ of a single positive thin lens 27
2-15 Achromatic case, where the blue and red foci show the same intersection length. The green focal length is shorter. 28
2-16 Lateral color $\Delta \bar{y}'$ of a single positive thin lens 29
2-17 Bar plots of Seidel surface contribution for a given lens design. 31

2-18 Monochromatic intrinsic and induced ray aberration parts 33

3-1 Intrinsic and induced color aberration parts 37
3-2 Classification of different color aberration orders exemplary shown, starting at (a) paraxial intersection lengths s and (b) image height y. The green and yellow colored quantities mark the well-known Seidel and Buchdahl coefficients, respectively. The blue framed quantities include induced color aberrations. 38
3-3 Overview of the current state of the induced color aberration problem and the new derived quantities within this thesis. Please note, Since Wynne identified a way to determine the contribution of induced axial and lateral color by tracing two paraxial rays with different wavelengths, his induced terms are not wrong, but can be simplified within this new approach. 39
3-4 Refraction of two paraxial marginal rays with different wavelengths (black and blue line) at an arbitrary surface S 40
3-5 Refraction of the marginal ray at a thick lens. The marginal ray heights and angles are y_1 and u_1 as well as y_2 and u_2 at surface S1 and surface S2, respectively. 44
3-6 Refraction of two paraxial chief rays with different wavelengths (black and blue line) at an arbitrary surface S. The intermediate images show different lateral color aberrations $\Delta\bar{y}_1$ and $\Delta\bar{y}'_1$, whereby the image position is defined by the intersection length of the marginal ray (dashed line) 47
3-7 Refraction of two paraxial chief rays with different wavelengths (black and blue line) at an arbitrary surface S. The intermediate images show lateral color aberrations $\Delta\bar{y}_1$ and $\Delta\bar{y}'_1$, which also leads to a chromatic defocused image of the stop position Δp. 52
3-8 Refraction of the marginal ray and chief ray (dashed and solid line) at a thick lens with an refractive index of n. The marginal ray heights and angles are y_1 and u_1 as well as y_2 and u_2 at surface S1 and surface S2, respectively. The chief ray heights and angles are $\bar{y}_0$ and $\bar{u}_0$, $\bar{y}_1$ and $\bar{u}_1$ as well as $\bar{y}_2$ and $\bar{u}_2$ at the intermediate image, surface S1 and surface S2, respectively. 54
3-9 Parameters defining the spherical aberration conditions. Here, capital letters refer to real ray and small letter to the paraxial ray parameters. 58

3-10 Quantities defining spherochromatism. Here, the solid black line parameters refer to the real ray path and dashed black line parameters to the paraxial ray path of the primary wavelength λ_1. The second wavelength λ_2 is represented by blue lines. Again, capital letters belong to the real rays and small letters to the paraxial rays. 59
3-11 Longitudinal aberration plot corresponding to the relations, shown in Figure 3-10 for wavelength λ_1 and wavelength λ_1. Here, the intersection length s for λ_1 provides the reference. Δs describes the difference in z-direction to this reference and h_p characterizes the relative pupil height. 60
3-12 Extended considerations on a chromatically varying marginal ray. Here, the solid line parameters again refer to the marginal ray of the primary wavelength λ_1 and the blue line parameters to the marginal ray of the second wavelength λ_2. Additionally, the chief ray of λ_1 is plotted as a dotted line. The intersection length s of the marginal ray characterizes the intermediate image for λ_1. At this image, an axial color aberration Δs is present. The position of the imaged stop in front of the surface is defined by the intersection length p of the chief ray. Here, a chromatic varying stop size characterized by $\Delta\bar{y}_p$ is present. The same considerations are applied for the primed quantities after the surface. 63

4-1 Example design composed of two lenses, each in a 4f- arrangement. (a) shows the marginal raytrace for two different wavelengths (dashed and dotted line), illustrating the axial color parameters and (b) shows the chief raytrace of two different wavelengths (solid and dotted line) illustrating the lateral color parameters. 74
4-2 Thick meniscus lens with same radii of $R = 15\,\text{mm}$ and a thickness of $t = 10\,\text{mm}$. 77
4-3 (a) Schupmann achromatic design, where a positive lens with f'_{L1} and negative lens with $f'_{L2} = -f'_{L1}$ are set up together, separated by an airspace of $d = 2f'_{L1}$. (b) Schupmann design improved by a third lens with $f'_{L3} = 1/2f'_{L1}$, positioned exactly at the intermediate image between the two lenses. 78
4-4 Longitudinal aberration plots for (a) the two-lenses N-BK7 Schupmann design and (b) the same Schupmann design improved by a third N-BK7 thin lens with positioned exactly at the intermediate image between the two lenses. 79
4-5 Thick meniscus lens with same radii of $R = 15\,\text{mm}$ and a thickness of $t = 10\,\text{mm}$. 82

4-6 (a) a classical unsplit achromat and (b) a split achromat with a air space between the lenses. 85
4-7 Longitudinal aberration plots for (a) the classical unsplit achromat and (b) the split achromat with a air space between the lenses. The first, positive lens is made of NBK7 and the second, negative lens of NSF5. . 85
4-8 Lens drawing of the microscopic lens. [BSW] 90
4-9 Axial color aberration represented by the Zernike wavefront aberration coefficient for defocus A_{02} from 425 nm to 800 nm. [BSW] 90
4-10 Lens drawing of the microscopic lens described in [BSW] combined with a standard tube lens package, described in [War19]. 91
4-11 Optical Performance plots of the microscopic lens at $NA = 1.0$ (a) Spot diagram, (b) polychromatic MTF, (c) Longitudinal aberration plot and (d) paraxial chromatic focus shift 91
4-12 Longitudinal Seidel surface coefficients of axial color (1st AXC) for 450 nm and 700 nm. Surface numbers 1 to 3 are immersion surfaces. Surface numbers from 4 to 21 and 23 to 26 are the microscopic lens surfaces and the tube lens with glass block, respectively. The last bar shows the sum over the total system and its exact values above. 93
4-13 Longitudinal Seidel surface coefficients of axial color (1st AXC) for 450 nm and 546 nm. Surface numbers are the same as in Figure 4-12. . 93
4-14 Longitudinal Seidel surface coefficients of axial color including 1st- and 2nd-order contributions for 450 nm and 700 nm. Surface numbers 1 to 3 are immersion surfaces. Surface numbers from 4 to 21 and 23 to 26 are the microscopic lens surfaces and the tube lens with glass block, respectively. The last bar shows the sum over the total system and its exact values above. 95
4-15 Longitudinal Seidel surface coefficients of axial color including 1st- and 2nd-order for 450 nm to 546 nm. Surface numbers are the same as in Figure 4-14. 95
4-16 Longitudinal aberration plot of the microscopic lens. 97
4-17 Longitudinal surface coefficients including axial color (1st- and 2nd-order) and spherochromatism (GA) for 450 nm to 700 nm. Surface numbers 1 and 3 are immersion surfaces. Surface numbers from 4 to 21 and 23 to 26 are the microscopic lens surfaces and the tube lens with glass block, respectively. 98
4-18 Longitudinal surface coefficients including axial color (1st- and 2nd-order) and spherochromatism (GA)for 450 nm and 546 nm. Surface numbers are the same as in Figure 4-17. 98

4-19 Longitudinal surface coefficients of axial color, distinguishing between intrinsic and induced aberration parts. Surface numbers 1 and 3 are immersion surfaces. Surface numbers from 4 to 21 and 23 to 26 are the microscopic lens surfaces and the tube lens with glass block, respectively. 100
4-20 Longitudinal surface coefficients of spherochromatism, distinguishing between intrinsic and induced aberration parts. Surface numbers are the same as in Figure 4-19. 100
4-21 Separation of the different wavelengths at the first surface of the middle group of the microscopic lens as well as at the first surface of the tube lens. 101

List of Tables

4.1 Axial color contributions for the example system for case (1). The wavelength range is $\lambda_1 = 486\,\text{nm}$ to $\lambda_2 = 656\,\text{nm}$. 74

4.2 Axial color contributions for the example system for case (2). The wavelength range is $\lambda_1 = 486\,\text{nm}$ to $\lambda_2 = 656\,\text{nm}$. 75

4.3 Lateral color contributions for the example system for case (1). The wavelength range is $\lambda_1 = 486\,\text{nm}$ to $\lambda_2 = 656\,\text{nm}$. 75

4.4 Lateral color contributions for the example system for case (2). The wavelength range is $\lambda_1 = 486\,\text{nm}$ to $\lambda_2 = 656\,\text{nm}$. 76

4.5 Induced and intrinsic axial color contributions of a meniscus lens for a wavelength range from 486 nm (F-line) to 587 nm (d-line). 78

4.6 G^L coefficients of the two-lens Schupmann design for the prior summed up 1st-order color aberrations AXC^L and LAC_p^L and the intrinsic and induced parts of G^L 80

4.7 Seidel wavefront aberration coefficient S_I by two single ray traces and the comparison to the spherochromatic coefficient G. 82

4.8 Wavefront aberration coefficients of the mirror design example for the prior summed up chromatic aberrations AXC_{1st} and $LAC_{p,1st}$ and the intrinsic and induced parts of G. 83

4.9 Conversation of Seidel's spherical aberration coefficients and of the spherochromatism coefficient G into longitudinal aberrations SPH and GA 84

4.10 Numerical solution for three variable radii $R1, R2$ and $R3$ of the unsplit achromat. The Seidel contributions for axial color AXC and 3rd-order spherical aberration S_I as well as the Buchdahl-Rimmer 5th-order contributions $B5$ are given. 86

4.11 Numerical solution for three variable radii $R2, R3$, $R4$ and a variable air space thickness t of the split achromat. The Seidel contribution for axial color AXC and 3rd-order spherical aberration S_I as well as the Buchdahl-Rimmer 5th-order contributions $B5$ and the Spherochromatism contributions G are given. 88

4.12 Numerical solution for three variable radii $R2, R3$, $R4$ and a variable air space thickness t of the split achromat. The spherochromatism contributions G and its intrinsic as well as its induced parts are given. 89

Zusammenfassung

Der Schwerpunkt dieser Arbeit lag auf der Untersuchung von Farbaberrationen höherer Ordnung sowie der Differenzierung ihrer induzierten und intrinsischen Aberrationsanteile.
In analoger Weise zu den monochromatischen Abbildungsfehlern, erzeugen Fehler niedrigerer Ordnung induzierte Fehler höherer Ordnung, welche sich Fläche für Fläche innerhalb des optischen System aufsummieren. Diese induzierten Aberrationsanteile existieren im Falle der Farbfehler jedoch bereits im paraxialen Bereich, da auch paraxiale Strahlen durch Dispersion beeinflusst werden.
Folglich wurde in dieser Arbeit zunächst eine neue Klassifikation der Aberrationsordnungen eingeführt. Im Falle von Farbfehlern beziehen sich die unterschiedliche Ordnungen neben der Feld- und Pupillenabhängigkeiten der Strahlen zusätzlich auf die Abhängigkeit von Dispersion.
In dem anschließenden Kapitel wurde ein neuer analytischer Ansatz beschrieben, der den Einfluss von Dispersion, beginnend bei den paraxialen Parametern der Schnittweite und der Bildhöhe bishin zu ihrer Auswirkung auf die monochromatischen Aberrationen 3. Ordnung, beschreibt. Basierend auf den kumulativen Eigenschaften von induzierte Aberrationen war eine flächen- und linsenaufgelöste Beschreibung erforderlich. Im Abschnitt 3.2, 3.3, 3.4 und 3.5 konnte eine komplexe analytische Untersuchung zeigen, dass sich der Einfluss der Dispersion durch die chromatischen Unterschiede in den Strahlhöhen (Δy und $\Delta\bar{y}$) und den Strahlwinkeln (Δu und $\Delta\bar{u}$) des Rand- bzw. Hauptstrahls identifiziert lässt. Somit konnte die im Kapitel 2.5 aufgezeigte analytische Lücke bzgl. induzierter Farbfehler durch die vier Hauptergebnisse dieser Arbeit geschlossen werden. Diese vier Gleichungen (3.107), (3.108), (3.109) und (3.110) zeigen den direkten Zusammenhang zwischen den benannten, durch Dispersion verursachten Rand- und Hauptstrahlvariationen und den zuvor im optischen System aufsummierten, niedrigeren Farbfehlern 1. Ordnung, AXC, LAC, AXC_p and LAC_p. Unter Berücksichtigung dieser Relationen konnten neben dem Farblängs- und Farbquerfehler 2. Ordnung nun auch die chromatischen Variationen der Sphärischen Aberration, Koma, Astigmatismus, Bildfeldwölbung und Verzeichnung analytisch bestimmt und auf ihre induzierten und intrinsichen Anteile untersucht werden.
Diese Erweiterung der bekannten Flächenkoeffizientenformeln bietet dem Optikde-

signer ein neues Analysewerkzeug, welches zeigt, wie und warum Farbfehler höherer Ordnung, im speziellen induzierte Farbfehler, auftreten und ermöglicht somit dem Designer ein tieferes Systemverständnis zu erlangen. Daher wurden in dem zweiten Teil dieser Arbeit zunächst fünf klassische Beispiele für induzierte Farbaberrationen diskutiert. Alle Beispielsysteme sind simpel gehalten, da diese am besten zum besseren Verständnis der Eigenschaften und möglichen Einflüsse von induzierten und intrinsischen Farbfehlern beitragen. Insbesondere das katadioptrische System in 4.1.4 und der aufgesplittete Achromat in 4.1.5 sind in der Literatur häufig zitierte Beispiele für induzierte Farbeffekte. Jedoch war ihre genaue analytische Untersuchung bis jetzt nicht möglich. Hier konnten nun die neuen Flächebeitragsformeln, die in dieser Arbeit gefunden wurden, angewendet werden und erklären, wie die optischen System unter der Berücksichtigung von induzierten Fehleranteilen funktionieren.
Schließlich stellt dann ein komplexeres optisches System mit höherer Praxisrelevanz für einen Optikdesigner das finale Beispiel dar. Dieses letzte Systembeispiel war ein aufwendiges Mikroskopobjektiv. Hierbei handelt es sich um ein Design aus einer Vielzahl von Linsen in einer kompakten Anordnung sowie unterschiedlichen Glaskombinationen. Eine detaillierte Designanalyse ergab, dass unter Berücksichtigung der verfügbaren Standardanalysewerkzeuge für Farbfehler, wie z. B. die Seidel'sche flächenaufgelöste Analyse sowie dem chromatischen Fokusverschiebungsdiagramm, unzureichende Ergebnisse auftraten. Nur durch die Erweiterung dieser Standardwerkzeuge mit den neuen Farblängsfehlerkoeffizienten 2. Ordnung und durch Hinzufügen der ausgleichenden Anteile des Gaußfehlers konnte die vorliegende beugungsbegrenzte Abbildungsleistung erklärt werden. Die neuen Flächenkoeffizientendiagramme zeigten anschaulich, wie sich die intrinsische und induzierte Farblängsfehler 1. und 2. Ordnung sowie die Gaußfehleranteile ausbalancieren und wo die performance-dominierenden Systemflächen und Linsen waren. Vergleicht man dies mit der in diesem Beispiel unzureichenden Seidelanalyse, befähigte erst das neue Analysetool den Designer das Mikroskopsystem zu verstehen und dominierende Flächen bzw. Linsen zu identifizieren.

Ehrenwörtliche Erklärung

Ich erkläre hiermit ehrenwörtlich, dass ich die vorliegende Arbeit selbstständig, ohne unzulässige Hilfe Dritter und ohne Benutzung anderer als der anegegebenen Hilfsmittel und Literatur angefertigt habe. Die aus anderen Quellen direkt oder indirekt übernommenen Daten und Konzepte sind unter der Angabe der Quelle gekennzeichnet. Bei der Auswahl und Auswertung folgenden Materials haben mir die nachstehenden aufgelisteten Personen in der jeweils beschriebenen Weise unentgeltlich geholfen:

(1) Die für die Berechnung und Analyse der optischen Systeme genutzte Software (Oase, OpticsStudio, Matlab, Mathematica) wurde von der Corporate Research&Technology der Carl Zeiss AG (Dipl.-Ing. M. Hanft, Director Design Jena) zur Verfügung gestellt.

(2) Ewa Kasperkiewicz, Studentin der Friedrich-Schiller-Universität, erarbeitete im Rahmen ihrer Werksstudententätigkeit bei der Carl Zeiss AG auf der Grundlagen, der in Kapitel 3.2 und 3.3 beschriebenen Theorie, einen Mathematica Code zur Berechnung der induzierten Flächenbeiträge an optischen Beispielsystemen.

(3) Yasmin Abou Laban, Studentin der Friedrich-Schiller-Universität, implementierte im Rahmen ihres Research Lab Praktikums einen Macro Code für OpticStudio.

Weitere Personen waren an der inhaltlich-materiellen Erstellung der Arbeit nicht beteiligt. Insbesondere habe ich hierfür nicht die entgeltliche Hilfe von Vermittlungs- bzw. Beratungsdiensten in Anspruch genommen. Niemand hat von mir unmittelbar oder mittelbar geldwerte Leistungen für Arbeiten erhalten, die im Zusammenhang mit dem Inhalt der vorgelegten Arbeit stehen.
Die Arbeit wurde bisher weder im In- noch Ausland in gleicher oder ähnlicher Form einer anderen Prüfungsbehörde vorgelegt. Die geltende Promotionsordnung der Physikalisch-Astronomischen Fakultät ist mir bekannt. Ich versichere, daß ich nach bestem Wissen die reine Wahrheit gesagt und nichts verschwiegen habe.

Jena, _____ _____

Danksagung

Okay, dies ist nun wirklich die allerletzte Seite, die ich innerhalb dieser Arbeit tippe. Im Gegensatz zu den restlichen Kapiteln habe ich mich dazu entschlossen nicht zu googeln, wie man eine gute Danksagung formuliert, sondern sie einfach zu schreiben.

Als allererstes fallen mir die drei wichtigsten Männer ein, die es mir nicht nur ermöglicht, sondern mich auch in jeglicher Weise dabei unterstützt und geleitet haben, diese Dissertation zu schreiben. Herbert, Willi Ulrich und Marco, ihr wart für mich die besten Ermöglicher und Mentoren, die ich mir vorstellen konnte. Nicht nur aus fachlicher Sicht (das weiß, denke ich, jeder aus der Community) war es für mich immer etwas Besonderes euch drei in meinem Rücken zu wissen. Vielen Dank dafür und vor allem vielen Dank, dass ihr an mich geglaubt habt.
Jetzt, meine Family... Auf diesen Abschnitt habe ich mich schon seit fast 5 Jahren gefreut! Ich weiß, ihr wusstet es nicht. Vielleicht habt ihr es geahnt, wegen Thessas "Verplapperer" auf meiner Einzugsparty oder dem Geburtstagsvideo zu meinem 30. Jedenfalls haltet ihr jetzt diese Arbeit in der Hand und lest diese Danksagung an euch. Ich hoffe, ihr seid nicht bös, dass ich es nicht erzählt habe, aber ohne es zu wissen, wart ihr ein entscheidender Teil dieser Arbeit. Ohne euch, Ma und Pa, wäre ich nie bis nach Jena und zu ZEISS gekommen. Ihr habt mich immer unterstützt, habt alle Fragen zu Mathe und Physik mit mir am Wohnzimmertisch durchgekaut, mir mein Studium ermöglicht und wart zusammen mit Chrissy, Bernd und der kleinen Klara in den letzten 5 Jahren, die Auszeitmöglichkeit, die ich brauchte. Dieses dicke Dankeschön habt ihr euch mehr als verdient!
Jetzt, meine zweite Family... dieses Mal die aus Jena, Essen, Hamburg, mittlerweile auch Peking und Sao Paulo. Ihr habt die Diss am direktesten mit- und abbekommen. Ohne euch Schnuffis, die ihr u.a. auch Diskussionschallenger, aber vor allem Supporter und Ablenkungsprogramm (am Strand von Holland, auf den Tanzflächen und auf den Beach- sowie Hallencourts Jenas) wart, hätte ich das nicht gepackt. Ihr seid die besten Freunde... und ich hoffe, ihr freut euch schon auf die Verteidigungsparty! Save the date ist hiermit raus.
Last but not least, gibt es natürlich auch noch viele Kollegen, die mich unterstützt haben und denen ich danken will. Ihr dürft natürlich auch zur Party kommen! Aber

am wichtigsten ist mir dabei einer, Thomas, der "alte Hase" aus unserem Bunny Nest. Herzlichen Glückwunsch, du bist die meist zitierte Quelle in dieser Arbeit und auch die wichtigste. Ich bin echt froh, dass Marco dich neben mich gesetzt hat. Du warst der einzige, der mir verloren in meinen Rechnung und bei den ganzen Details helfen konnte. Ohne diese Hilfe bei den unzähligen kleinen und großen Fragen zwischendurch wäre ich wahrscheinlich irgendwo mittendrin untergegangen. Vielen, vielen Dank dafür!

Andrea

PS: Danke Grenouille.